THESIS FOR DEGREE OF DOCTOR OF PHILOSOPHY

LNG as the future marine fuel

Waste Heat Recovery Systems & Cold Ironing solutions for eco-friendly maritime transport

PhD Candidate: Michele Laviola
Supervisor: Prof. Marco Altosole
DITEN, POLYTECHNIC SCHOOL, UNIVERSITY OF GENOA, ITALY

MICHELE LAVIOLA, Department of Naval, Electrical, Electronic and Telecommunication Engineering (DITEN), University of Genoa, Italy.

ABSTRACT

Nowadays a regulatory framework regarding the pollutant emissions abatement, both at international and local level, significantly interests the maritime sector. To comply with the latest environmental rules, a new approach to ship design and a renewed way to operate the ship are need both in navigation and in harbour. This PhD Thesis aims to investigate on the positive features offered by the LNG fuel, more eco-friendly than the traditional marine fuel oils. In the first part of the research, the performance comparison between two marine engines, fuelled by natural gas and diesel oil respectively is reported. Two different simulation codes, one for each engine, validated by means of geometrical and performance data provided by the manufacturer have been developed to extend the comparison to the whole working area of the examined engines. In the second part of the research, a LNG-repowering study of a cruise ferry is presented. The study is enhanced by the investigation on possible Waste Heat Recovery (WHR) systems aiming at the reduction of Green House Gas (GHG), pollution, and money saving. A computational code has been developed to carry out the sizing and to analyse the energetic performance and economical aspects of the several examined WHR layout systems. The more eco-friendly layout for the considered ship is proposed to comply with in force rules. The third part of the PhD Thesis is focused on studying some maritime technical solutions for the electric energy generation and delivery to ships moored in port, by means of LNG fuelled generators installed on board a floating unit. Two different scenarios, regarding the LNG supply chain, are considered and some options for producing cleaner electric energy are then investigated. The reference area examined in this study is the old port of Genoa, where the traffic of both passenger and cargo ships takes place. The analysis is carried out by means of a MATLAB numerical code to calculate the most important features of the floating unit, as dimensions and weights and the most significant characteristics of the electric generation equipment, as the average load factor, fuel consumption and energy cost. From an economical point of view, the externalities costs abatement, thanks to the technical solution proposed are investigated. The study also focuses on the estimation of governmental incentives to promote and sustain the use of the proposed power supply barge, resulting into a fully positive technical solution.

Keywords: Marine engines simulation code, LNG-fuelled ship, Waste Heat recovery systems, Power supply barge, Alternative fuels, LNG, High Voltage Shore Connection, Cold ironing technologies, Air pollution, Cost benefit analysis, Socio-economic impact, External health costs, Investment cost, Incentive-based emissions reduction

CONTENTS

ACKNOWLEDGMENTS

I would like to express my sincere gratitude to my supervisor Professor Marco Altosole and Professor Massimo Figari who supported my work and helped me to get results of better quality.

I would like to thank Raffaello Corradi, Technical manager of Rimorchiatori Riuniti Group for suggesting to me the idea of the power supply barge as topic of the my PhD thesis and for several inspirations from a technical point of view.

I would like to express my full love for my family, the Arche of my life.

List of Acronyms

AS	Alternative Sources
BDC	bottom dead centre
COND	Condenser
CWP	Circulating Water Pump
DE	diesel engine
ECA	emission control area
ECO	Economizer
EEDI	energy efficiency design index
EPA	environment protection agency
EVA	Evaporator
FWP	Feed Water Pump
GHGs	greenhouse gases
GVU	Gas Valve Unit
GW	Glycol Water
HFO	heavy fuel oil
HP	High Pressure
HRSG	Heat Recovery Steam Generator
HWT	Hot Water Tank
IMO	international maritime organization
LNG	Liquefied Natural Gas
LP	Low Pressure
MDO	marine diesel oil
MGE	Main Gas Evaporator
NCR	normal continuous rating
NG	natural gas
PBE	Pressure Build-up Evaporator
RR	Rolls Royce

SD	Steam Drum
SI	spark ignition
SS	Steam Service
ST	Steam Turbine
SUP	Super heater
TC	turbocharger
TDC	top dead centre
VVT	variable valve timing system
WHR	Waste Heat Recovery
WHRS	Waste Heat Recovery System

Nomenclature

A_w	cylinder wall area
A_{ch}	cylinder head area
A_R	valve head area
b.m.e.p	brake mean effective pressure
b.s.f.c	brake specific fuel consumption
B	bore
c_1, c_2	constant values
C	brake torque
C_D	discharging coefficient
E	heat exchanger efficiency
f.m.e.p	mechanical friction mean effective pressure
h	thermal conductivity
H_i	inlet specific enthalpy

H_o	outlet specific enthalpy
H_f	fuel lower heating value
i.m.e.p	gross indicated mean effective pressure
J	polar moment of inertia
k_g	ratio of specific heats at constant pressure and volume
K_a, K_m	constants in Wiebe equation
K_{id}	ignition delay constant
m_i	inlet mass flow rate
m_o	outlet mass flow rate
M	mass
M_f	fuel mass
M_i	gas mass at manifold inlet
M_o	gas mass at manifold outlet
n	rotational speed
p	pressure
p_c	cylinder mean pressure
p_i	pressure inside the cylinder
p_o	pressure in the exhaust duct
p_{dr}	pressure in dragged engine condition
p.m.e.p	pumping mean effective pressure
P	power
P_C	compressor power
P_T	turbine power

Q	heat
Q_b	heat in combustion phase
Q_w	heat exchanged between fluid and cylinder wall
Q'	shaft torque
R	gas constant
S	piston stroke
t	time
T	temperature
T_{coo}	coolant temperature
T_{ex}	exhaust gas temperature
T_i	inlet temperature
T_g	gas temperature
T_i	outlet temperature
T_{Db}	combustion temperature in burning zone of diesel engine
T_{Dub}	combustion temperature in non-burning zone of diesel engine
T_{SI}	spark ignition temperature of gas engine
T_w	cylinder wall temperature
U	specific internal energy
v	gas speed inside the cylinder
v_m	piston mean velocity
V	volume, displaced volume
V_{ex}	manifold volume
W	work
x	piston displacement or generic variable

x_b	fraction of fuel mass burned
α	air mass/fuel mass ratio
β	turbocharger compressor pressure ratio
Δ	difference
η	efficiency
η_V	cylinder volumetric efficiency
ϕ	equivalence ratio
ω	angular velocity
θ	crank angle
θ_{id}	ignition delay crank angle
θ_{ign}	combustion starting angle
ρ	volumetric compression ratio
ρ_o	density
ζ	ratio between crank radius and rod length

INTRODUCTION

On a global scale, by 2030 the United Nations have planned goals dealing with energy efficiency and cleaner fossil-fuel management, promoting investments in both infrastructure and technology for a more eco-friendly environment. This new kind of scenario will involve the maritime activities and the international shipping as confirmed by Annex VI of IMO's pollution prevention treaty (MARPOL, IMO). The infrastructure and upgrade technology for supplying modern and sustainable energy services will affect the technical requirements of the ships and the related port activities. The strong interest to cut emissions from maritime shipping is supported by a regulatory framework consisting of international regulations, European directives and national laws regarding the emissions thresholds from ships in port, and possible solutions to comply with this need. The current regulations relating to such issues are:

- EU Directive 2005/33/EC, requiring for marine fuels a maximum sulphur content of 0.1% and 1.5% by mass in European ports and in exclusive economic zones respectively
- EU Directive 2014/94/EU, requiring the installation of LNG refuelling stations placed in the core TEN-T ports by 2025
- Annex VI of the MARPOL, establishing sulphur limits and abatement of NOx content up to limit threshold values in pollutant emission from marine fuels
- EU Directive 2006/339/EC, involving the installation of electric power stations in the port for supplying energy to ships while at berth
- EEDI (MEPC, IMO), requiring a minimum energy efficiency level for new ships
- Masterplan issued by the Italian Government for promoting the use of natural gas as fuel, thus reducing the environmental impact of transport by sea and road
- EU MRV (Monitoring, Reporting, Verification) regulation entered into force on 1 July 2015, and it requires ship owners and operators to annually monitor, report and verify CO_2 emissions for vessels larger than 5000 gross tonnage (GT) calling at any EU and EFTA (Norway and Iceland) port. Data collection takes place on a per voyage basis and starts on 1^{st} , 2018.

To comply with the latest environmental rules is necessary to upgrade the technological layout and operational profiles of ships. In addition, it is also proper to provide the shore-land with appropriate technologies, to make more eco-friendly the maritime activities during the interaction ship-shore. The use of a different fuel as the LNG could represent a keystone in the next decades of maritime transport activities. In this study, two different LNG applications are presented. One regards the LNG repowering of a Ro-Pax ferry (originally fuelled by HFO), while the other one concerns the feasibility study of a power supply barge (delivering electric energy to ships when at berth) equipped with gas generators. The case study regarding the second session of the study is focused on the old port of Genoa and the ships involved are both passenger and cargo carriers. Specifically for this port, a cold ironing solution based on the existing grid appears to be an unfeasible solution, due to the high power demand and the current rating of the electrical distribution infrastructure in the interested area. For this reason, suitable solutions to satisfy ships energy demand in port could be the adoption of

power supply floating units equipped with LNG-fuelled generators. Since a great deal of attention has been paid in recent years to optimize the use of energy resources in the maritime transport and in land activities, a possible introduction of a waste heat recovery system, to be applied both to the examined ship and to the power supply barge, has been considered. The possibilities to recover the heat released by the combustion processes of the main engines and to increase the fuel chemical energy exploitation could be favourable for ship-owners, environment and human health.

1 DESIGN PRINCIPLES OF LNG-FUELLED VESSELS

1.1 GENERAL ASPECTS OF LNG –FUELED SHIPS

LNG as ship fuel is now a proven solution. The number of ships using LNG as fuel is increasing day per day, and more and more infrastructures projects to make available this kind of resource are proposed or already completed. ECA limits should involve other water areas in the next future, this fact has involved an increase of LNG-fuelled fleet in the 2010-2014 period, and a further increase is expected in the future (Campora et al., 2016). Today, up to one hundred LNG-fuelled ships are operating on the global sea and other ones will be in use, as confirmed by the ship order book (Tellkamp J. & Mohn H., 2015). Figure 1.1 represents the sharing between flagships of existing and next order booked LNG-fuelled ships. The use of LNG as marine fuel is advantageous from a commercial and ecological point of view, reducing significantly air pollution emissions.

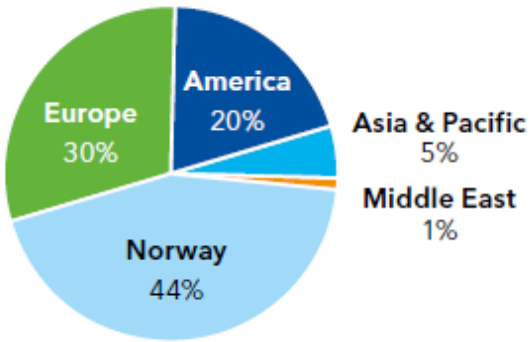

Figure 1.1. All confirmed projects. LNG-fuelled ships in operation & on order

Technical layout of a typical LNG-fuelled ship solution consists of:

- Proper LNG tanks for storing gas fuel
- Tank connection system (integrated with the tank), which is a gas-tight space with all gas hazardous equipment (evaporator system, piping, valves, instrumentation)
- The water-glycol circuit to evaporate LNG, consisting of a heat exchanger that uses the engine cooling water (or exhaust gases) as the source of heat.
- Bunker stations, connecting the tanks with vacuum insulated (or foam insulated) lines for LNG loading operations A vapour return line is usually provided.
- Gas supply lines, to transfer the gas from the evaporator to the gas valve unit of each engines
- The control system and the safety system
- Gas-fuelled engines

The Figure 1.2 shows the general arrangement of the gas system for LNG-fuelled ship.

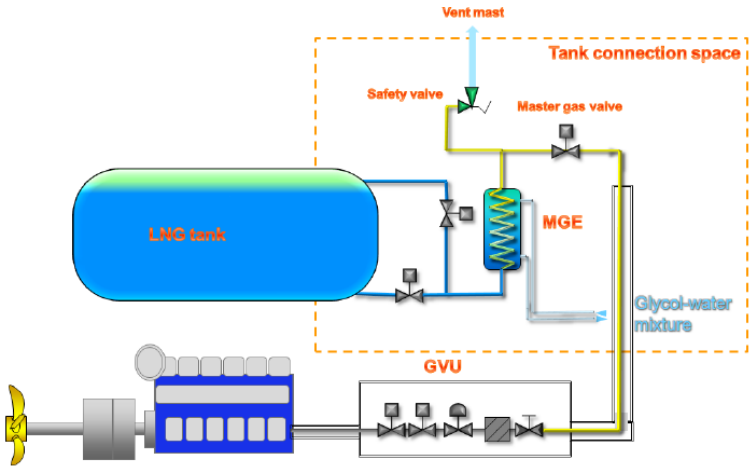

Figure 1.2. Gas system for LNG-fuelled ship (WARTSILA GAS SYSTEM, 2014)

Figure 1.3 shows the basic principles of bunkering and storage of LNG and for gas supply to the engines.

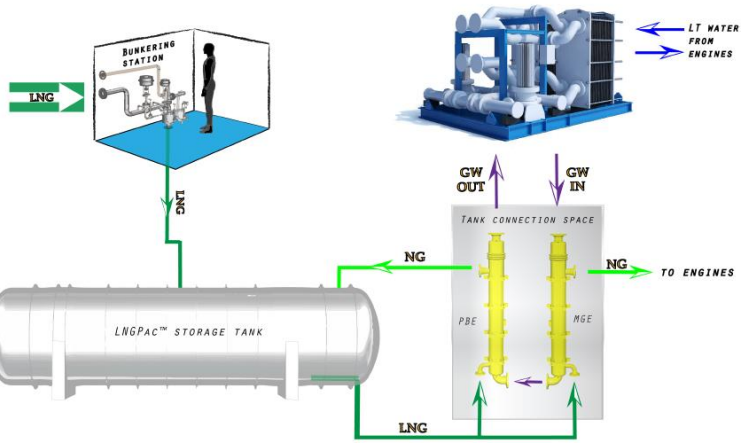

Figure 1.3. Simplified flow diagram of bunkering and storage of LNG and gas supply

1.1.1 LNG tanks

Different types of ship tanks for storing LNG are available on the market. The main characteristics of the several tank types are reported in Table 1.1.

Table 1.1. Main characteristics of the different tank types (WPCI-LNG FUELLED VESSELS)

Tank type	Description	Pressure	Pros	Cons
A	Prismatic tank, adjustable to hull shape; full secondary barrier	<0.7 barg	Space-efficient	Boil-off gas handling. More complex fuel system required High costs
B	Prismatic tank, adjustable to hull shape; partial secondary barrier	<0.7 barg	Space-efficient	Boil-off gas handling. More complex fuel system required High costs
	Spherical tank; partial secondary barrier		Reliably proven in LNG carriers	Boil-off gas handling. More complex fuel system required
C	Pressure vessel, cylindrical with dished ends	>2 barg	Allows pressure increase Simple fuel system Little maintenance Easy installation Lower costs	On board space requirements

Regarding the tank design principle to prevent the LNG spill in case of failure, the behaviour of the different kinds of LNG tanks could be summarized as follows (Wursig, 2013):

- *Type A and Membrane Tank → Gas release has to be handled in case of large leaks.* Complete first barrier failure has to be taken into account as hazard scenario
- *Type B Tank → Limited gas release from leaks has to be handled.* Only minor leaks of the tank structure is considered as possible leakage scenario. This kind of tank is designed under the "leak before break" criteria (Kokarakis, 2015)
- *Type C → leaks are possible only from valves*

Figure 1.4 shows an image of the different LNG tanks.

Figure 1.4. LNG Tanks (Kokarakis, 2015). Type C tank (left side above), Type B tank (left side below), Type A tank (right side above), Membrane tank (right side below).

One of the main characteristics describing a LNG tank is represented by the type of insulation, able to stem for the holding time (the time before the pressure relieve valve opens in case of an overpressure occurred inside the tank). There are different ways to get insulation, the commonly used are (Van Kreij J., 2015):

- Mechanical insulation, typically polyurethane insulation (the cheaper initial investment solution), usually used for large tanks.
- Vacuum insulation, the most used, typically obtained through perlite or multilayer insulation. In the annular space, a molecular sieve is present in order to absorb the remaining gas and the released gas fuel eventually coming from the inside wall.

The cons of mechanical insulation solutions are:

- a higher leak compared to vacuum
- the supports of the mechanically insulated tanks are more difficult to be insulated
- more space is required
- no secondary containment, which means that it needs some sort of containment around the tank (making the system more complicated).

The location of the tank is the main issue of the LNG-fuelled ship design and it is highly regulated through the pertinent international rules (IGF Code). The consequences related to a possible hazardous scenario are represented by the occurrence of fire, explosion or cryogenic leakage. The risk of fire in the space closed to the LNG tank room could cause over pressure inside the LNG tank due to the temperature increases (Bond S., 2011). In this regard, the fuel spaces must be segregated from sources of ignition by a cofferdam (IGF Code). Concerning the risk of leaked flammable product (natural gas) causing fire/explosion, a segregation should exist from sources of ignition; in this regards, the rules suggest an area classification to prevent a hazardous scenario. Where the term area is defined as (ABS, 2015):

Area means an area in which an explosive gas atmosphere is, or may be expected to be, present in quantities such as to require special precautions for the construction, installation and use of equipment. Hazardous areas are divided into:

- *Zone 0 is an area in which an explosive gas atmosphere is present continuously or for long periods or frequently.*
- *Zone 1 is an area in which an explosive gas atmosphere is likely to occur in normal operation occasionally.*
- *Zone 2 is an area in which an explosive gas atmosphere is not likely to occur in normal operation but, if it does occur, will persist for a short period only.*

Non-Hazardous area means an area in which an explosive gas atmosphere is not expected to be present in quantities such as to require special precautions for the construction, installation and use of equipment.

The potential risk associated to a leaked cryogenic fluid leads to a loss of structural integrity, so some containments and protections need to be provided (e.g. full secondary barrier and devices to promptly warn about a potential hazardous situation, by means of gas and temperature detection). The con of LNG as ship fuel is the large space demanding, so a possible solution is to reduce the operational range or best by improving the efficiency of the design (Nichita C. et al., 2014). The LNG tanks adopted by gas-fuelled ships are designed with doubled barrier containment, vacuum insulated type and around 4 bars of operating pressure. The outer shell is made of stainless steel as well as the Tank Connection Space, which is considered the secondary barrier of LNG piping/nozzles place inside of it (for this reason it is considered as a gas safe area). The best effective solution of the determination of the LNG tank location takes into account different aspects as the minimization of bending moments, cargo loss and stability considerations and the risk associated to collisions, fire, explosion, mechanical damage.

Finally, the position of the LNG tanks is constrained by:

- The distance from shell specified by IMO IGF code
- Minimum inspection space between tanks
- Required foundation space
- Space requirements

The location of the gas storage tanks can be either on open deck or in enclosed spaces. It is acceptable to install the storage tanks in enclosed spaces if a maximum gas pressure of 10 bar occurs. The IGF code gives some references regarding the position of the gas storage tanks to be installed on board. The minimum distance of the tanks should be the lesser of B/5 or 11.5 m from the shipside, the lesser of B/15 and 2 m from the bottom plating and not less than 800 mm from the shell plating. A cofferdam of at least 900 mm should be interposed between the machinery space A and the tank space hold (if the gas storage is of type C, the cofferdam can be removed as this type of tank has got a secondary barrier increasing the level of safety in case of leakage from the inner containment space). Drip trays should be provided underneath the tank (especially where leakage is likely occurred such as welded connection or joints) and should be of sufficient capacity to contain the volume that could escape in the event of a pipe connection failure.

1.1.2 Tank Connection Space

Tank Connection Space is a fuel gas conditioning and preparation space; it is located outside of the engine room. For smaller vessels using Type C fuel storage tanks, the Connection Space is typically combined with the tank and represents the "coldbox", i.e. a gas-tight enclosure equipped with all piping, valves, evaporation equipment and instrumentation. Regarding the safety of the gas handling process, the gas-hazardous space is confined to the "coldbox". A simplified representation of the tank connection space layout is reported in Figure 1.5.

The cold box consists of:

- Tank penetrations
- Valves
- LNG evaporator
- Instrumentation
- Control system

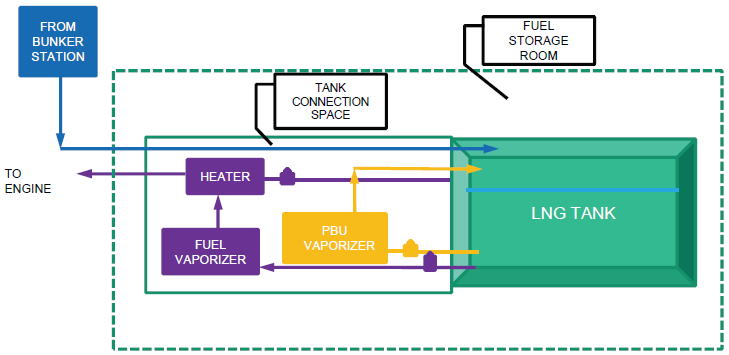

Figure 1.5. Tank Connection Space (Bond S., 2011)

The gasification of the LNG stored in the liquefied natural gas tank, to be employed subsequently by the Gas utilization unit, occurs in the LNG evaporator installed inside the "coldbox". Usually, the temperature of the supplied gas into the engines must be in a span of 5°C and 40°C, typically the value is around 20°C (Theotokatos G. et al., 2015). The Glycol-Water unit is the equipment used to heat the LNG by means of an appropriate heating medium that usually is a mixture of 50% ethylene-glycol and water, entering into the evaporator at 50°C (Theotokatos G. et al., 2015). The characteristics of this fluid are excellent at both high and low temperatures, so it can be also used as anti-freezer. It is the most used heat transfer fluid in marine applications because of its high safety level and the relatively low associated operational risks and costs (Theotokatos G. et al., 2015). The pressure built-up unit (PBU in Figure 1.5) ensures that the pressure inside the tank is kept constant to a proper value to feed the engines. The gasification system needs to be located near the Tank Hold Space in order to minimize the length of the LNG piping and consequently mitigating the risks of possible cryogenic liquid leakages.

1.1.3 Gas handling Equipment

IGF code provides two options to choose the system configurations of the gas machinery spaces. The first one refers to the concept of gas-safe machinery space in which the spaces are considered gas safe under normal and abnormal conditions. A simplified representation of the engine room layout in case of gas-safe machinery option is reported in Figure 1.6. The second one is the Emergency Shutdown (ESD) protected machinery space that requires that in case of gas detection, all non-safe equipment (ignition sources) and machinery have to be automatically shut-down.

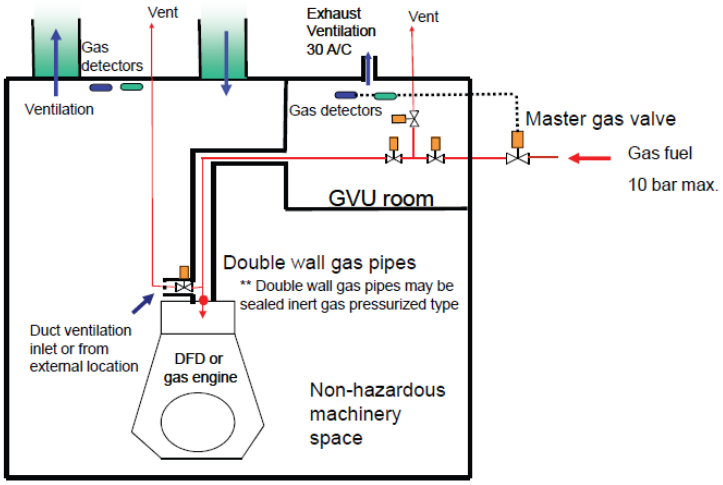

Figure 1.6. Gas safe machinery layout (Bond S., 2011)

For the ESD (Emergency Shut-down system) layout the structure, surrounding the hazardous components (engine room), are designed to minimize the damages to the vessel/structures in the event of an explosion; so the engine room is a closed chamber, continuously ventilated with gas detection alarm systems (Esoy V. et al., 1998). A simplified representation of ESD option layout is reported in Figure 1.7.

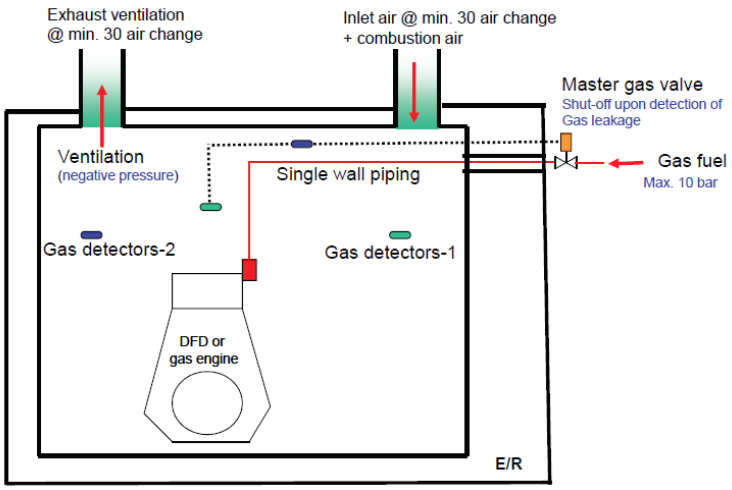

Figure 1.7. ESD machinery layout (Sea Bond, ABS, 2011)

The gas safe machinery option is suitable for retrofit cases (Theotokatos G. et al., 2015). For this purpose, the engine room is not required to be explosion-proof and the engines do not need to be placed in individual closed chambers for containing possible gas leaks. To strengthen the level of safety, the gas line inside the engine room should be a double-walled pipe, and mechanical ventilation (IGF Code) in the annular space needs to be provided (or alternatively a nitrogen pad needs to be provided). Gas detectors are placed inside the annular space and a removal system, to vent gas leaked from the inner gas pipe to the atmosphere, is provided. The gas safe machinery space concept allows to reduce the construction cost, system complexity and weight (Theotokatos G. et al., 2015). All gas pipes must be of stainless steel. Gas detectors have to be provided in the Tank Connection Space, Tank Hold Spaces, all ducts around gas pipes, engine rooms, ventilation trunks, compressor rooms, and other enclosed spaces containing gas piping or other gas equipment. The exhaust system should have a constant upward slope to prevent gas from accumulating in the system. The layout of arrangement of a Tank Hold Space is reported in Figure 1.8.

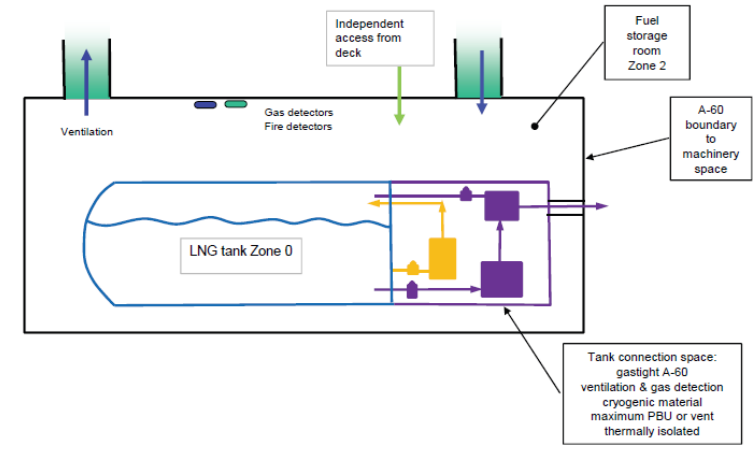

Figure 1.8. Tank Hold Space (Bond S., 2011)

In the ESD option, the gas line inside the engine room is based on the single wall-piping concept (only low pressure with a maximum value of 10 bar is allowed). The engine room must contain only engines and the minimum necessary equipment. The gas detection alarm rings at 20% lower explosive limit (LEL) and, if 40% LEL is verified, the gas supply is shut off and the machinery is shutdown. The electrical equipment placed inside the engine room needs to be a zone 0, certified safe type IEC 92-502. Ventilation fans should ensure a ventilation capacity of at least 30 air changes per hour and a full redundancy is required (IGF Code). The possible gas release rooms need to be provided with double self-closing doors for entrance and exit of crew. The engine room is equipped with two independent gas-monitoring systems and the locations of gas detectors need to be tested by smoke tests or a gas dispersion analysis. Single wall pipe is allowable on open deck, on the contrary a double wall is needed in enclosed spaces in order to create a safe gas tight zone. All LNG pipes have to be structurally verified through a stress analysis that is applied for all pipe containing liquid at -110 °C.

1.1.4 Fuel Gas Supply System Operational Principles

Regarding the natural gas feeding system, the following safety requirements must be fulfilled (IGF Code):

- The gas fuel pipes shall not be located less than 800 mm from the shipside.
- Gas fuel piping should not run through accommodation or services spaces and control stations. If gas pipes pass through enclosed spaces, enclosed air-ventilated ducts need to be provided or double wall piping should be employed.
- In order to mitigate the consequence of gas leakage and so to isolate the possible damage where it occurs, stop valves should be fitted at least every 40 m. As alternative, the gas line system may be divided into more sections, each one equipped with control

valves that are located in a safe and readily accessible zone (not involved in case of fire).

In order to isolate the engine room from a gas leakage occurring in the fuel system inside, a master gas valve may be located outside machinery space. According to the kind of engine, there are two main categories of gas supply systems:

- Low pressure fuel gas supply system
- High pressure fuel gas supply system

Low pressure fuel gas supply system provides fuel gas at 4-5 bar, typical value of gas fuel feeding four strokes engine, both single gas or dual fuel. The pressure is kept constant at the required value inside the tank through the PBU system, or through a cryogenic pump submerged at the bottom of tank. The Figure 1.9 reports the simplified layout of a gas fuel supply system for low-pressure engines.

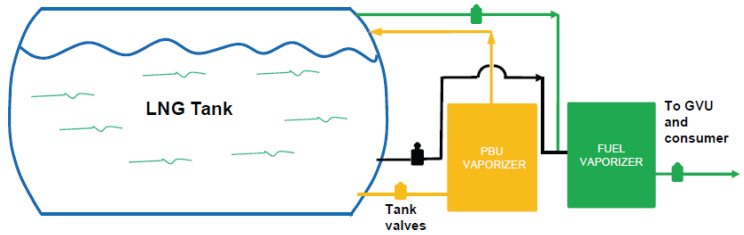

Figure 1.9. PBU system for low-pressure gas fuel (Bond S., 2011)

For high-pressure gas fuel applications (typical for two strokes engines), the gas fuel pressure is required to be around 250 bar, so the cryogenic pump (HP Pump in Figure 1.10) is used to increase the pressure. The Figure 1.10 reports the simplified layout of a gas fuel supply system for a two strokes engine.

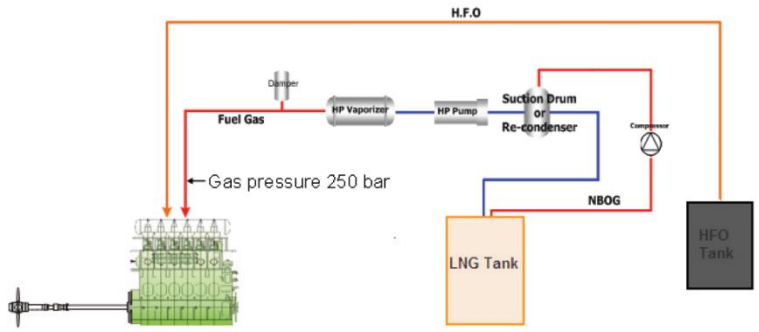

Figure 1.10. PBU system for high-pressure gas fuel (Bond S., 2011)

1.1.5 Gas Valve Unit

Each gas user installed on board needs to be provided with an individual Gas Valve Unit (GVU), in order to ensure a fast and reliable shutdown in normal conditions or in case of an emergency and for adjusting the gas feeding pressure as required by the user. The GVU consists of two quick closing valves and an interposed ventilation valve (Karlsson S. et al., 2013). The two quick closing valves provide 100% of redundancy since they are connected in series. In case of gas leakage from the inner pipe, the system control provides an immediate closing of the valves and the gas is vent through the ventilation valve to the atmosphere. The scheme representing the GVU arrangement is reported in Figure 1.11.

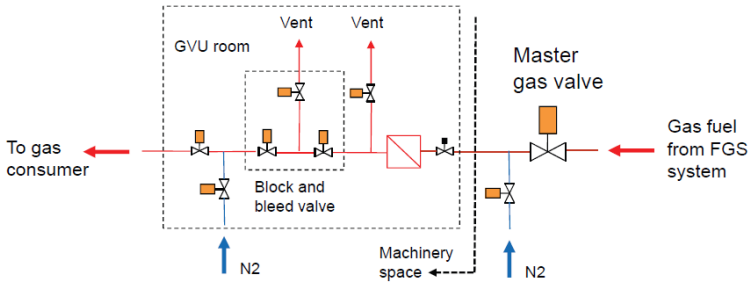

Figure 1.11. Gas Valve Unit system (Bond S., 2011)

The GVU may be placed into a separate room that has to be gas tight and considered as a zone 1 hazardous area. All electrical equipment has to be hazardous zone 1 compatible. The access through the gas valve room is made possible only through an airlock system that provides gas tight condition when it is in use. A maximum distance of 10 m from the GVU and the engine is recommended. As alternative to the air lock system, the GVU can be boxed in a gas tight enclosure containing all the process components, such as the valves, actuators and sensors.

1.1.6 Ventilation system

The IGF code recommends to split ventilation system in two separate sections, one related to hazardous spaces and the other related to non-hazardous spaces. The electric fan motors should not be located in ventilation ducts. Another important aspect to take into account in a LNG-fuelled vessel design is the location of the vent mast. IGF code recommends a minimum height of 6 m from any working deck and it needs to comply with a minimum distance of 10 m from any opening to machinery or accommodation. When the double-wall piping is chosen to move gas to the users, the air ventilated in the annular space will be discharged to the open air by a ventilation fan located at the beginning of each pipeline after the evaporator unit. The ventilation fan is equipped with a filter, a demister unit and a waterproof protection cover.

1.1.7 Gas-fuelled engine

Many engines in all power ranges are available on the marine market; the best-known engine manufacturers for marine propulsion offer a wide selection of dual fuel or single gas engines. Single gas engines are of four stokes type and are available only for small-medium size of power; on the contrary, dual fuel engines can be more powerful. Dual fuel engines are available both as four strokes type and two strokes type. Two types of dual fuel engines are currently available on the market and they differ for the combustion mode (Theotokatos G. et al., 2016):

a) gas injected at high pressure into the combustion chamber (Diesel cycle mode);
b) a low-pressure air-gas mixture introduced in the inlet manifold (Otto cycle mode).

The low-pressure mode means that fuel gas pressure is approximately 5 up to 6 bar. The feeding fuel could be provided directly from a pressurized storage tank. High-pressure mode means that the gas requires to be pumped up to 300 bar before to be injected. Engines running only on gas mode use a spark plug to ignite the combustion. In dual fuel engine, the combustion occurs through the ignition provided by a small amount of pilot fuel that is injected into the cylinder and burns causing the high temperature of the gas air mixture at the end of the compression phase.

A deep simulation analysis is presented in the next chapter to investigate the thermodynamic behaviour of a four-stroke marine gas engine, in comparison with a diesel engine of similar power.

1.1.8 Bunkering station

LNG is bunkered at cryogenic temperature so special equipment has to be adopted. During bunkering operations a water curtain system is activated which shields the ship structure against possible spillages of LNG during this phase. In Figure 1.12 a frame of a bunkering operation for a small quantity of LNG is reported. Besides, stainless steel drip trays are fitted below the pipe connection where possible leakages can occur.

Figure 1.12. Bunkering operation

Normal bunkering procedures require that no gas have to be discharged into atmosphere. Key Bunkering stations need to be installed in sufficient natural ventilation. Remote control and monitoring have to be provided. The system may be equipped with manual and remote ESD valves. A correct bunkering operation is preceded by draining, purging and inerting the bunkering line before the transfer of fuel start. Gas detectors should be installed for possible gas spillages in the bunkering lines.

2 PERFORMANCE SIMULATION OF A MARINE GAS ENGINE

In this chapter, the behaviour of a marine four-stroke gas engine is simulated to assess its pollutant emissions in comparison with a traditional diesel engine. As know, The CO_2 engines emissions can be reduced/avoided employing fuels characterized by low carbon content like methane or zero content as hydrogen (Benvenuto et al., 2015a). The present study is addressed to four-stroke engines of the second typology, for which Rolls Royce (RR) has started to commercialize a new generation of medium speed four-stroke marine engines, named "Bergen Marine Engines" (Rolls-Royce, 2012). This family of engines is divided into B and C series, both incorporating diesel engines (fuelled only by diesel oil) and gas engines (only NG fuel). In RR production, the overall power range is 1800÷8000 kW for diesel engines, and 1400÷7000 kW for NG engines. This paper presents a comparison, obtained by numerical simulation, between the following Bergen engines of the C series:

- C25:33-series diesel engine (DE), with power range: 1460÷3000 kW, operating speed range: 720÷1000 rpm

- C26:33-series NG engines with power range: 1400÷2430 kW, operating speed range: 900-1000 rpm.

Two simulation codes, based on thermodynamic laws of the real cycles, have been developed in Simulink® (MATLAB toolbox) language, for DE and the NG engine respectively, in order to compare the two engines in their whole working area. Both simulators have been fine-tuned and validated through the performance data provided by the manufacturer. The comparison concerns mainly the following engine characteristics: dimensions and weights, overall efficiency, carbon dioxide emissions. Other issues as installation on board, fuel storage and safety, load capacity of the ship, fuel and maintenance costs are not taken into account. The results show a significant differentiation between the two examined engines, as regards efficiency and emissions of carbon dioxide. In order to explain the different behaviour, a comparison of the respective real cycles and a thermodynamic analysis of the two combustion modes are carried out. This last analysis is also used to justify (theoretically) the relevant differences in nitrogen oxides emissions.

2.1 LOW EMISSIONS PROPULSION AND POWER GENERATION SYSTEM

The compliance with the emission limits requires the adoption of propulsion and power generation systems, alternative to the current solutions. The almost zero emissions of sulphur dioxide and particulate matter in the exhaust gas of NG engines are due to the sulphur absence in the NG fuel and to the typical combustion process of the spark ignition engines. Similar motivations can be repeated for the hydrocarbons emissions. As regards NO_x emissions, the RR Bergen engines considered in this study present a good performance, as certified by EPA (Environment Protection Agency). In fact the NG engine C26:33, characterized by a lean-burn combustion (i.e. fuel-air equivalence ratio Φ, defined as the ratio of the fuel-to-oxidizer ratio to the stoichiometric fuel-to-oxidizer ratio, equal to 0.5 at high and medium loads, and slightly greater, around 0.55, at low loads) has obtained the IMO Tier III certification, as shown in Figure 2.1. The same figure shows also that the DE engine C25:33 satisfies the IMO Tier II specifications.

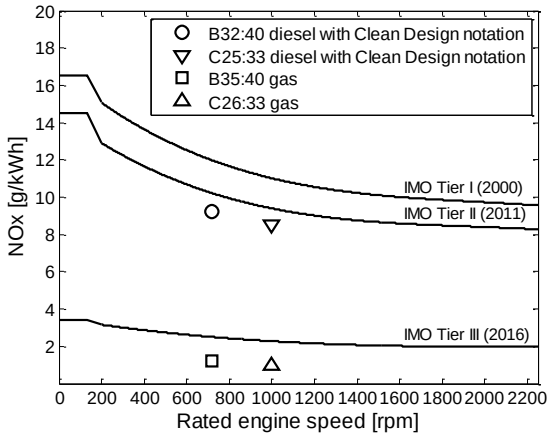

Figure 2.1. NOx emission for Bergen engines (Rolls-Royce, 2012)

A brief explanation about the lower NO_x emissions of the NG engines, compared to diesel engines, is given in the following.

2.1.1 Nitrogen oxides emission

The combustion process of NG engines and diesel engines is quite different. In the first engines type, the reference cycle is the Otto cycle, where the combustion (originated by a sparking plug) is developed like a flame front in a homogeneous air-fuel mixture, as schematized in Figure 2.2. On the contrary, in the Diesel cycle the combustion process occurs in the burning zone illustrated in Figure 2.3. In a range of load conditions near to the NCR, the equivalence ratio ϕ of both considered engines is quite similar and equal to about 0.5, but this value is the same throughout the volume of the cylinder for NG engines (Figure 2.2), while represents an average value in the cylinder volume for diesel engines. In the latter case, the value of ϕ is about 1 (stoichiometric value) or slightly less in the cylinder burning zone of Figure 2.3, and approximately equal to zero in the non-burning one. Consequently the combustion temperature of the Diesel cycle (in the burning zone) is much greater than that of the Otto cycle (reference cycle of a spark ignition NG engine), at equal overall equivalence ratio ϕ. This is shown in Figure 2.8, where the temperature values are normalized with respect to the maximum temperature in the burning zone of the diesel engine. The temperature values, depending on crank angle θ, are determined by means of two simulation codes, a two-zone diesel engine model (Benvenuto et al., 1998) and a spark ignition NG engine model (Benvenuto et al., 2013) respectively, both applied to engines characterized by the same rotational speed, volumetric compression ratio, pressure and temperature in the cylinder. As known, according to the thermal Zel'dovich mechanism (Zel'dovich YB., 1946), a higher combustion temperature is responsible for an increase in the production of nitrogen oxides.

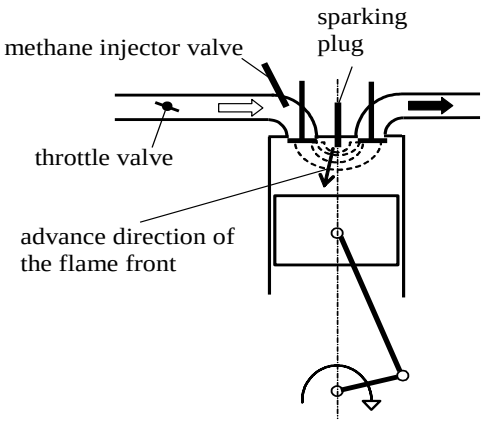

Figure 2.2. Spark ignition engine combustion scheme

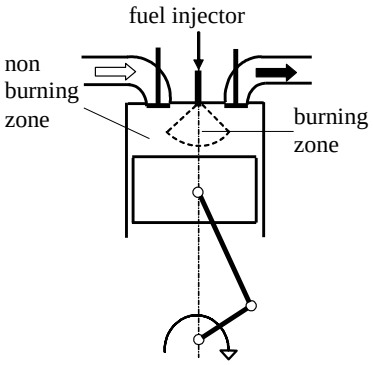

Figure 2.3. Diesel engine combustion scheme

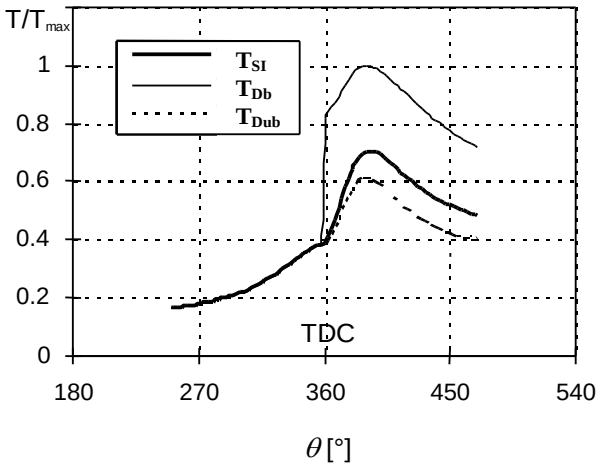

Figure 2.4. Typical trend of combustion temperatures versus crank angle in the diesel engine burning (TDb) and non- burning (TDub) zone, and inside the flame front for the NG spark ignition engine (TSI)

2.2 MAIN DESIGN FEATURES OF THE EXAMINED ENGINES

The diesel engine RR C25:33L6P and the gas engine RR C26:33L8PG are considered for the comparison, due to their similar maximum continuous rating (MCR) power (2 MW and 2.16 MW respectively) at the same rotational speed (1000 rpm). Table 2.1 reports the main design characteristics of the two engines, drawn from the pertinent project guides.

Table 2.1. Main design and performance parameters (at MCR conditions) of the considered engines

Engine parameters	C25:33L6P	C26:33L8PG
fuel type	HFO or MDO	NG
cylinders number	6L	8L
bore [mm]	250	260
stroke [mm]	330	330
brake power [kW]	2000	2160
(b.m.e.p.) [bar]	24.7	18.5
speed [rpm]	1000	1000
b.s.f.c. [g/kWh]	185	154
charge air pressure [bar]	4.2	2.8
charge air temperature [°C]	55÷60	55

The C25:33L6P diesel engine can burn both HFO (with viscosity up to 700 cSt at 50° C) and MDO. The fuel system uses mechanical fuel injectors with electronic control of fuel pressure and injection timing. As regards the C26:33L8PG gas engine, the adopted NG fuel is composed by clean and dry methane gas, with minimum quantity of other substances. The gas pressure is controlled by an electronic governor, as well as the fuel injectors and ignition timing. Both the DE and the NG engine are equipped with a Variable Valve Timing (VVT) system, acting on the intake and exhaust valves of the cylinders. When the engines are running at low loads, the valve opening/closing timing is set to perform conventional diesel or spark ignition gas cycles. Otherwise, in case of medium or high loads, the VVT system is arranged to perform a Miller thermodynamic cycle. As known, the Miller cycle, through a specific setting of the valve opening/closing timing, produces a compression phase less extended than the expansion phase (Andreola M., 2011.), allowing a greater thermodynamic efficiency in comparison with conventional diesel or spark ignition cycles. At low loads, the Miller cycle is not convenient because it reduces the delivered engine torque. As for dimensions and weights of the selected engines (their side and front views are given in Figure 2.5), the data reported in Table 2.2 do not show significant differences, except for the NG engine length that is greater (around 18%) because of a larger number of cylinders than DE (eight instead of six).

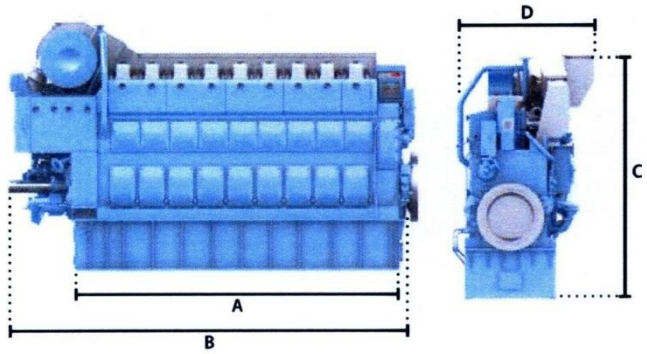

Figure 2.5. Side and front view of the Rolls-Royce Bergen marine propulsion engine (Rolls Royce, 2012)

Table 2.2. Weights and dimensions of the considered Bergen engines

Engine characteristics	C25:33L6P	C26:33L8PG
Engine length (A) [mm]	3170	3930
Overall engine length (B) [mm]	4036	4796
Height (C) [mm]	3195	3195
Width (D) [mm]	1775	1748
Dry weight [kg]	19650	20700

2.3 SIMULATION MODELS

In order to increase the amount of information necessary for the comparison of the Bergen diesel and NG engines, two “real cycle” simulation codes, based on thermodynamic laws, have been developed in Simulink® language. A literature review of the simulation models concerning reciprocating internal combustion engines can be found in (Benvenuto et al., 1998). In general, three levels of complexity can be defined. A first level of models can be identified, where engine performance calculations are based on maps or empirical correlations, linking together the main engine variables. In these models, the dynamics of the engine and relative subsystems (turbocharger) is often taken into account by means of time constants. The approach used is quite simple and suitable only for a rough simulation of engine dynamic behaviour. The second level refers to those models in which the thermodynamic processes in the cylinders, including combustion, are calculated stepwise as functions of the crank angle (Altosole et al., 2017c; Benvenuto et al., 2016). These thermodynamic calculations are combined with an analysis of the dynamic behaviour of the turbocharger and of the circuit linking it with the cylinders (intercooler, air and exhaust gas receivers, etc.). In many studies, the combustion scheme adopted corresponds to a "single zone" approach, which allows a fairly realistic prediction of cylinder pressure versus time. This combustion scheme, however, is not suitable for the evaluation of the exhaust emissions in diesel engines. From this point of view, a significant improvement is represented by the «two-zone» approach, which provides distinct calculations for the burning and non-burning zone, thus allowing to obtain the flame temperature, whose value is required by the correlations for the exhaust emissions (Benvenuto et al., 1998). Finally, very complex diesel engine models (third level), though described in the literature, are not taken into consideration in this overview: they are not deemed suitable for the concerned dynamic simulation, because of too long calculation times. The simulation codes developed for the present study, belonging to the second

level described above, with a “single-zone” combustion model, are able to assess the performance of all main components of the engine (i.e. cylinder, turbocharger, inlet and exhaust manifolds, intercooler), in steady state and dynamic working conditions, in the whole operating area. The engines simulation approach is based on the “filling and emptying” method. Figure 2.6 shows the overall Simulink® scheme adopted for the supercharged Bergen engines. Similar simulation approaches have been recently used also by (Tadros et al., 2015) and (Altosole et al., 2014) for the performance representation of a two-stroke diesel engine and a marine gas turbine, respectively.

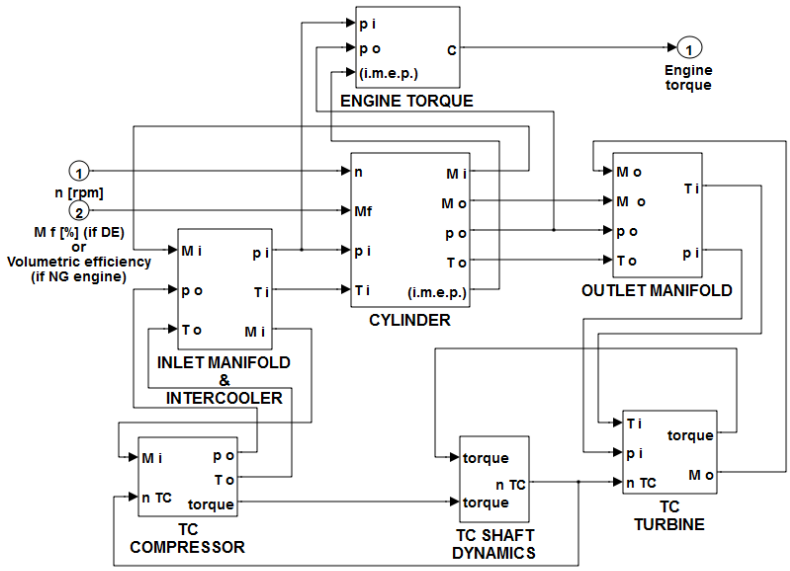

Figure 2.6. Simulink® scheme adopted to represent the examined Bergen engines

The scheme configuration is the same for the two different types of engines (DE and NG), but the input variables relating to the fuel supply (the second input data in Figure 2.6) are different: the fuel mass percent in the case of the diesel engine and the cylinder volumetric efficiency for the gas engine. The model consists of the following main subsystems:

1) cylinder

2) inlet manifold and intercooler

3) outlet manifold

4) turbocharger compressor

5) turbocharger turbine

6) turbocharger shaft dynamics

7) engine torque

Each block includes a set of performance maps, algebraic and differential equations, mathematical operators, describing the subsystem behaviour. Obviously, the characteristics of the components are depending on the considered engine typology, mainly as regards the combustion process simulation in the cylinder module and the torque governor. Simulations are performed at environmental conditions corresponding to atmospheric pressure and air temperature equal to 25°C.

2.2.2. *Cylinder simulation*

The physical phenomena occurring inside the cylinders of the engine are modeled taking into account the whole process, consisting of different phases: intake, compression, combustion, expansion, and exhaust. It is supposed that the thermodynamic properties of the fluid, according to a zero-dimensional approach, are depending on the temperature and chemical composition of the mixture inside the cylinder, with a difference between the two engines combustion processes: two-zones model for DE (Benvenuto et al., 1998) and single zone for the gas engine (Benvenuto et al., 2013). In the NG engine, the fuel is considered completely vaporized and mixed with air. The cylinder calculations are performed by increasing step by step the crank angle θ (the independent variable). From the crankshaft angular velocity (ω) and crank angle increment (dθ), the pertinent time interval (dt) is determined. In the intake phase the piston moves from the top dead centre (TDC) to the bottom one (BDC). The piston displacement (X) from the TDC is:

$$x = \frac{S}{2}\left[1 + \frac{1}{\zeta} - \cos\theta - \frac{1}{\zeta}\sqrt{\left(1 - \zeta^2 \sin^2\theta\right)}\right] \tag{2.1}$$

Where S is the piston stroke and the ratio between crank radius and rod length. The consequent cylinder volume variation is easily calculated from cylinder bore and volumetric compression ratio. The amount of air M (in DE), or air and NG mixture introduced into the cylinder is expressed by:

$$M = \rho_o V \eta_V \tag{2.2}$$

In equation (2.2) ρ_o is the fluid density at the intake valve while V is the displaced volume. The volumetric efficiency (η_v) value, as explained in (Ferrari G., 2008), depends on the reference cycle (for instance it is lower for the Miller cycle). The compression phase calculation starts from the BDC piston position, or in a higher position in the case of Miller cycle. In the latter, the pressure is maintained constant until the closing of the intake valve. The heat exchanged between the working fluid and the cylinder walls (dQw) is calculated as follows:

$$dQ_w = \frac{h\, A_w}{\omega}\left(T_g - T_w\right)d\theta \tag{2.3}$$

Where T_g is the gas temperature and T_w is the cylinder wall temperature, evaluated as reported in (Benvenuto et al., 1998). The fluid-cylinder wall thermal conductivity h, as proposed by (Woschni G., 1967) is determined by using the expression:

$$h = 3.26\, B^{-0.2}\, p^{-0.8}\, T^{-0.53}\, v^{0.8} \tag{2.4}$$

Where B is the cylinder bore and p, T and v are the fluid pressure, temperature and speed. The fluid speed inside the cylinder may be calculated with the expression given by (Ferrari G., 2008):

$$v = c_1\, v_m + c_2 \frac{V\, T_{ref}}{p_{ref}\, V_{ref}} \left(p - p_{dr}\right) d\theta \tag{2.5}$$

Being c_1 and c_2 are numerical constants, v_m is the piston mean velocity and $p_{ref}, V_{ref}, T_{ref} p_{ref}$, T_{ref} and V_{ref} are reference values of pressure, temperature and cylinder volume; p_{dr} is the cylinder pressure during the dragged engine condition (i.e. absence of combustion). The area of the cylinder walls (A_w), involved in the heat exchange, is determined as:

$$A_w = \pi\, B\, x + A_{ch} \tag{2.6}$$

A_{ch} being the cylinder head area and x the piston displacement from TDC determined by equation (2.1). In the phases in which the engine operates at closed valves (i.e: compression, combustion, expansion), the pressure variation inside the cylinder is calculated by integrating in the time domain the following differential equation:

$$\frac{dp}{dt} = \frac{k_g - 1}{V}\frac{dQ}{dt} - \frac{k_g}{V}\, p\, \frac{dV}{dt} + \frac{k_g - 1}{V}\, m_i H_i - \frac{k_g - 1}{V}\, m_o H_o \tag{2.7}$$

derived from the equation of energy for a closed system, combined with the ideal gas law (Laviola M. & Martelli M., 2014). In the equation, V is the cylinder mean volume pertinent to the considered $d\theta$ step while m_i, H_i and m_o, H_o are the mass flow rates and specific enthalpies in inlet and outlet sections; k_g is the ratio of specific heats at constant pressure and volume. In the calculation of all phases of the cycle, the working fluid temperature is obtained by applying the ideal gas equation. The term dQ, in equation (2.7) takes into account the heat generated by the fuel combustion and the heat exchanged with the cylinder walls:

$$dQ = Q_b\, dx_b - dQ_w \tag{2.8}$$

where Q_b is the heat released during the combustion phase, depending on burned fuel mass M_f and lower heat value H_f:

$$Q_b = M_f\, H_f \tag{2.9}$$

and x_b is the mass fraction of burned fuel, calculated according to equation of (Wiebe I., 1956), as follows:

$$dx_b = 1 - \exp\left[- K_a \left(\frac{\theta - \theta_{ign}}{\Delta\theta} \right)^{K_m+1} \right] \tag{2.10}$$

In equation (2.10) $\theta\theta_{ign}$ is the angle at the beginning of the combustion, jK_a and K_m are numerical constants depending on the engine type (Ferrari G., 2008). Always in equation (2.10), $\Delta\theta$ represents the combustion phase duration in terms of crank angles. As regards the NG engine model, $\Delta\theta$ is determined considering an appropriate flame propagation speed, the space covered by the flame and the engine speed (Benvenuto et al., 2013). The $\Delta\theta$ values obtained in this way are confirmed by reference data (Farzaneh-Gord M., 2009). In the case of DE model, i.e. without spark ignition, $\Delta\theta$ is determined by considering the time required for the fuel to enter into the cylinder through the holes of the injector, as detailed in (Benvenuto et al., 1998). The initial combustion angle (θ_{ign}) is evaluated taking in account the ignition delay crank angle (θ_{id}), given by (Benvenuto et al., 1998):

$$\theta_{id} = K_{id} n\, p^{-0.388} \left(\frac{40}{CN} \right)^{0.69} \exp\left(\frac{4.644}{T} \right) \tag{2.11}$$

Depending on ignition delay constant K_{id}, engine speed n, cylinder pressure and temperature p and T, and fuel cetane number CN. As regards the NG engine model, the initial combustion angle (θ_{ign}) is not affected by ignition delay, so θ_{ign} simply corresponds to the moment when the initial spark is generated from the spark plug. After the phases of combustion and expansion, during the exhaust phase, the gas flow through the exhaust valve is governed by the following equation (compressible gas through a flow restriction):

$$\frac{dM}{dt} = \frac{C_D A_R p_i}{(RT_i)^{0.5}} \left(\frac{p_o}{p_i} \right)^{\frac{1}{k_g}} \left\{ \frac{2k_g}{k_g - 1} \left[1 - \left(\frac{p_o}{p_i} \right)^{\frac{k_g - 1}{k_g}} \right] \right\}^{0.5} \tag{2.12}$$

or, in the case of choked flow, by:

$$\frac{dM}{dt} = \frac{C_D A_R p_i}{(RT_i)^{0.5}} \sqrt{k_g} \left(\frac{2}{k_g + 1} \right)^{\frac{k_g + 1}{2(k_g - 1)}} \tag{2.13}$$

where the choked flow condition is expressed by the following relationship:

$$\left(\frac{p_o}{p_i} \right) \leq \left(\frac{2}{k_g + 1} \right)^{\frac{k_g}{k_g - 1}} \tag{2.14}$$

In the previous expressions, the values of p_i and T_i are the pressure and temperature in the cylinder respectively, while p_o is the pressure in the exhaust duct. The value of the discharging coefficient C_D

is assumed equal to 0.7, as proposed by (Farzaneh-Gord M., 2009). In the same equations, the reference area A_R is the valve head area and R is the gas constant. The exhaust gas temperature T_{ex} is calculated through the blow-down equation (Ferrari G., 2008):

$$T_{ex} = T_i \left[1 - \left(\frac{k_g - 1}{k_g} \right) \left(1 - \frac{p_i}{p_o} \right) \right] \tag{2.15}$$

Where the pressure inside the exhaust manifold, is calculated by integrating the following differential equation:

$$\frac{dp_o}{dt} = \frac{M_i - M_o}{V_{ex}} R\, T_{ex} \tag{2.16}$$

V_{ex} being the volume of the manifold. The values of M_i and M_o represent the gas masses entering and leaving the manifold respectively. The work produced by the piston in all phases of the cycle is calculated by integrating (with respect to the crank angle variable θ) the differential equation:

$$dW = p_c dV \tag{2.17}$$

where p_c is the cylinder mean pressure during the step dθ, and dV is the cylinder volume change in the same step.

2.2.3. Inlet manifold and intercooler

These two components are considered together in the corresponding block of Figure 2.6. The inlet manifold, located after the turbocharger compressor, is considered as a control volume where mass and energy accumulation are determined by the continuity and energy dynamic equations:

$$dW = p_c dV \tag{2.18}$$

$$\frac{d(\rho_o U)}{dt} = \frac{m_i H_i - m_o H_o + Q - P}{V} \tag{2.19}$$

Where U is the specific internal energy and subscripts represent the inlet and outlet conditions of mass flow rates and specific enthalpies. In the second equation, the power exchanged P is assumed to be zero (rigid walls of the components), while the heat flow between the walls and the contained gas (Q) is neglected. The air cooling effect is evaluated, in the intercooler simulation, by the equation:

$$T_o = T_i - E(T_i - T_{coo}) \tag{2.20}$$

Where T_{coo} is the coolant temperature and the heat exchanger efficiency (E) is supposed constant. The pressure drop of the whole set is evaluated as a constant fraction of the inlet pressure.

2.2.4. Outlet manifold

This engine component, located after the cylinders and before the turbocharger turbine (Figure 2.6), is considered as a control volume where mass and energy accumulation are governed by the equation (2.18) and equation (2.19) respectively. The mean temperature in the exhaust manifold is evaluated by describing the cylinder blow-down process with the simple procedure proposed by (Ferrari G., 2008).

2.2.5. Turbocharger

In reference to Figure 2.6, turbocharger simulation is performed via three blocks: TC COMPRESSOR, TC TURBINE and TC SHAFT DYNAMICS. In the compressor module, steady state performance maps, provided by the manufacturer, are used. They allow to estimate the compressor mass flow rate and efficiency, as functions of the compressor pressure ratio and of the non-dimensional shaft speed. More in detail, a steady state compressor map given by the Manufacturer is used in 2D matrix form. Compressor pressure ratio (β=po/pi) and isentropic efficiency (ηc) are evaluated as a function of the corrected volume flow rate $V'_{Cc} = V'_{C}\sqrt{T_{ref}/T_a}$ and corrected rotational speed $n_{Cc} = n_{TC}\sqrt{T_{ref}/T_a}$ according to the procedure reported in (Cohen et al., 1987). The turbine performance calculation is very similar to that used for the compressor. Steady state maps are used again, providing mass flow rate and efficiency as functions of the expansion ratio (in terms of pressures) and of the kinematic ratio (i.e. ratio between the rotor tip speed and the isentropic expansion velocity). The turbocharger shaft dynamics is calculated, in the specific module shown in Figure 2.6, by the time integration of the momentum equation:

$$\frac{d\omega}{dt} = \frac{1}{J\omega}\left(P_T - P_C\right) \tag{2.21}$$

Where J is the inertia of rotational masses and P_T and P_C are the power provided and required by turbine and compressor.

2.2.6. Engine torque

The torque delivered by the engine is calculated in the corresponding module of the simulator scheme of Figure 2.6, in terms of the brake mean effective pressure b.m.e.p.:

$$\text{b.m.e.p.} = \text{i.m.e.p.} + \text{p.m.e.p.} - \text{f.m.e.p.} \tag{2.22}$$

Where i.m.e.p. is the gross indicated mean effective pressure, while p.m.e.p. is the pumping mean effective pressure, evaluated as the difference between the inlet and outlet pressures of the cylinder: both the pressures enter as input variables into the engine torque module (Figure 2.6). The mechanical friction mean effective pressure f.m.e.p. of equation (2.22) is evaluated by:

$$\text{f.m.e.p.} = f_1(n) + f_2(\text{i.m.e.p.}) \tag{2.23}$$

Where $f_1(n)$ and f_2(i.m.e.p.) are specific functions depending on engine speed n and i.m.e.p., properly developed for each considered engine (diesel or gas engine), on the basis of data provided by the engines manufacturer. At last, the brake torque C, in the case of four-stroke engine, is given by:

$$C = (\text{b.m.e.p.})\, V \frac{1}{4\pi} \tag{2.24}$$

2.2.7. Engine power control

As known, the engine delivered power is given by:

$$P = C\omega \tag{2.25}$$

C being the brake torque and ω the angular speed, proportional to the engine rotational speed (n), that is an input variable of the engine simulator. As a consequence, if the engine works at constant speed, the engine power depends only on the delivered torque, proportional to the brake mean effective pressure (b.m.e.p.), which in turn depends on the three mean pressures on the right side of equation (2.22). As regards the diesel engine, the delivered torque is governed by the variation of the fuel mass injected into the cylinders, thus varying mainly the indicate mean effective pressure. In the case of a spark ignition engine, such as the examined NG engine, the delivered torque is governed by varying the cylinders volumetric efficiency through the throttle valve. In this type of engine, characterized by a constant equivalence ratio φ, the variation of η_v affects the mean pressures i.m.e.p. and p.m.e.p., changing b.m.e.p. and consequently the engine torque represented by equation (2.24).

2.4 SIMULATION RESULTS AND VALIDATION

The numerical models have been validated for different steady state load conditions, by comparing the simulation results with reference data provided by the manufacturer of the engines. Table 2.3 shows the percentage errors of the simulators, referred to MCR load conditions, expressed in the form:

$$\text{error} = \frac{\text{calculated value} - \text{referencevalue}}{\text{referencevalue}} 100\ [\%] \tag{2.26}$$

Table 2.3. Simulation percentage errors of the two Bergen engines

Data error [%]	C25:33L6P (DE)	C26:33L8PG (NG)
brake power	-0.031	0.388
b.m.e.p.	-0.060	0.351
b.s.f.c	0.031	0.624
cylinder inlet air pressure	0.142	-1.964
cylinder inlet air temperature	-0.080	-1.910
cylinder inlet air mass flow	0.803	1.230
cylinder outlet gas mass flow	0.511	1.834
TC inlet turbine temperature	-4.390	-3.054
TC outlet turbine temperature	-2.484	-3.970

The table shows a substantial good agreement between calculated and references data, with percentage errors lower than 2% for most of the examined parameters. Only the inlet and outlet temperatures of the turbocharger turbine are characterized by an error greater than 2% but lower than 5%. This is probably due to input data, relative to the turbocharger, not properly tuned. More in detail, Figure 2.7 shows a very good accuracy in the simulation of the NG engine brake specific fuel consumption (b.s.f.c.), both at constant MCR engine speed and along the nominal propeller curve indicated by the manufacturer. The latter is shown as a dash line in the engine load diagram of Figure 2.8, together with the curves at constant efficiency calculated by the simulator. The values reported in both diagrams are normalized with respect to MCR conditions.

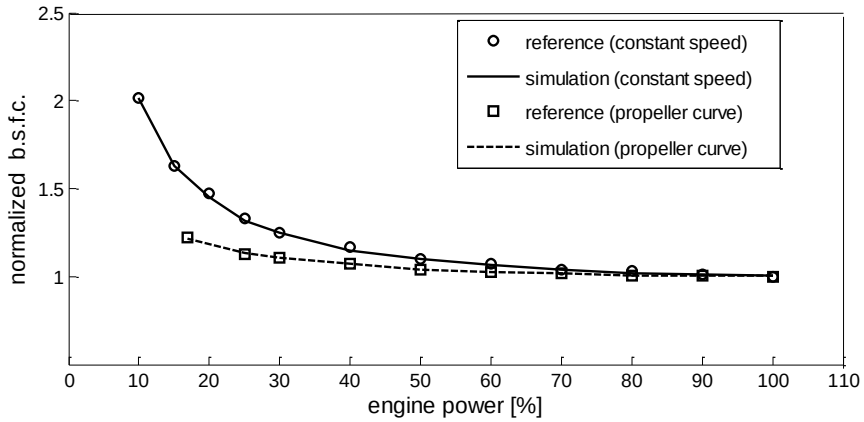

Figure 2.7. b.s.f.c. simulation accuracy (NG engine)

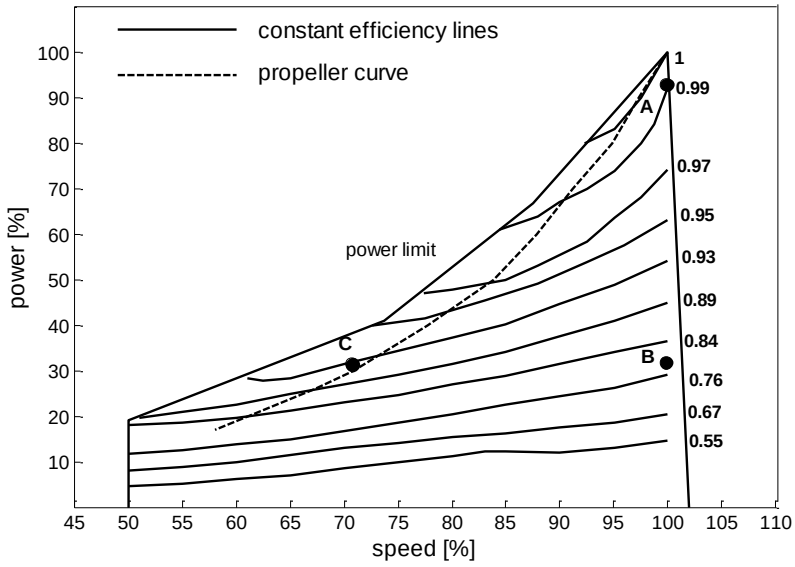

Figure 2.8. Efficiency map (NG engine)

As regards the validation of the diesel engine simulation, a comparison is made in terms of overall efficiency, between simulation results and engine reference data provided by the manufacturer. In the DE load diagram of Figure 2.9, the power and speed values are normalized with respect to the design conditions (MCR) of the NG engine, differently from the curves at constant efficiency, which are normalized with respect to the DE design conditions (MCR).

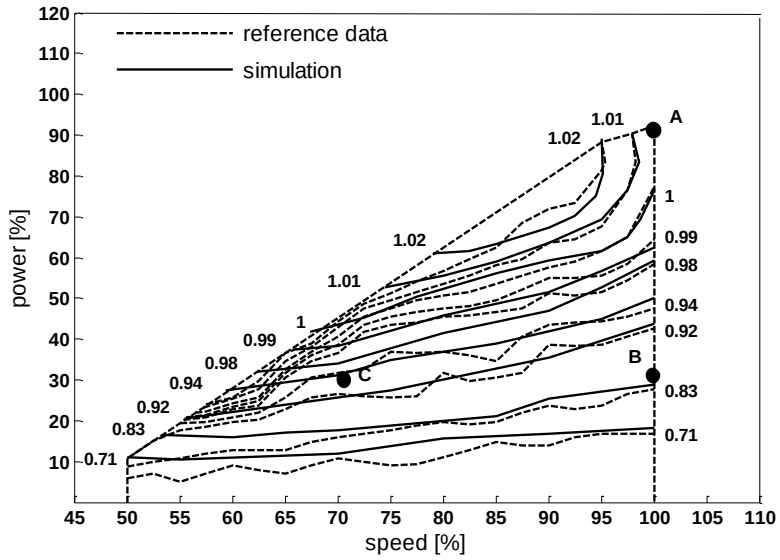

Figure 2.9. Diesel engine efficiency map

The tuning of the diesel engine simulator was particularly difficult, due to the irregular shape of the reference constant efficiency curves (dash lines in Figure 2.9). This atypical behaviour (quite different in comparison with traditional DE performance maps) is responsible for a minor accuracy of the simulator results, especially at low loads and revolutions. However, the achieved simulation results are considered enough reliable for a parametric analysis throughout the working area of the engine. The simulation reliability is confirmed by the calculated values of the cylinder peak pressure, with errors lower than 1%, for both engines.

2.5 PERFORMANCE COMPARISON

A first comparison between the two examined engines is already presented in Table 2.1, as for cylinders number, bore, stroke and main performance data in design conditions, while in Table 2.2 weights and dimensions are reported too. The significant difference relative to the b.m.e.p. (24.7 bar for the diesel engine and 18.5 bar for the NG engine), is motivated by the need to get optimal performance for the NG engines characterized by a lean-burn combustion (Wärtsilä, 2013). In this section, the comparison concerning the overall efficiency and CO_2 emissions is added. The diagram of Figure 2.10 shows the percentage difference ($\Delta\eta$) between the overall efficiencies η_{NG} (i.e. NG engine efficiency) and η_D (i.e. DE efficiency) of the two engines, calculated as follows:

$$\Delta\eta = \frac{\eta_{NG} - \eta_D}{\eta_D} 100 \tag{2.27}$$

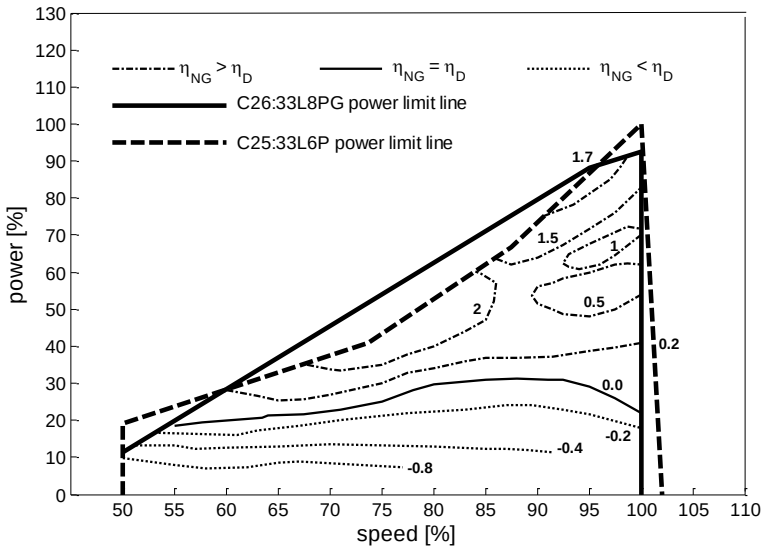

Figure 2.10. Curves of constant differential efficiency (NG engine vs diesel engine)

In the diagram, the power and speed values are normalized with respect to the design conditions of the NG engine (the engine speed is the same for both engines), while the efficiency difference curves are normalized according to DE design conditions. As shown in Figure 2.10, the NG engine is characterized by a greater efficiency than DE at high loads. This is due to several factors including: the greater lower heating value of the NG fuel compared to HFO and the influence of this fact in this working area characterized by about the same volumetric compression ratio and a similar equivalence ratio, the differences between the mean effective pressures (see Table 2.1), the different combustion modes, and so on. The advantage in the efficiency of the NG engine gradually decreases when the engine load is reduced, up to zero (black solid line in Figure 2.10). For a further load reduction, the DE efficiency increases with respect to NG engine. In order to provide an explanation of these results, two working conditions at partial load are analysed, corresponding to points B and C illustrated in the load diagrams of Figure 2.8 and Figure 2.9. The respective values of brake power and speed, the same for the two engines, are reported in Table 2.4.

Table 2.4. Performance evaluation of the engines at partial load conditions

		C25:33L6P (DE)		**C26:33L8PG (NG)**	
Reference data	Working points	B	C	B	C
	brake power [kW] (30% of MCR_D)	600	600	600	600
	speed [rpm]	1000	710	1000	710
Simulation data	Difference in η_E [%]	-16.6	-8.8	-21.8	-13.4
	Difference in (i.m.e.p.) [%]	-67.2	-59.0	-61.9	-51.4
	Difference in TC speed [%]	-12.1	-13.2	-36.2	-47.6
	Difference in φ [%]	-13.8	13.4	0.0	0.0
	Difference in β_C [%]	-57.4	-55.3	-45.5	-53.1
	Difference in cylinder inlet air mass [%]	-54.1	-69.2	-62.2	-66.2

Simulation data of Table 2.4 are obtained by evaluating the difference among the numerical values in B and C conditions and the design load value (working point A). This last value is used to normalize the numerical difference for each engine parameter x, according to:

$$\Delta x = \frac{x_{B,C} - x_A}{x_A} 100 \tag{2.28}$$

By analysing the data reported in Table 2.4, it can be observed that the reduction of the efficiency (η_E) is more consistent in the NG engine; the contrary happens as regards the i.m.e.p. parameter. The smaller reduction of this value, in the case of the NG engine, is also confirmed by the comparison of the real cycles illustrated in the Figure 2.11 (DE) and Figure 2.12 (NG engine), corresponding to the load conditions defined by the points A (2MW, 1000 rpm), B (0.6 MW, 1000 rpm) and C (0.6 MW, 710 rpm).

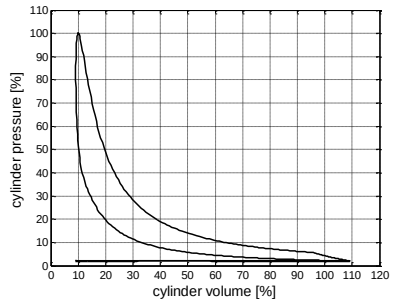

(A)

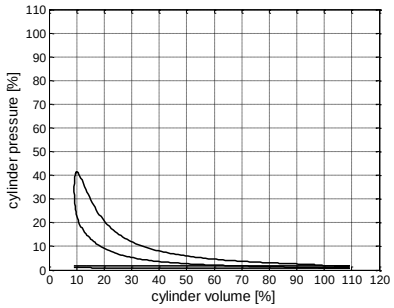

(B)

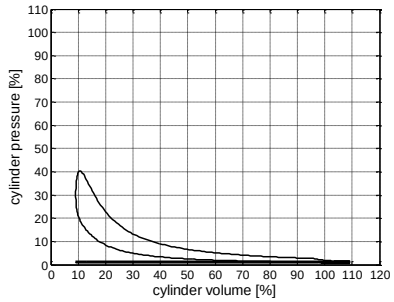

(C)

Figure 2.11. Normalized diesel Miller cycles, corresponding to the working points (A), (B), (C)

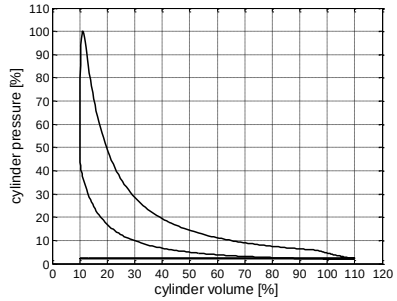

(A)

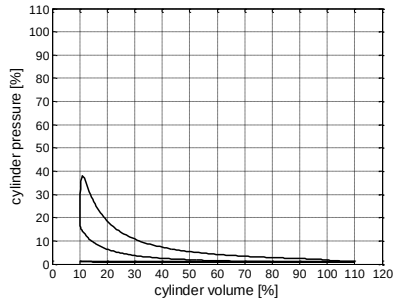

(B)

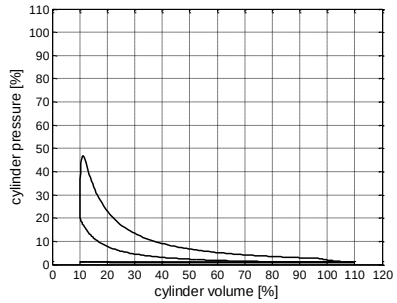

(C)

Figure 2.12. Normalized natural gas Miller cycles, corresponding to the working points (A), (B), (C)

Always from Table 2.4 it can be observed that the reduction of the turbocharger speed is more significant in the NG engine than in DE (in the point B but especially C). As regards the equivalence ratio φ, a small reduction is presented by DE, while in the NG engine the ϕ value is maintained constant by the fuel injection governor, excepting a small increase at very low load conditions. Despite the sensible difference in the turbocharger speed, the two engines present similar values as regards the consistent reduction of the TC compression ratio β_C at partial loads. This is mainly due to the different torque control logics adopted for the two engines: variation of the fuel mass injected in the cylinders for DE, and variation of the cylinders volumetric efficiency (η_v) through the throttle valve for the gas engine. These different control logics also explain the low differences in air mass

flow entering into the cylinders, despite the rather different TC speed reductions between the two engines. From the foregoing considerations it can be deduced that the main reason of the efficiency reduction of the NG engine, compared to DE, for decreasing loads, is the increase of the pumping mean effective pressure (p.m.e.p.), due also to the adopted torque control logic. Concerning the emissions of carbon dioxide, Figure 2.13 shows the CO_2 curves in terms of percentage difference between NG engine DE.

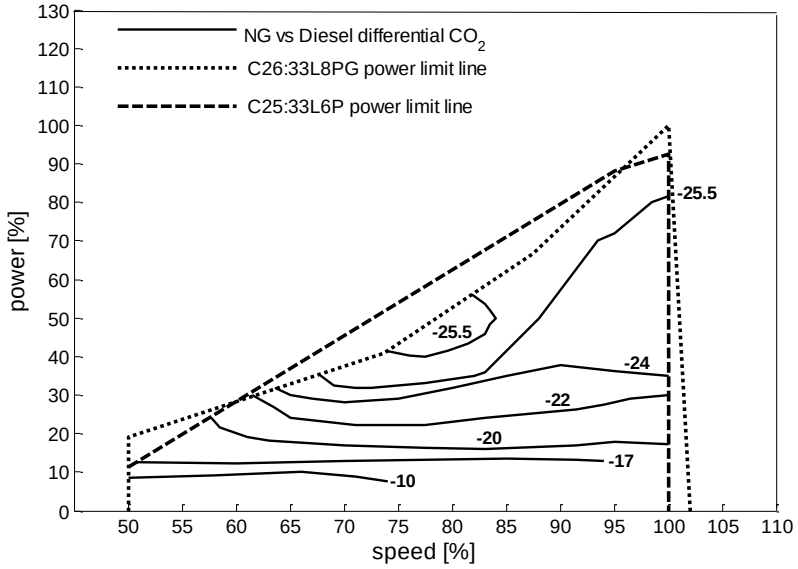

Figure 2.13. NG vs DE differential CO_2 emissions

The carbon dioxide mass of the two engines (i.e. $M_{CO_2\,NG}$ and $M_{CO_2\,D}$) is estimated, for each working point of the engines maps, by the respective fuel mass consumption and fuel type (NG or HFO), following the procedure proposed by the Marine Environment Protection Committee (MEPC, 2012). The formula for the calculation of the differential Δ_{CO_2} emissions is:

$$\Delta_{CO_2} = \frac{M_{CO2\,NG} - M_{CO2D}}{M_{CO2D}} 100 \tag{2.29}$$

The comparison results presented in Figure 2.13, covering the overall working areas of the two engines, show a significant reduction of CO_2 emissions (around 25%) for the NG engine, in a wide part of the performance map (this result confirms pertinent data reported in (Livanos G. A. et al., 2012)). Only for power values lower than 30%, the NG engine advantage shows a progressive reduction at decreasing loads. This reduction is easily explained by the corresponding efficiency reduction of NG engine in comparison with diesel engine, as shown in Figure 2.10.

2.6 REMARKS

The introduction of natural gas, as an alternative to traditional fuel oils used in ship propulsion, is very interesting especially for environmental implications. This issue is addressed in the present study by comparing two marine engines, produced by the same manufacturer: a spark-ignition engine fuelled by natural gas and a compression-ignition engine powered by liquid fuel (diesel oil), in order to obtain detailed information on their performance and possible applications. The two engines, characterized by similar design power and equal rotational speed range, are compared not only on the basis of data provided by the manufacturer (weights, dimensions, operational data), but also in terms of pollutant emissions into the atmosphere and overall efficiency in their whole working areas. The comparative assessment of these parameters is carried out in view of the recent IMO regulations. It is based on data taken from literature as regards SOx and NOx emissions, while the evaluation of CO_2 emissions is the result of a specific numerical simulation. The attention paid to this last aspect is the main contribution of the present study. Finally, a detailed comparison of several parameters is achieved by simulation, for different loads and speed conditions of the engines. The main results of the comparison can be summarized as follows:

- a greater overall efficiency of the gas engine (percent increase up to 2%) is evident for high-medium loads but it decreases at low loads (percent decrease around 1%);

- in terms of CO_2 emissions reduction, the advantage of the gas engine is greater in a wide zone of the load diagram (CO_2 reduction up to 26% in nominal working conditions), with a small decrease at low loads.

The examined methane engine can be reasonably considered a representative sample of the current marine four stroke gas engines, demonstrating significant advantages over the traditional diesel propulsion, at least for short routes of the ship. For the sake of completeness, other issues will be addressed in a forthcoming analysis, such as: on board installation of the engines, fuel storage and safety, influence on the ship load capacity, fuel and maintenance costs, as well as the problem of methane slip.

3 WASTE HEAT RECOVERY SYSTEM FOR MARITIME SECTOR

3.1 STEAM PLANT FOR WASTE HEAT RECOVERY

The possibility of obtaining high thermal efficiency values, typical of medium-high power combined systems, is a valuable advantage to meet the regulations on CO_2 emission restrictions. The Marine Environment Protection Committee (MEPC), by IMO, has focused in recent years on the energy efficiency, both as ship design and management. To quantify the energy efficiency of the vessel, the EEDI (Energy Efficiency Design Index) index was introduced, expressed in grams of carbon dioxide per ship's capacity-mile, and gives an indication of project engineering efficiency. The regulations relating to this issue have been entry in force since January 1, 2013 and give a clear indication of the increasingly growing interest on the marine transport with regard to the optimization of the exploitation of energy resources. In addition to the environmental aspect, economic considerations, related to the uncertainties on the cost of fuels, encourage nowadays the search for even more efficient solutions to be adopted in energy conversion plants for ship power and propulsion systems (Altosole et al. 2017b). Despite the efficiency of this type of engines is rather high (slightly lower than 50%), due to the uncertainty about fuel prices and the growing international attention to environmental issues, the marine diesel engines manufacturers are constantly striving to increase the efficiency of these engines, mainly through an increment of the thermodynamic efficiency and a reduction of mechanical losses. However, these improvements appear to be slow and difficult to achieve. An emerging alternative way to increase the overall efficiency of both propulsion and power systems of the ship is represented by the possibility to recover part of the considerable amount of thermal energy released by these engines and currently dispersed into the environment (Benvenuto et al., 2015b). The ability to adopt new devices and technical solutions to maximize the use of fuel energy can make ships of the latest generations compatible with modern standards. Heat recovery is carried out by means of a recovery boiler in which the water-steam gas heat exchange occurs. The defining of thermal recovery is reached with a careful study of the pressures within the water-vapour duct and the appropriate exchange temperature choice. The recovered heat fraction can be increased using boilers with multiple levels of pressure, but in the marine field, single or double pressure configurations are adopted in order to avoid an excessive increase in costs, weights and space requirements. The steam turbine, combined with this type of plant, is characterized by very loaded stages and a high expansion ratio to reduce weights and spaces. The thermal energy recovery from exhaust gases can be carried out on each ship equipped with a thermal engine able to produce propulsion/electric power; unfortunately, there are technical and economic constraints (initial plant investment) that limit the adoption of recovery devices. Ships characterized by high propulsion power and significant demand values for electricity are the best candidates for energy recovery systems. The technological innovation focused on heat recovery, resulting into the development of the so-called TES systems (MAN Diesel & Turbo, 2007). These systems consist of various combinations of steam turbines (using steam produced in a heat exchanger) and power gas turbine (which uses part of the exhaust gas bypassed by turbocharger). Waste heat recovery (WHR) for power generation is already a well-established reality for ships with medium-high power and requiring a high fraction of power used to meet electric power consumption, as in the case of large containerships (Tigges K., 2011). WHR systems can also be installed on board passenger ships where the steam production is used to

meet heat demand by thermal users and electricity demand is significant. All WHR systems manufacturers (SIEMENS, Dresser Rand, Mitsubishi Heavy Industries, MAN, Wartsila) include in their portfolio this modern recovery system that combines power turbine and steam turbine. An article published by MAN (MAN Diesel & Turbo, 2012) explains that the most appropriate recovery energy system is based on the power range installed on board:

- Installed power less than 15 MW: WHR systems with only a power gas turbine are recommended, the advantage of which is the simplicity of the system due to the possibility of avoiding the installation of large and heavy machinery such as the heat steam generator. Alternatively, the Organic Rankine Cycles systems that can better heat up at low temperatures and thus have better energy performance than the typical Hirn cycle when the amount of recoverable energy is low.
- Installed power between 15 MW and 25 MW: WHR systems with a single power gas turbine or only a steam turbine are recommended.
- Installed power greater than 25 MW: the modern WHR systems with both gas turbine and steam turbine are recommended.

By examining several articles and brochures of the major recovery system suppliers, it can be seen how some of them (MHI, MAN and Wartsila) propose plants coupled with Diesel 2T both single and double pressure, depending on the electrical requirements of the ship and the return of investment of the plant. An example of a single pressure WHR system layout is shown in Figure 3.1.

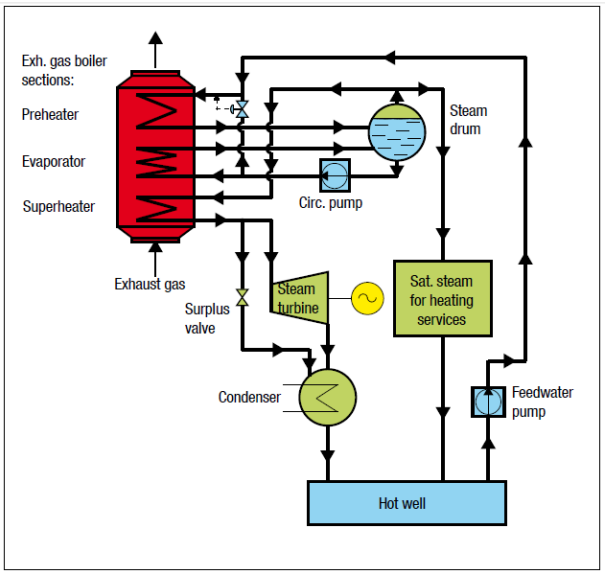

Figure 3.1. Single-pressure heat recovery system proposed by MAN (MAN Diesel & Turbo, 2012)

Through the installation of a single pressure recovery system, it is possible to produce power between 4% and 7% (MAN Diesel & Turbo, 2012) of the power of the main engine. Another aspect to consider in the design of a recovery plant is the possibility to recover heat from other waste heat

sources of the engine such as jacket water and charge air cooler. As regard the double pressure option, low-pressure steam could be characterized by a low saturation temperature that could reduce the exhaust gas temperature below the threshold temperature. A good practice, as mentioned in literature (MAN Diesel & Turbo, 2004) is not exceeding to cool down exhaust gas temperatures below 165 ° C, in order to avoid the sulphuric acid production, which is extremely corrosive in contact with metallic parts. Therefore, all the manufacturers (MAN, Wartsila, SIEMENS, MHI, Dresser Rand) provide for preheating the feed water by means of heat recovery from the jacket water or charge air cooler. Alternatively to the use of the other heat sources, as stated by a study carried out by MAN (MAN Diesel & Turbo, 2007), the inlet water into the exhaust steam generator could be preheated through saturated vapour bled by the high-pressure system. In case of ship powered by gas engines, there is no constraint regarding the exhaust gas outlet temperature because of the substantial absence of sulphur in NG (the eventually sulphur content in the diesel oil of the pilot ignition is negligible, since the fuel oil injected is about 1% of NG mass, (Altosole et al., 2017a)). To increase the specific enthalpy of the steam it is possible to superheat it through the adding of another heat exchanger. The so-called superheater is an expensive component that requires frequent maintenance but that allows to obtain steam with higher steam quality so less damaging to turbine blades (Singh D. V. & Pedersen E., 2016). Another technical/design aspect to be taken into account in designing a double pressure steam systems is the feeding of the high-pressure section of the heat exchanger steam generator; two different plant options can be listed:

- Feeding of the high-pressure section by taking part of liquid saturated vapour from the low-pressure steam drum (as shown in Figure 3.2).
- Feeding of the high-pressure section by water to be taken downstream of the preheating carried out with other heat sources (as shown in Figure 3.3).

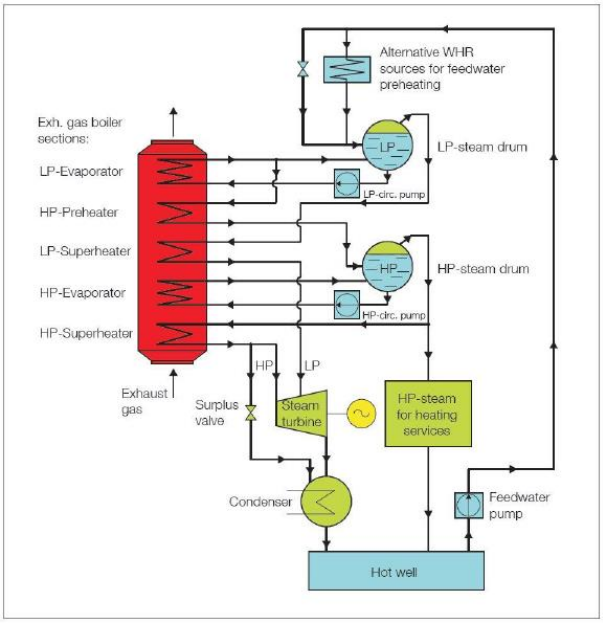

Figure 3.2. Double-pressure heat recovery system proposed by MAN (MAN Diesel & Turbo, 2012)

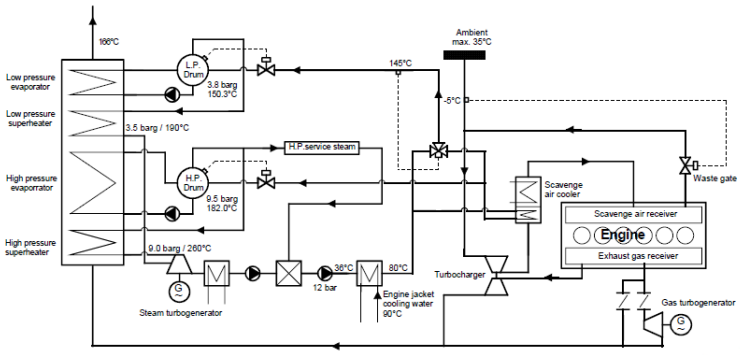

Figure 3.3. Waste heat recovery system proposed WARTSILA (Schmid H., 2005)

By installing a double-pressure steam recovery plant, it is possible to reach steam turbine power ranging between 5 and 8% (MAN Diesel & Turbo, 2012) of the power of main engine. Heat exchangers used in the marine field are vertical finned tube operating in counter flow pattern. Figure 3.4 shows a representation of this type of heat exchanger.

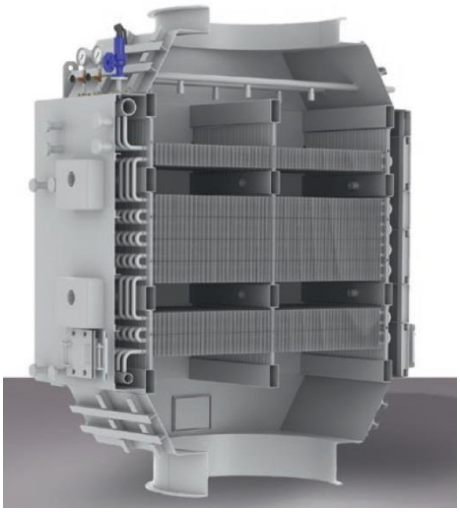

Figure 3.4. Heat exchangers by SAACKE (SAACKE MARINE SYSTEMS)

Due to the small size of the turbines usually used for waste heat recovery on-board ships, the backpressure turbine could be not cost-effective. As regards the steam condenser the coolant fluid used is the seawater either intermediate fresh-water circuit or not. A representation of a condenser is shown in Figure 3.5.

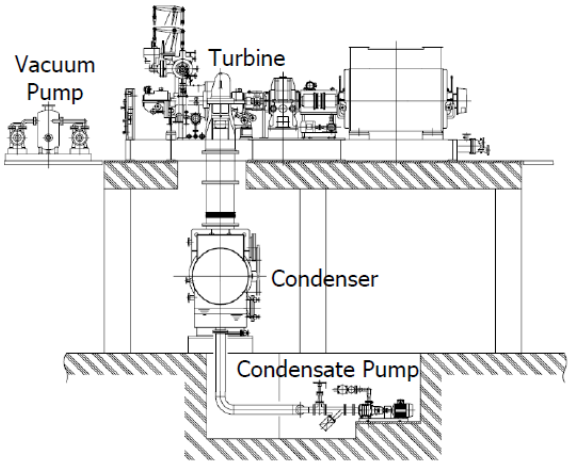

Figure 3.5. Condenser layout downward exhaust connection (MITSUBISHI HEAVY INDUSTRIES)

The steam turbines installed on board ships are action type one (thanks to weight, compactness and reliability of this kind of machines), axial, condensing (to maximize the power produced), single or double steam inlets.

3.2 POWER TURBINE

The power turbines commonly used for these plants are radial type: simple and compact, much more similar to supercharged turbines than the more elaborate gas turbines. This kind of turbines is fed by the exhaust gas bypassed by turbocharger (in the range of 8 to 12% of the mass flow of fumes (MAN Diesel & Turbo, 2012)) for main engine load greater than 50%. Scientific literature shows that the power that can be obtained by installing power turbines is about 3-5% of the power of the main engine (MAN Diesel & Turbo, 2012; MAN B & W Diesel A / S). Depending on the power required and the operating profile of the ship, the power turbine can be installed either coupled to steam turbine in a single pack (as shown in Figure 3.6) or installed individually.

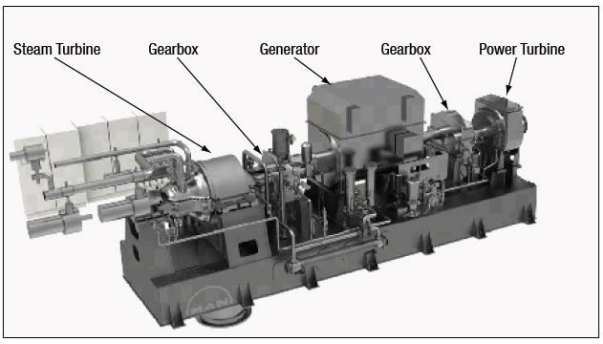

Figure 3.6. Power turbine and steam turbine compound system (MAN Diesel & Turbo, 2012)

The normal operating condition of this power pack provides that firstly the steam turbine couples the generator through a clutch once getting design speed, and in case of a further electrical power demand, the power turbine is coupled too. The combined running of steam turbine and power turbine makes it possible to reach an output power between 8 and 11% (MAN Diesel & Turbo, 2012) of the main engine power.

3.3 HEAT RECOVERY STEAM GENERATOR BASIC DESIGN

The design of the heat recovery steam generator was performed using an in-house code written in MATLAB environment. The code consists of two main parts, the first one concerns the evaluation of the heat exchanges between exhaust gas and steam-water, while the second one is dedicated to the heat exchanger sizing. The thermo-physical properties of the steam water were obtained from appropriate tables found in literature while the exhaust gases were considered as a mixture of water vapour and carbon dioxide (perfect combustion assumption), whose quantities are obtained in relation to the amount of fuel/air in the combustion mixture. The considered layouts of the heat recovery steam generators are of 4 types: single pressure and double pressure, both in saturated and superheated steam option. The heat exchanger taken in consideration are vertical finned tubes, operating in counter flow pattern. Heat transfer area was calculated using the logarithmic average temperature method. The heat flow exchanged between the two fluids can be estimated through equation (3.1).

$$\dot{m}_h\left(H_{i,h} - H_{o,h}\right) = \dot{m}_c\left(H_{o,c} - H_{i,c}\right) \tag{3.1}$$

Where:

- $\dot{m}_h$ is the mass flow rate of hot fluid;
- $\dot{m}_c$ is the mass flow rate of cold fluid;
- $H_{i,h}$ ($H_{i,c}$) inlet enthalpy of hot fluid (cold fluid);
- $H_{o,h}$ ($H_{o,c}$) outlet enthalpy of hot fluid (cold fluid).

In the case of a single-phase fluid (gas), enthalpy can be calculated by equation (3.2).

$$H = c_p\, T \tag{3.2}$$

Where:

- c_p is the specific heat at constant pressure;
- T is the gas temperature.

Regarding the heat exchange surface, the thermal flow can be assessed as in equation (3.3).

$$\Phi = K_e\, A\, LMTD\, F \tag{3.3}$$

Where:

- K_e is the heat transfer coefficient;
- A is the heat exchange area;
- $LMTD$ is the Log Mean Temperature Difference;
- F is a correction factor that takes into account the type of heat exchanger and the inlet and outlet temperatures.

The heat transfer coefficient K_e is evaluated using the equation (3.4).

$$\frac{1}{K_e} = \frac{1}{h_e} + \frac{1}{h_i}\frac{A_e}{A_i} + R_e + R_i\frac{A_e}{A_i} + \frac{s}{k}\frac{A_e}{A_{ml}} \tag{3.4}$$

Where:

- h_e and h_i are the convection coefficients for internal and external flow, respectively;
- A_e, A_i e A_{ml} are the inner area of the wall, the outer area and their average logarithmic, respectively;
- R_e and R_i are fouling factor, caused by the deposit;
- s is the thickness of the tube;
- k is the thermal conductivity of the wall material.

In the case of thin walls, the A_{ml} can be approximated with the arithmetic mean.

In the case of finned tubes, the effective heat exchange surface is evaluate through the calculation of the global efficiency, as reports in equation (3.5).

$$\eta = \frac{A_0}{A} + \eta_a\frac{A_a}{A} \tag{3.5}$$

Where:

- $A = A_0 + A_a$ (A_0 is the naked surface while A_a is the finned surface);
- η_a is the fin efficiency, calculated by the use of diagram reported in Figure 3.7.

The evaluation of the fin efficiency is related to these following terms:

- δ is the thickness of the fin;
- r_b is the inner radius of the fin;
- r_a is the outer radius of the fin;
- $m = \sqrt{2h/(k\delta)}$,
- h is the convection coefficient of the outer fluid.
-

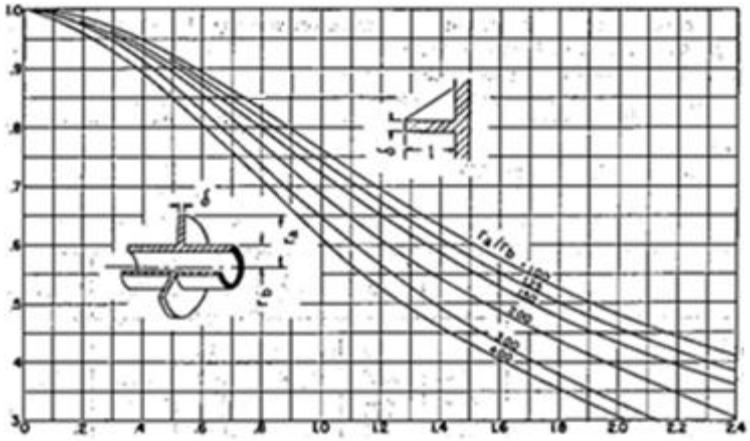

Figure 3.7. Fin efficiency correlation

The value of the convective coefficient h_i is determined by the number of Nusselt, expressed as:

$$Nu = \frac{hD}{k} \tag{3.6}$$

Where D is the inner diameter of the tube.

Nu calculation is possible through Dittus and Boelter correlation, as reported in equation (3.7):

$$Nu = 0.023\, Re_D^{0.8}\, Pr^n \tag{3.7}$$

Where n is 0.3 in the case of external convection and 0.4 in the case of internal convection, while Re_D and Pr are respectively the number of Reynolds and Prandtl calculated as in equations (3.8) and (3.9).

$$Re_D = \frac{vD}{\upsilon} \tag{3.8}$$

$$Pr = \frac{\mu c_p}{k} \tag{3.9}$$

Where:

- v is the fluid velocity;
- υ is the kinematic viscosity of the fluid;
- μ is the dynamic viscosity of the fluid.

The value of the external coefficient h_i is obtained by equation (3.10), in which the Colburn factor (j_H) is derived from statistical correlations through the Reynolds number Re_D such as those shown in Figure 3.8.

$$h_e = \frac{j_H \, G \, c_p}{Pr^{2/3}} \tag{3.10}$$

In equation (3.10) G is the mass flow per surface unit defined as in equation (3.11).

$$G = v \, \rho \tag{3.11}$$

Where ρ is the fluid volumetric mass density.

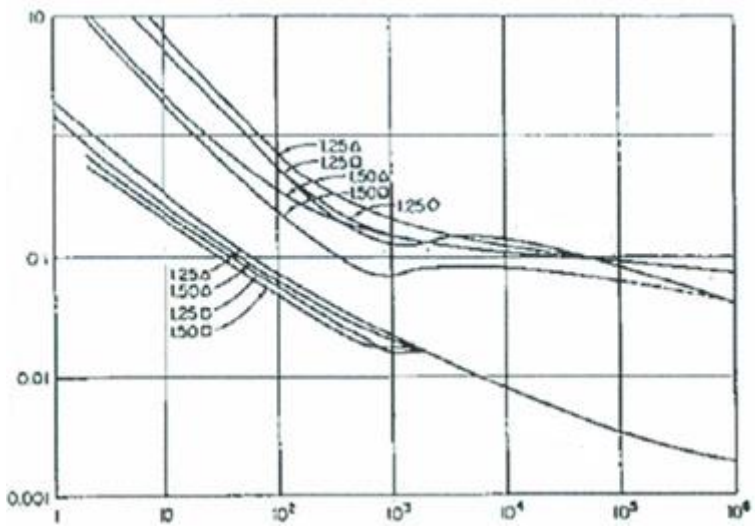

Figure 3.8. Colburn factor

The correction factor F of equation (3.3) can be obtained through the graph in Figure 3.9 by knowing the values of the R and P parameters calculated as in equation (3.12) and (3.13), respectively.

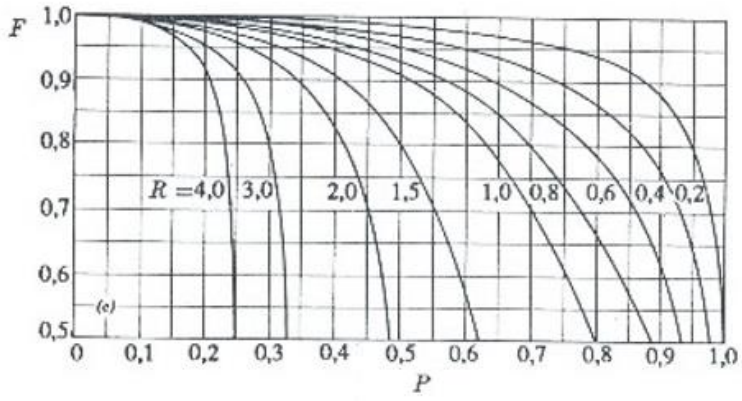

Figure 3.9. Correction factor F

$$P = \frac{t_2 - t_1}{T_1 - t_1} \tag{3.12}$$

$$R = \frac{T_1 - T_2}{t_2 - t_1} \tag{3.13}$$

The t and T are the temperatures referred to water vapour and gas respectively, while the subscripts 1 and 2 refer to the exchanger's inlet and outlet. $LMTD$ is calculated through the equation (3.14).

$$LMTD = \frac{\Delta T_2 - \Delta T_1}{ln\frac{\Delta T_2}{\Delta T_1}} \tag{3.14}$$

Where ΔT_1 and ΔT_2 are respectively:

$$\Delta T_1 = T_{h,i} - T_{c,o} \tag{3.15}$$

Where:

- $T_{h,i}$ is the inlet temperature of the hot fluid;
- $T_{c,o}$ is the outlet temperature of the cold fluid.

$$\Delta T_2 = T_{h,o} - T_{c,i} \tag{3.16}$$

Where:

- $T_{h,o}$ is the outlet temperature of the hot fluid;
- $T_{c,i}$ is the inlet temperature of the cold fluid.

Piping thickness was obtained by consulting the RINA Classification Registry where the following calculation correlation is reported:

$$t = \frac{pD_e}{2K + p} + 0.3 \tag{3.17}$$

Where:

- p is the steam pressure [MPa];
- D_e is the outer diameter [mm];
- K is a property of the strength of the material that can be obtained from a table according to the maximum operating temperature that occurs in the piping.

Once calculating the thickness of the pipe, it is necessary to compare it with the minimum value provided by the Register, and select the greater between them. The surface required by each heat exchanger is obtained from equation (3.3) by knowing these input terms:

- Inlet and outlet temperatures for each component of the heat exchanger
- Heat flow exchanged
- Heat flow coefficient

Pressure loss inside the tubes was considered negligible (Qiang Guo et. Al., 2012), while hot gas pressure loss was calculated through the correlation (3.18.

$$\frac{L_w}{g} = \frac{\lambda}{D}\frac{U^2 L}{2g} + \sum_i \xi_i \frac{U^2}{2g} \tag{3.18}$$

Where:

- L_w is head loss;
- g is the gravitational acceleration;
- U is the exhaust gas speed;
- L is the length of the tube;
- λ is calculated through the Colebrook correlation (equation (3.19)), as function of Reynolds number (Re) and roughness (ε);
- ξ_i is the coefficient of local loss.

$$\frac{1}{\sqrt{\lambda}} = -2log\left(\frac{2.51}{Re\sqrt{\lambda}} + \frac{\varepsilon}{3.71D}\right) \tag{3.19}$$

3.4 WASTE HEAT RECOVERY BASIC DESIGN

Input data for the design of a heat recovery steam generator are:

- Main engine power and specific fuel consumption (design condition)
- Exhaust gas temperature (design condition)
- Exhaust gas mass flow rate (design condition)
- Available space to arrange the heat exchanger
- Steam service for on-board users

Techno-constructive parameters used for the design of a heat recovery steam generators are the operating steam pressure and the main differences in temperature that occur between the two fluids, namely:

- p_{HP} high steam pressure
- p_{LP} low steam pressure
- p_{COND} condenser pressure
- ΔT_{pp} temperature difference at the pinch point (corresponding to the outlet hot gas temperature in the evaporator)
- ΔT_{ap} temperature difference at the approach-point (corresponding to the inlet hot gas temperature in the superheater)

- ΔT_{sc} subcooling temperature difference between the saturated steam temperature and inlet steam temperature in the evaporator

Recommended steam pressure not less than 7 bar (MAN Diesel & Turbo, 2004) to avoid so large heat exchange area for warming thermal users on-board the ship.

The condenser pressure should not be too low to prevent condensers with excessive surface exchange. A minimum value could be 0.065 bar as suggested in the literature (Livanos G. A. et al., 2014). ΔT_{sc} is recommended to avoid the risk of beginning evaporation in the economizer tubes resulting in temporary flow blocks due to vapour bubbles. In design practice are usual values at 10-15 ° C (Perdichizzi, 2011).

Geometrical properties of the heat steam generator are:

- Vertical and transverse tube spacing
- Outer diameter of the tube
- Fin pitch and dimensions of the fin

The spacing of the pipes in the vertical and transverse directions as well as the diameter was taken equal to the values obtained by product technical specification of a heat steam generator whose values are known. The fin pitch can range from 10 to 13 mm as found in the literature (MAN Diesel & Turbo, 2004).

The constraints to be met are:

- Maximum water-steam speed; no more than 40 m/s for saturated steam and 100 m/s for the superheated steam (The Engineering ToolBox) to avoid excessive wear on the tubular walls.
- Steam quality > 0.9 (Unipv), so less damaging to turbine blades
- Loss pressure of exhaust gas through the heat recovery not more than 150 mmWC (MAN Diesel & Turbo, 2004).
- Available space in the exhaust gas funnel to accommodate the HRSG
- Exhaust gas outlet temperature not higher than 165 ° C in case of using HFO (MAN Diesel & Turbo, 2004), to avoid the formation of particularly corrosive sulphuric anhydride.

Output data of significant interest are:

- Steam turbine power, calculated through the equation (3.20)
- Fuel exploitation index, calculated as in equation (3.21)

$$P_{ST} = \dot{m}_{ST} \, (H_{in} - H_{out}) \, \eta_{ST} \tag{3.20}$$

Where:

- $\dot{m}_{ST}$ is the steam mass flow rate expanded in the steam turbine;
- H_{in} and H_{out} are the inlet and outlet steam turbine enthalpies, respectively;

- η_{ST} is the turbine efficiency at design point, whose value taken equal to 0.67 has been found in literature (Dimopoulos G. G. et al., 2011).

$$I_{fuel} = \frac{P_B + P_{ST} + \Phi_{SS} - P_{FWP} - P_{CWP}}{(\dot{m}_{fuel} + \Delta\dot{m}_{fuel}) * LHI} \, 100 \tag{3.21}$$

Where:

- P_B is the brake power of the main engine;
- Φ_{SS} heat flux required by steam services;
- P_{FWP} is the power required by pump to boost feeding water, calculated through the equation (3.22);
- P_{CWP} is the power required by condenser cooling water pump , calculated through the equation (3.23);
- $\dot{m}_{fuel}$ is the fuel mass flow rate of the main engine;
- $\Delta\dot{m}_{fuel}$ is the increase of fuel consumption due to the backpressure provided by the heat steam generator. The evaluation of this adding fuel is calculated through a correlation found in literature (Mylaudy Dr. S. & Naveen. S., 2015);
- LHI is the lower heat value of fuel;
- Weight of the heat recovery steam generator, evaluated through a correlation related to the volume occupied;
- Vertical dimension of the heat recovery steam generator, evaluated knowing the size of the tube bundles and adopting a clearance as found in technical specification of a heat recovery steam generator available on the market (SAACKE MARINE SYSTEMS).

$$P_{FWP} = \frac{\dot{m}_{WF} \, g \, h}{\eta_P \, \eta_{EL}} \tag{3.22}$$

Where:

- $\dot{m}_{WF}$ is the feeding water flow rate;
- h is the pump head;
- η_P is the pump efficiency;
- η_{EL} is the electrical efficiency.

$$P_{CWP} = \frac{\dot{m}_{CW} \, g \, h}{\eta_P \, \eta_{EL}} \tag{3.23}$$

Where:

- $\dot{m}_{CW}$ è is the condenser cooling water flow rate, calculated through a simple balance equation of the heat flux occurring in the condenser.

3.5 SINGLE PRESSURE HEAT RECOVERY SYSTEM

As regards the single pressure steam plant, two types have been considered, one producing saturated steam (as shown in Figure 3.10) and one able to superheat the steam (as shown in Figure 3.11). The equations governing the heat exchange of the saturated steam plant are listed below:

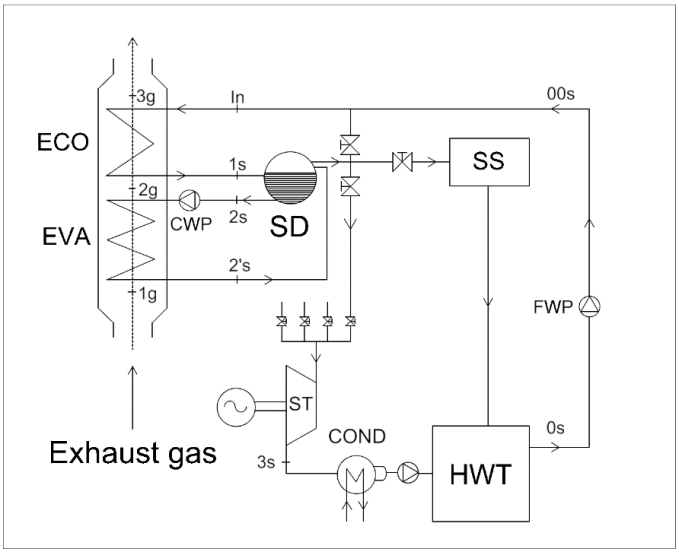

Figure 3.10. Waste heat recovery system (single pressure saturated steam) layout (Altosole et al., 2015)

$$\dot{m}_S = \dot{m}_{SS} + \dot{m}_{ST} + \dot{m}_{PH\ ECO} \tag{3.24}$$

Where:

- $\dot{m}_{SS}$ is the steam mass flow rate used for steam services;
- $\dot{m}_{PH\ ECO}$ is the steam mass flow rate bled from the steam drum and mixed with inlet feeding water in order to increase the temperature of inlet water to 130°C (Livanos G. A. et al., 2014).

$$\dot{m}_{S\ VAP} = \dot{m}_S + \dot{m}_{riliq} \tag{3.25}$$

Where:

- $\dot{m}_{S\ VAP}$ is the steam mass flow rate flowing in the evaporator;
- $\dot{m}_{riliq}$ is the part of $\dot{m}_{S\ VAP}$ that liquefies cause the subcooling difference temperature.

$$\dot{m}_S = \dot{m}_{PH\ ECO} + \dot{m}_{FW} \tag{3.26}$$

$$\dot{m}_{ST} = \dot{m}_S - \dot{m}_{PH\ ECO} - \dot{m}_{SS} \tag{3.27}$$

$$\dot{m}_S\,(H_{1S} - H_{In}) = \dot{m}_g\,c_{pg}\,(T_{2g} - T_{3g}) \tag{3.28}$$

Where:

- H_{1S} is the outlet enthalpy of water in the economizer, it is calculated as function of water pressure and temperature T_{1S}, as in equation (3.29);
- H_{In} is the inlet enthalpy of water in the economizer;
- $\dot{m}_g$ is the exhaust gas mass flow rate;
- c_{pg} is the specific heat at constant pressure;
- T_{2g} is the exhaust gas temperature at the inlet of economizer, calculated as in equation (3.30);
- T_{3g} is the exhaust gas temperature at the outlet of economizer.

$$T_{1S} = T_{2S} - \Delta T_{SC} \tag{3.29}$$

Where T_{2S} is the saturated steam temperature.

$$T_{2g} = T_{2S} + \Delta T_{pp} \tag{3.30}$$

$$\dot{m}_S\,(H_{2S} - H_{1S}) = \dot{m}_{riliq}\,(H_{2\prime S} - H_{2S}) \tag{3.31}$$

Where:

- H_{2S} is the enthalpy of steam at the inlet of evaporator;
- $H_{2\prime S}$ is the enthalpy of steam at the outlet of evaporator.

$$\dot{m}_{S\,VAP}\,(H_{2\prime S} - H_{2S}) = \dot{m}_g c_{pg}\,(T_{1g} - T_{2g}) \tag{3.32}$$

Where:

- T_{1g} is the exhaust gas temperature at the inlet of heat recovery steam generator;
- T_{2g} is the exhaust gas temperature at the outlet of the evaporator.

$$\dot{m}_{PH\,ECO}\,H_{2\prime S} + \dot{m}_{FW}\,H_{00S} = \dot{m}_S\,H_{In} \tag{3.33}$$

Where H_{00S} is the enthalpy of the feeding water.

$$H_{0S} = \frac{\dot{m}_{ST}\,H_{oCOND} + \dot{m}_{SS}\,H_{oSS}}{\dot{m}_{FW}} \tag{3.34}$$

Where:

- H_{oSS} is the enthalpy of steam at the outlet of steam services circuit;
- H_{oCOND} is the enthalpy of the water at outlet of the condenser;
- H_{0S} is the enthalpy of the feeding at the outlet of the hot well tank.

The unknowns of the problem are:

- $\dot{m}_{PH\ ECO}$
- $\dot{m}_S$
- $\dot{m}_{FW}$
- $\dot{m}_{S\ VAP}$
- $\dot{m}_{riliq}$
- $\dot{m}_{ST}$
- T_{3g}

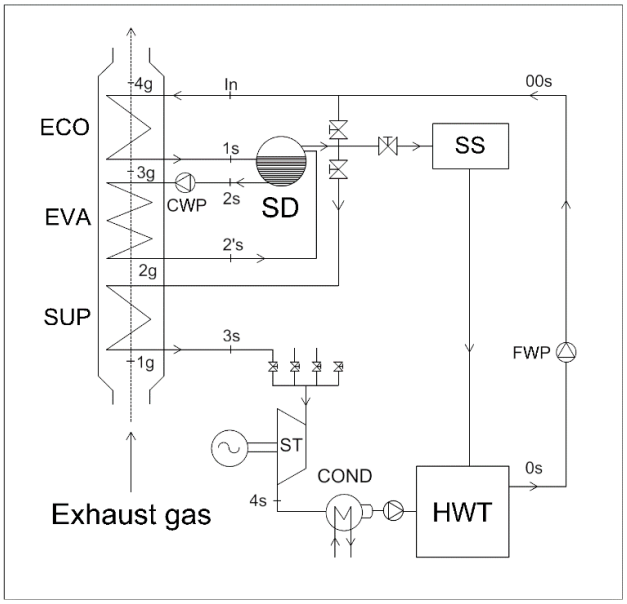

Figure 3.11. Waste heat recovery system (single pressure superheated steam) layout

The equations that model heat exchanges in the single pressure superheated steam plant are the equations: (3.24), (3.25), (3.26), (3.27), (3.30), (3.31), (3.33) and others as follows:

$$\dot{m}_S\ (H_{1S} - H_{In}) = \dot{m}_g\ c_{pg}\ (T_{3g} - T_{4g}) \tag{3.35}$$

Where:

- T_{3g} is the exhaust gas temperature at the outlet of the economizer;
- T_{4g} is the exhaust gas temperature at the outlet of the HRSG.

$$\dot{m}_S\ (H_{1S} - H_{In}) = \dot{m}_g\ c_{pg}\ (T_{3g} - T_{4g}) \tag{3.36}$$

$$T_{3g} = T_{2S} + \Delta T_{pp} \tag{3.37}$$

$$\dot{m}_{S\,VAP}\,(H_{2\prime S} - H_{2S}) = \dot{m}_g c_{pg}\left(T_{2g} - T_{3g}\right) \tag{3.38}$$

Where T_{2g} is exhaust gas temperature at the outlet of the superheater.

$$\dot{m}_{ST}\,(H_{3S} - H_{2\prime S}) = \dot{m}_g\,c_{pg}\left(T_{1g} - T_{2g}\right) \tag{3.39}$$

Where H_{3S} is the enthalpy at the inlet of the steam turbine, calculated as function of steam pressure and temperature T_{3S} that is calculated as in equation (3.40).

$$T_{3S} = T_{1g} - \Delta T_{ap} \tag{3.40}$$

The unknowns of the problems are:

- $\dot{m}_{PH\,ECO}$
- $\dot{m}_S$
- $\dot{m}_{FW}$
- $\dot{m}_{S\,VAP}$
- $\dot{m}_{riliq}$
- $\dot{m}_{ST}$
- T_{4g}
- T_{2g}

3.6 DOUBLE PRESSURE HEAT RECOVERY SYSTEM

With regard to the double pressure heat recovery system, two types have been considered, one operating with saturated steam (as shown in Figure 3.12) and one producing superheated steam (as shown in Figure 3.13). The equations governing the heat exchange of the saturated steam plant are listed below:

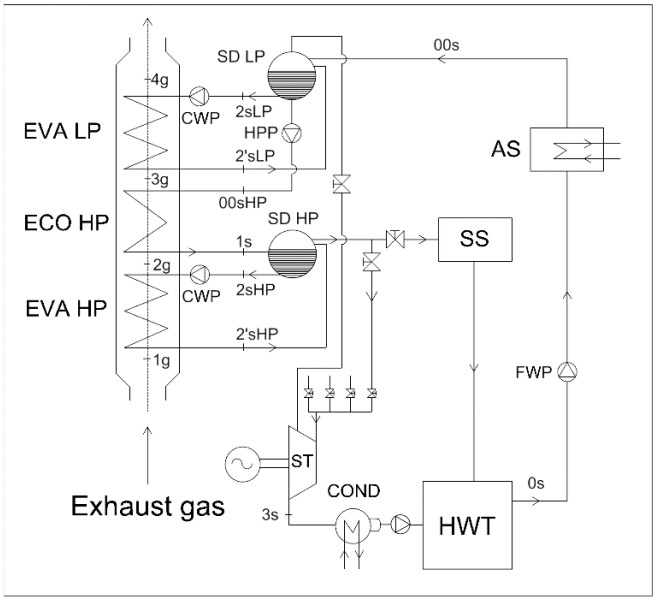

Figure 3.12. Waste heat recovery system (double pressure saturated steam) layout

$$\dot{m}_{S\,HP}\,(H_{1S\,HP} - H_{00S\,HP}) = \dot{m}_g\,c_{pg}\,(T_{2g} - T_{3g}) \tag{3.41}$$

Where:

- $\dot{m}_{S\,HP}$ is the steam mass flow rate at the outlet of high pressure evaporator;
- $H_{1S\,HP}$ is the steam enthalpy at inlet of high pressure economizer, calculated as function of the high pressure and the steam temperature $T_{1S\,HP}$;
- $H_{00S\,HP}$ is the enthalpy of the water at the inlet of high pressure economizer;
- T_{2g} is the exhaust gas temperature at the inlet of the high pressure economizer, calculated as in equation (3.30);
- T_{3g} is the exhaust gas temperature at the outlet of the high pressure economizer.

$$\dot{m}_{S\,HP}\,(H_{2S\,HP} - H_{1S\,HP}) = \dot{m}_{riliq\,HP}\,(H_{2'S\,HP} - H_{2S\,HP}) \tag{3.42}$$

Where:

- $H_{2S\,HP}$ is the enthalpy of saturated water at the inlet of high pressure evaporator;

- $\dot{m}_{riliq\ HP}$ is the part of steam that liquefies cause the subcooling difference temperature;
- $H_{2'S\ HP}$ is the enthalpy of dry steam of the high pressure circuit.

$$\dot{m}_{S\ VAP\ HP}\ (H_{2'S\ HP} - H_{2S\ HP}) = \dot{m}_g\ c_{pg}\ (T_{1g} - T_{2g}) \tag{3.43}$$

Where:

- $\dot{m}_{S\ VAP\ HP}$ is the mass flow rate of vaporized water in the high pressure evaporator tubes;
- T_{1g} is the exhaust gas temperature at the inlet of the HRSG.

$$\dot{m}_{S\ VAP\ HP} = \dot{m}_{S\ HP} + \dot{m}_{riliq\ HP} \tag{3.44}$$

$$\dot{m}_{S\ LP}\ (H_{2S\ LP} - H_{1S\ LP}) = \dot{m}_{riliq\ LP}\ (H_{2'S\ LP} - H_{2S\ LP}) \tag{3.45}$$

Where:

- $\dot{m}_{S\ LP}$ is the mass flow rate of water at the inlet of HRSG;
- $H_{2S\ LP}$ is the enthalpy of saturated water at the inlet of low pressure evaporator;
- $\dot{m}_{riliq\ LP}$ is the part of steam that liquefies cause the subcooling difference temperature;
- $H_{2'S\ LP}$ is the enthalpy of dry steam at the outlet of low pressure evaporator;
- $H_{1S\ LP}$ is the enthalpy of the water at the inlet of low pressure economizer, calculated as function of pressure and the temperature $T_{1S\ LP}$ that is evaluated through the equation (3.29).

$$\dot{m}_{S\ VAP\ LP}\ (H_{2'S\ HP} - H_{2S\ HP}) = \dot{m}_g\ c_{pg}\ (T_{3g} - T_{4g}) \tag{3.46}$$

Where:

- $\dot{m}_{S\ VAP\ LP}$ is the mass flow rate of vaporized water in the low pressure evaporator tubes;
- T_{4g} is the exhaust gas temperature at the outlet of the HRSG, calculated as in equation (3.30).

$$\dot{m}_{S\ VAP\ LP} = \dot{m}_{S\ LP} + \dot{m}_{riliq\ LP} - \dot{m}_{S\ HP} \tag{3.47}$$

$$\dot{m}_{ST\ LP} = \dot{m}_{S\ LP} - \dot{m}_{S\ HP} \tag{3.48}$$

Where $\dot{m}_{ST\ LP}$ is the low-pressure mass flow rate of steam expanding in the steam turbine.

$$\dot{m}_{ST\ HP} = \dot{m}_{S\ HP} - \dot{m}_{SS} \tag{3.49}$$

Where $\dot{m}_{ST\ HP}$ is the high-pressure mass flow rate of steam expanding in the steam turbine.

The unknowns of the problem are:

- $\dot{m}_{S\,HP}$
- T_{3g}
- $\dot{m}_{riliq\,HP}$
- $\dot{m}_{S\,VAP\,HP}$
- $\dot{m}_{S\,LP}$
- $\dot{m}_{riliq\,LP}$
- $\dot{m}_{S\,VAP\,LP}$
- $\dot{m}_{ST\,LP}$

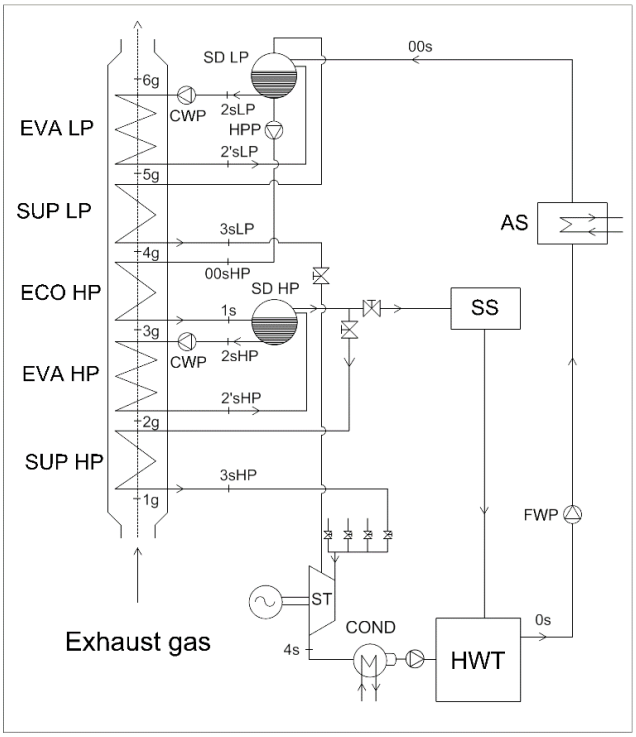

Figure 3.13. Waste heat recovery system (double pressure superheated steam) layout

$$\dot{m}_{S\,LP}\,(H_{2S\,LP} - H_{In}) = \dot{m}_{riliq\,LP}\,(H_{2'S\,LP} - H_{2S\,LP}) \tag{3.50}$$

$$\dot{m}_{S\,VAP\,LP}\,(H_{2'S\,LP} - H_{2S\,LP}) = \dot{m}_{g}\,c_{pg}\,(T_{5g} - T_{6g}) \tag{3.51}$$

Where:

- T_{5g} is the exhaust gas temperature at the inlet of low pressure evaporator;
- T_{6g} is the exhaust gas temperature at the outlet of the HRSG.

$$\dot{m}_{S\,VAP\,LP} = \dot{m}_{S\,LP} + \dot{m}_{riliq\,LP} - \dot{m}_{S\,HP} \tag{3.52}$$

$$\dot{m}_{ST\,LP} = \dot{m}_{S\,VAP\,LP} - \dot{m}_{riliq\,LP} \tag{3.53}$$

$$\dot{m}_{ST\,LP}\,(H_{3S\,LP} - H_{2'S\,LP}) = \dot{m}_g\,c_{pg}\,(T_{3g} - T_{4g}) \tag{3.54}$$

Where:

- $H_{3S\,LP}$ is the enthalpy of the low pressure steam at the inlet of steam turbine, that is calculated as function of pressure and temperature $T_{3S\,LP}$ (calculated as in equation (3.55);
- T_{4g} is the exhaust gas temperature at the inlet of low pressure superheated.

$$T_{3S\,LP} = T_{3g} - \Delta T_{ap\,LP} \tag{3.55}$$

Where T_{3g} is the exhaust gas temperature at the outlet of low pressure superheated, calculated as in equation (3.56).

$$T_{3g} = T_{2S\,HP} + \Delta T_{pp\,HP} \tag{3.56}$$

$$\dot{m}_{S\,HP}\,(H_{1S\,HP} - H_{00S\,HP}) = \dot{m}_g\,c_{pg}\,(T_{4g} - T_{5g}) \tag{3.57}$$

$$\dot{m}_{S\,VAP\,HP}\,(H_{2'S\,HP} - H_{2S\,HP}) = \dot{m}_g\,c_{pg}\,(T_{2g} - T_{3g}) \tag{3.58}$$

Where T_{2g} is the exhaust gas temperature at the outlet of high pressure superheated.

$$\dot{m}_{S\,HP}\,(H_{2S\,HP} - H_{1S\,HP}) = \dot{m}_{riliq\,HP}\,(H_{2'S\,HP} - H_{2S\,HP}) \tag{3.59}$$

$$\dot{m}_{S\,VAP\,HP} = \dot{m}_{S\,HP} + \dot{m}_{riliq\,HP} \tag{3.60}$$

$$\dot{m}_{ST\,HP} = \dot{m}_{S\,HP} - \dot{m}_{SS} \tag{3.61}$$

$$\dot{m}_{ST\,HP}\,(H_{3S\,LP} - H_{2'S\,LP}) = \dot{m}_g\,c_{pg}\,(T_{1g} - T_{2g}) \tag{3.62}$$

Where $H_{3S\,HP}$ is the enthalpy of steam at inlet of steam turbine that is calculated as function of the pressure and temperature $T_{3S\,HP}$, calculated as in equation (3.55).

$$T_{3S\,HP} = T_{1g} - \Delta T_{ap\,HP} \tag{3.63}$$

The unknowns of the problem are:

- $\dot{m}_{S\ HP}$
- $\dot{m}_{riliq\ HP}$
- $\dot{m}_{S\ VAP\ HP}$
- T_{2g}
- T_{4g}
- T_{5g}
- $\dot{m}_{ST\ LP}$
- $\dot{m}_{ST\ HP}$
- $\dot{m}_{S\ LP}$
- $\dot{m}_{riliq\ LP}$
- $\dot{m}_{S\ VAP\ LP}$

4 CASE STUDY

4.1 CUURENT AND RENEW POWERING OF A RO/RO PAX FERRY

The vessel selected as a case study is a Ro/Ro Pax Ship of the Grandi Navi Veloci shipping company, built in 2002. Currently the ferry operates the Genoa-Palermo route sailing six days per week in the winter months and seven days per week in the summer months. The daily operating profile includes 19 hours of navigation, one hour of manoeuvre and 4 hours for the goods/passenger embarking/disembarking phase. Figure 4.1 shows the longitudinal view of the ferry while the main characteristics of the ship are shown in Table 4.1.

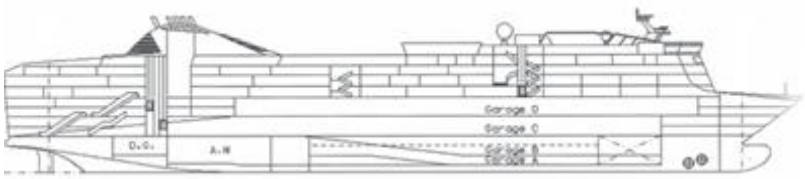

Figure 4.1. Longitudinal section of the cruise ferry

Table 4.1. Main characteristics of the ship

SHIP		
Length overall	[m]	211.5
Breadth (maximum)	[m]	30.4
Draught	[m]	7.83
Gross tonnage	[gt]	49257
Service speed	[kt]	23.5
Lane capacity	[m]	2800
Pax capacity	[-]	2920

The propulsive system consists of 2 propellers driven by 2 diesel engines per shaft (under normal navigation conditions, only one engine per shaft running at about 80% of the maximum load). The generation of electricity is carried out by 4 generator sets. The characteristics regarding propulsion and power generation are shown in Table 4.2.

Table 4.2. Main characteristics of the ship propulsion and electrical system

PROPULSION AND ELECTRIC GENERATORS		
Engine Type		4*16V46C
Nominal power	[kW]	16800
Nominal speed	[rpm]	500
Fuel	[-]	HFO
Generator set type		4*6R32LNE
Nominal power	[kW]	2430
Nominal speed	[rpm]	720
Fuel	[-]	HFO/MDO

The electrical load required according to the different operating profiles and the number of running electric generators to supply it are shown in Table 4.3.

Table 4.3. Electric power demand for different operating conditions

		Summertime sea going	Wintertime sea going	Manoeuvring	Port staying
Electric power	[kW]	4565	3374	4786	2886
# Running generators	[-]	3	2	3	2

The steam users demand on board the ferry is about 2708 kWt at 3 t/h of saturated steam at 6/7 bar. There are currently 4 economizers and 2 oil-fired boilers. Figure 4.2 shows the diagram of the current on board steam generation system.

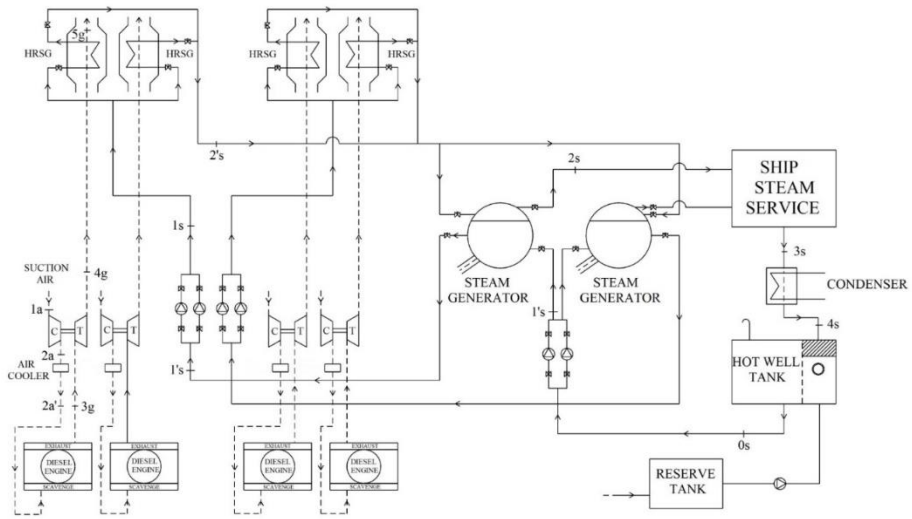

Figure 4.2. Current layout of the steam generation plant installed on board

In this study, the replacement of current engines and diesel generators powered by HFO with dual fuel engines has been considered. The main features of the selected engines are shown in Table 4.4.

Table 4.4. Main characteristics of the ship propulsion and electrical system selected for repowering case

DF PROPULSION AND ELECTRIC GENERATORS		
Engine Type		4*18V51/60 DF
Nominal power	[kW]	17550
Nominal speed	[rpm]	500
Fuel	[-]	NG/HFO
Generator set type		4*6L35/44 DF
Nominal power	[kW]	2953
Nominal speed	[rpm]	720
Fuel	[-]	NG/MDO

Considering that the use of natural gas as fuel would not require any heating compared to the HFO, then the renew demand for thermal flow is 815 KW (value communicated by the chief engineer of the ship). In this study, it was considered that the use of HFO occurs only in the event of a failure of the gas supply system and so the amount of HFO required could be calculated as for a round trip. Since this amount of HFO should be always ready for the use and therefore warm to be pumped as needed. The new required heat flow is 1893 KW. This quantity is calculated considering that the heat flow is proportional to the amount of fuel on board. The input data considered as a design point, needed to estimate the best recovery system solution, are reported in Table 4.5.

Table 4.5. Input data design point

INPUT DATA		
Engine Type		18V51/60 DF
Running engines	[-]	2
Nominal power	[kW]	17550
Load factor	[-]	0.75
Exhaust gas temperature after turbine	[°C]	350
Exhaust air flow	[kg/s]	24.883
Exhaust fuel flow	[kg/s]	0.675
Fuel	[-]	NG

Figure 4.3 shows a section of the casing of the economizers of the ship. Consulting the technical drawings and thanks to the advisory of marine superintendent of this ship, it has been set that the max footprint to accommodate the heat recovery steam generators could be 1.85 m x 2.1 m. (the original are 1.65 m x 1.9 m).

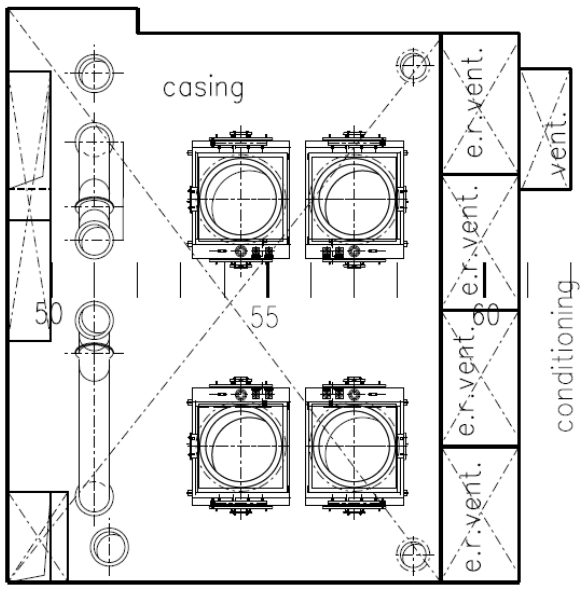

Figure 4.3. Layout of current steam generators on-board the ship

With regard to the maximum vertical dimension that could be used to accommodate the heat steam generator, the max value is 7 m. The geometry of the tube bundles is shown in Table 4.6 and a representation is shown in Figure 4.4.

Table 4.6. Characteristics of the Heat recovery components

HEAT RECOVERY GEOMETRY		
Type		Tube bundle
De	[mm]	38
S_T	[mm]	76
S_H	[mm]	76
h_f	[mm]	12.7
t_f	[mm]	2
L_f	[mm]	11

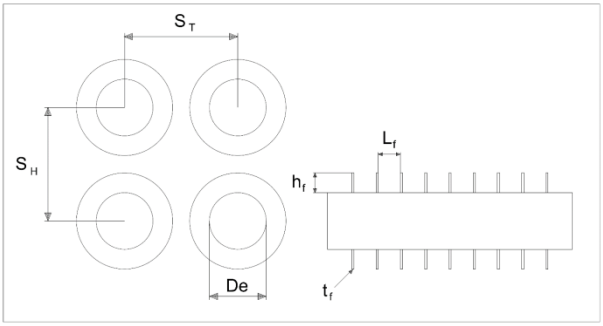

Figure 4.4. Tubular heat exchanger

4.2 SELECTION OF THE PARAMETERS SET

In order to get the set of parameters that maximizes fuel exploitation, a MATLAB code was written. The code implements the energy balance equations and the equations dedicated to the sizing of the heat recovery steam generator as described above. The computing code executes the calculations for different parameters values that are systematically changed. The value of the parameters and the step used for each type of the examined recovery plant is reported in Table 4.7 (where number 1 refers to the saturated steam single pressure plant, number 2 refers single pressure superheated steam, number 3 refers to the double pressure saturated steam plant and number 4 refers to the double pressure superheated plant). The optimal parameter set is the one maximizing fuel exploitation.

Table 4.7. Parameters and values for optimisation calculations

PARAMETERS AND VALUES					
		WHR TYPOLOGY			
		1	2	3	4
p_{HP}	[bar]	7 - 12	7 - 12	7 - 12	7 - 12
p_{LP}	[bar]	-	-	3.5 - 4.5	3.5 - 4.5
p_{COND}	[bar]	0.065 - 0.2	0.065 - 0.2	0.065 - 0.2	0.065 - 0.2
$\Delta T_{pp\,HP}$	[°C]	30 - 90	30 - 90	40 - 100	30 - 90
$\Delta T_{pp\,LP}$	[°C]	-	-	40 - 100	50 - 90
$\Delta T_{ap\,HP}$	[°C]	-	50 - 110	-	50 - 110
$\Delta T_{ap\,LP}$	[°C]	-	-	-	50 - 110

Table 4.8 shows the set of parameters that maximize the fuel utilization index of each recovery system considered.

Table 4.8. Set of parameters values for optimized design

SELECTED VALUES					
		WHR TYPOLOGY			
		1	2	3	4
p_{HP}	[bar]	7	7	9.9	10
p_{LP}	[bar]	-	-	3.7	3.6
p_{COND}	[bar]	0.13	0.065	0.13	0.065
$\Delta T_{pp\,HP}$	[°C]	37	34	90	73
$\Delta T_{pp\,LP}$	[°C]	-	-	52	68
$\Delta T_{ap\,HP}$	[°C]	-	104	-	62
$\Delta T_{ap\,LP}$	[°C]	-	-	-	68

Table 4.9 shows the main results obtained for each recovery plant studied.

Table 4.9. Results of optimized solutions

MAIN RESULTS OF STUDY					
		WHR TYPOLOGY			
		1	2	3	4
I_{fuel}	[%]	50.82	51.04	51.18	51.21
$P_{\%}$	[%]	4.55	5.20	5.50	5.55
P_{ST}	[kW]	1198	1370	1447	1461
$\Delta\dot{m}_{fuel}$	[%]	1.32	1.47	1.465	1.45
Δp_{HRSG}	[mmWC]	133.94	148.48	148.28	146.6
T_{EG}	[°C]	199	193	192	208
x_S	[-]	0.9	1	0.9	0.95
H_{HRSG}	[m]	6.38	6.66	6.71	6.44
W_{HRSG}	[ton]	16.85	17.72	17.88	17.25
$Fuel\ saving$	[%]	3.39	3.81	4.03	4.08
$Payback$	[years]	4.43	4.53	5.21	5.06

The installation of a recovery plant as the ones described in Table 4.9 allows turning off one diesel-generators during navigation. Choosing the best plant design depends on many factors; one of the most important to be considered is the fuel saving (calculated by equation (4.1). From Table 4.9 it is noted that this value does not have significant deviations based on the selected plant solution.

$$I_{fuel} = \frac{m_{fuel} - m_{fuelWHRS}}{m_{fuel}} 100 \quad (4.1)$$

Where:

- m_{fuel} is the amount of fuel burned per year without the adoption of a recovery system;
- $m_{fuelWHRS}$ is the amount of fuel burned per year considering the installation of a recovery system.

Through the WHR 1, it is possible to achieve the lowest payback time (calculated as in equation (4.2)), and it is the easiest type of system to build and install (the presence of a superheater leads to increased maintenance costs).

$$Payback\ Time = \frac{C_{WHRS}}{(m_{fuel} - m_{fuelWHRS})\, C_{fuel}} \quad (4.2)$$

Where:

- C_{WHRS} is the cost of the WHRS which includes the cost of the steam turbine generator (steam turbine + alternator + condenser) computed as in equation (4.3); and the cost of steam generator (Livanos G. A. et al., 2014).
- C_{fuel} is the cost of fuel, taken as 477 €/ton (Livanos G. A. et al., 2014)

$$C_{ST} = \alpha_C\, {P_{ST}}^{0.9} \quad (4.3)$$

The equation (4.3) is structured for modelling the economy of scale, and the coefficient α_C was calibrated through data obtained from bibliography (Livanos G. A. et al., 2014). With regard to double pressure systems, a cost increase of 20% was assumed.

Summing up, the advantages offered by a plant at a saturated steam pressure level:

- No overheating (lower maintenance cost)
- Simplicity of system (compared to double pressure levels)
- Greater reliability
- Less weight
- Minor exchange area with less backpressure

Figure 4.5 shows the heat exchanged in the heat recovery steam generator and the temperature regarding the selected plant.

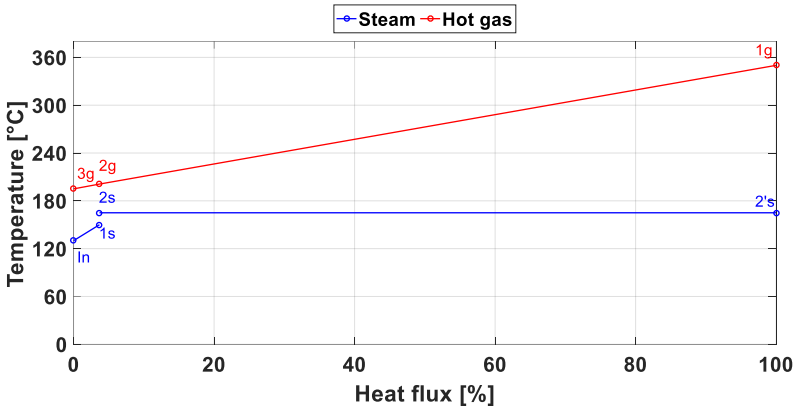

Figure 4.5. Temperature vs heat flux in WHR 1

4.3 OFF-DESIGN CONDITION

The selected plant for the study in off-design is the WHR 1. For the evaluation of the performance in off design condition, a MATLAB code was written. The geometry of the recovery system and the upstream conditions of the exhaust gases are the input data. The conceptual layout of the code is shown in Figure 4.6.

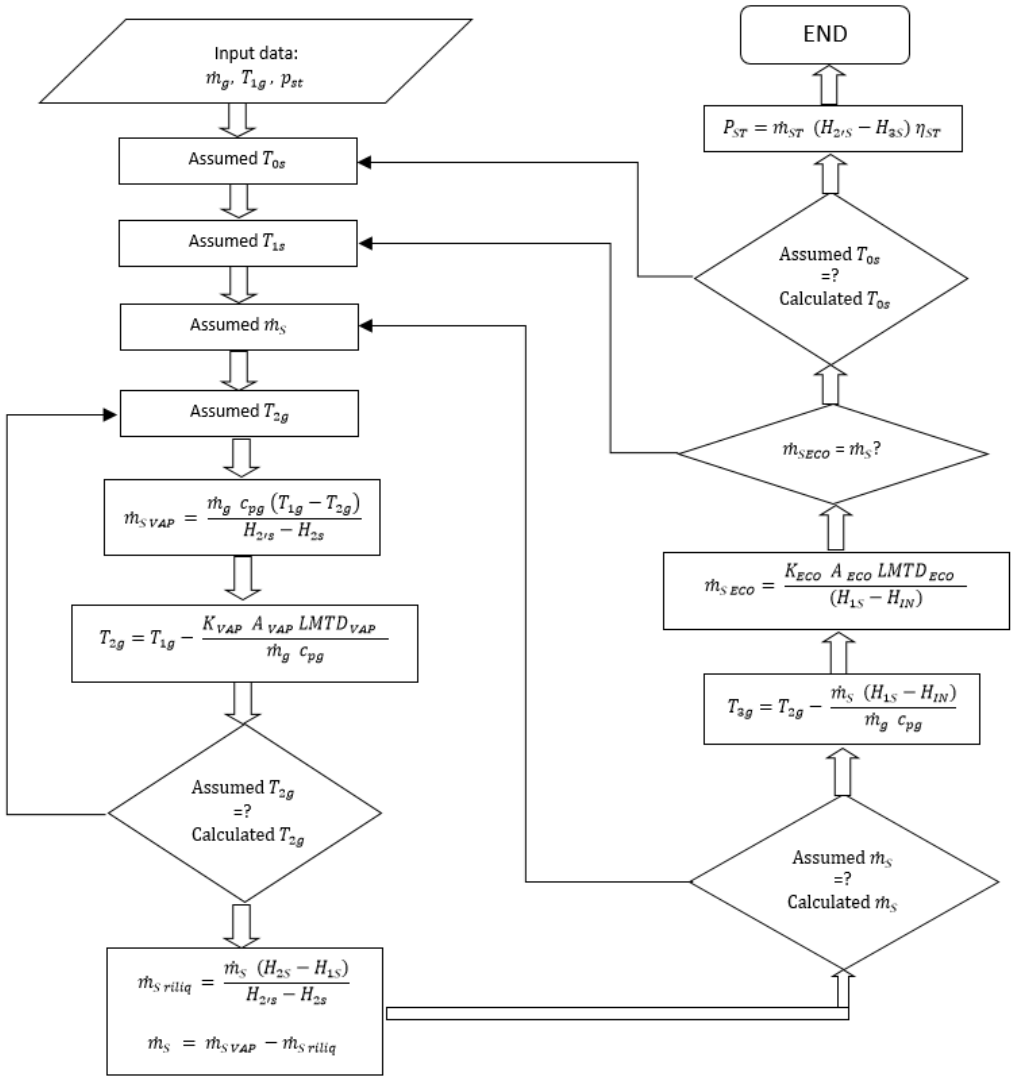

Figure 4.6. Flow chart of conceptual layout for off design condition

When operating the HFO, the backpressure in heat recovery plant increases due to excess air of diesel engine. To solve this problem, it is advisable to bypass some of the exhaust gases in an alternative duct. The calculation code evaluates the maximum amount of exhaust gas that flow through the recovery system at each load condition both in gas and in HFO mode. The heat balance of the mixed gas calculates the exhaust gas temperature at the funnel outlet. The sizing of the bypass duct, considering an acceptable maximum speed of 40 m/s (MAN 51/60DF Project Guide) referring to the 100% maximum load condition by burning HFO, is carried out. The performances of the steam turbine (so the value of the machine efficiency) vary by the steam mass flow rate expanding in the turbine. The variation of the performance is carried out adopting the same values found in bibliography (Dimopoulos G. G. et al., 2011). Table 4.10 shows the main results of the simulation for different load conditions related to gas mode operation, while in Table 4.11 those pertinent to diesel mode.

Table 4.10. Off-design results gas mode

GAS MODE/OFFDESIGN					
		ENGINE LOAD			
		0.5	**0.75**	**0.85**	**1**
m_g	[kg/s]	17.31	25.45	25.57	29.44
T_{1g}	[°C]	387	350	358	341
$m_{gBYPASS}$	[kg/s]	0	0	0	2.43
T_{EG}	[°C]	187	199	200	211
Δp_{HRSG}	[mmWC]	63.65	133.94	136.33	150
P_{ST}	[kW]	1012	1198	1275	1177
I_{fuel}	[%]	51.34	50.82	50.47	50.26

Table 4.11. Off-design results diesel mode

DIESEL MODE/OFFDESIGN					
		ENGINE LOAD			
		0.5	**0.75**	**0.85**	**1**
m_g	[kg/s]	21.21	31.11	32.45	35.59
T_{1g}	[°C]	338	297	313	323
$m_{gBYPASS}$	[kg/s]	0	3.46	5.05	8.31
T_{EG}	[°C]	192	205	214	226
Δp_{HRSG}	[mmWC]	91.45	150	150	150
P_{ST}	[kW]	826	703	872	985
I_{fuel}	[%]	49.29	48.23	49.03	48.34

Note that at the 0.75 diesel mode the turbine power decreases as much as the T1g is low.

Figure 4.7 shows the power produced by the steam turbine for different engine loads.

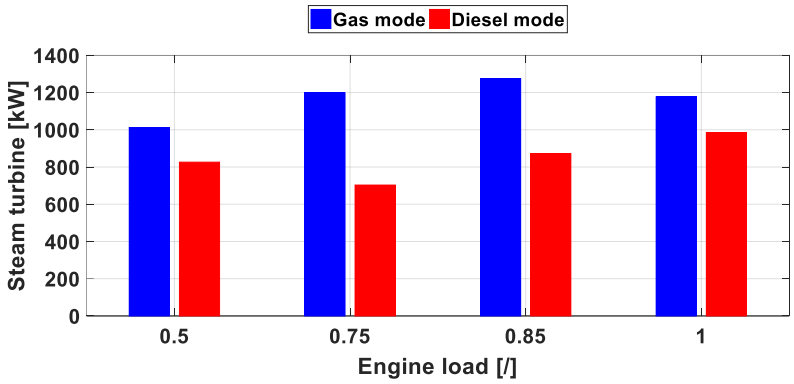

Figure 4.7. Steam power turbine vs engine load

4.4 CONSIDERATIONS ON LNG TANK ANS INVESTMENT COST

Yearly LNG consumption of vessel operation (considering the saving benefit offered by the selected WHR) is 32603 tons (consumption of main engines, generating sets and boilers for steam production during the time at berth). Considering that the storage of LNG on board allows averagely a range of 400 miles (Alberto Quarati, 2015) and considering that the sea route of the examined ferry is around 427 miles, the refuelling will have to be carried out before every departure. The capacity required by of the gas tanks is calculated as in equation (4.4).

$$LNG_{Tank} = \frac{LNG_{cons}\ FD}{Days\ \rho_{LNG}\ FL\ N_{Tanks}} \tag{4.4}$$

Where:

- LNG_{cons} is the total consumption of LNG per year;
- $Days$ are the 365 days in a solar year;
- ρ_{LNG} is the mass density, considered equal to 0.43 kg/m^3;
- FL is the filling limit of tank, supposed equal to 0.95 (WARTSILA Gas Systems, 2014) ;
- N_{Tanks} is the number of LNG tanks installed on board: two tanks were considered.
- FD is the factor design introduced to take into account the increased consumption due to adverse sea conditions or other reasons why gas consumption may increase. An increase of 30% of fuel on board was decided.

The calculated tank capacity of is 131 m^3. Referring to the LNGPAC product guide, the 145 m^3 capacity has been selected; the main technical data are shown in Table 4.12. Regarding the amount of MDO burned for DG's operation, one week of endurance is considered. Considering that the amount of pilot flame is equal to 1% (Livanos G. A. et al., 2014) of LNG consumption, an amount of MDO equal to 6.32 tons is needed.

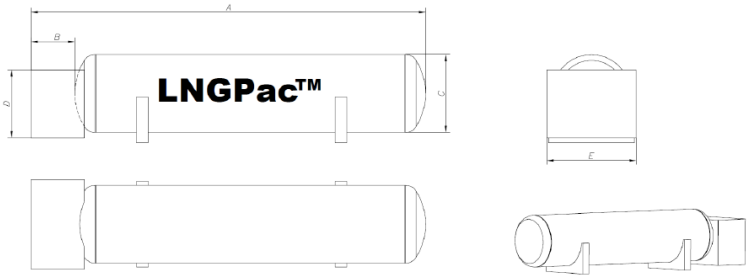

Figure 4.8. LNG tank layout

Table 4.12. Features of selected LNG tank

WARTSILA LNGPAC		
A	[m]	19.2
B	[m]	2.3
C	[m]	4.1
D	[m]	3.2
E	[m]	3.0
Inner volume	[m^3]	145
Operational weight	[ton]	140

As for steam turbine installation, dimensions and weights can refer to products available on the market (MHI, Steam turbine generator); the features considered for this study are shown in Table 4.13.

Table 4.13. Features of selected steam turbine installation

MAIN FEATURES OF TURBOGENERATOR		
Width	[m]	1.6
Length	[m]	3.785
Height	[m]	1.89
Weight	[ton]	6

Table 4.14 reports the main features in terms of weight and dimensions of old and new engine set.

Table 4.14. Features new and old main engine and generating set

PROPULSION AND ELECTRIC GENERATORS			
Engine Type		16V46C	18V51/60 DF
Width	[m]	5.35	4.73
Length	[m]	12.345	12.088
Height	[m]	5.5	5.517
Weight	[ton]	225	265
Generator set type		6R32LNE	6L35/44 DF
Width	[m]	2.49	2.958
Length	[m]	8.5	10.17
Height	[m]	3.745	4.631
Weight	[ton]	57	85

4.5 CONSIDERATIONS ON SHIP STABILITY

In order to check the stability and trim of the gas fuelled ferry configuration, the Table 4.15 reports the main hydrostatic properties (gotten from stability booklet) at full load summer condition.

Table 4.15. Hydrostatic properties from Stability booklet of the ship. Full load condition (Original condition)

ORIGINAL HYDROSTATIC PROPERTIES		
T_O	[m]	7.83
Δ_O	[ton]	28358
VCG_O	[m]	13.215
LCG_O	[m]	83.914
GMT_O	[m]	3.693

An appropriate area where placing the LNG tanks on board would require a very detailed study. In this first stage of feasibility study, it would be possible to arrange the LNG tank inside the ship's hull beside the engine room in an area that is currently part of the garage deck at the third level, as shown in Figure 4.9.

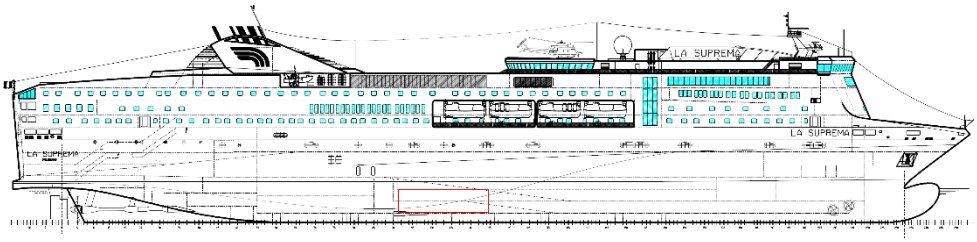

Figure 4.9. Possible installation of LNG tank (red box)

This kind of choice presents the following advantages:

- Low centre of gravity of the ship
- Reduction of gas piping, so less leakage in case of failure
- Most protected area against mechanical damage
- Not visible to passenger eyes
- Less heat dispersion especially in summer, so less boil-off
- Easy access to bunkering stations

Table 4.16 lists the weights and positions of the main items embarked and landed.

Table 4.16. Loading and unloading items

NEW LAYOUT OF SHIP			
Loading items	z [m]	x [m]	weight [ton]
4 * 18V51/60 DF	4.5	65.62	1060
4 * 6L35/44 DF	8.3	38	340
4* HRSG	25.3	53.39	67.40
TURBOGENERATOR	8.3	38	6
CONDENSER	7	38	7
HFO	6	71	277
MDO	8.3	43.13	6.32
LNG TANK + FUEL	8.84	84.30	280
Unloading items			
4 * 16V46C	4.5	65.62	900
4 * 6R32LNE	8.3	38	228
4* ACTUAL HRSG	25.3	53.39	53
ACTUAL HFO	6	71	1665
ACTUAL MDO	8.3	43.13	181

Through the static moment theorem is possible to obtain information about the new configuration in hydrostatic terms as reported in Table 4.17.

Table 4.17. Hydrostatic properties. Full load condition (Renewed condition)

RENEWED HYDROSTATIC PROPERTIES		
T_R	[m]	7.63
Δ_R	[ton]	27315
VCG_R	[m]	13.51
LCG_R	[m]	84.59
GMT_R	[m]	3.65

4.6 TECHNICAL SOLUTIONS FOR NAVIGATION CONFORMITY IN THE MEDITERRANEAN SEA

The European Directive 2005/33 / EC provides the use of fuels with a maximum allowable sulphur content of 0.1% in European ports and 1.5% in territorial sea and exclusive economic zones. In addition, MARPOL ANNEX VI imposes the use of fuels with a sulphur content up to 0.5% from 2020. Another important maritime regulation, the MRV, is going to be introduced in Europe, addressing the ship-owners to cut CO_2 emissions in operating their ships. Several technical solutions are currently present on the maritime market in order to comply with this issue, as follows:

- Use of LNG in navigation, use of LNG in port (or cold ironing system) [TECHNICAL SOLUTION 1]
- Use of LSHF in navigation, MGO in port (or cold ironing system) [TECHNICAL SOLUTION 2]
- Scrubber system & HFO in navigation, MGO in port (or cold ironing system) [TECHNICAL SOLUTION 3]
- Scrubber system & HFO in navigation, Scrubber system & MDO in port (or cold ironing system) [TECHNICAL SOLUTION 4]

In the event that the Mediterranean becomes an NECA area, the following solutions were considered:

- Use of LNG in navigation, use of LNG in port (or cold ironing system) [TECHNICAL SOLUTION 1]
- SCR & MGO in navigation, SCR & MGO in port (or cold ironing system) [TECHNICAL SOLUTION 5]
- Scrubber system + SCR & HFO in navigation, Scrubber system + SCR & MDO for generating set (or cold ironing system in port) [TECHNICAL SOLUTION 6]

Considering as case study the ferry LA SUPREMA, Table 4.18 shows the calculated fuel consumption according to different scenarios. The calculation of the amount of fuel burned was made taking into account the fuel burned addition due to the backpressure of the HRSG generating steam for thermal users (Henriksson D. & Nymanvierto R., 2016), the presence of the scrubber (ABS, 2013) and the SCR (Fast Ferry Management, INC., 2007).

Table 4.18. Fuel consumption related to different Technical solutions investigated

FUEL CONSUMPTION [tons/year]			
	NAVIGATION	**MANOEUVERING**	**PORT**
TECHNICAL SOLUTION 1 (2020)			
ME	26453	-	
GS	4243	261	978
BOILER SS	-	57	114
TECHNICAL SOLUTION 2 (2020)			
ME	32590	-	-
GS	4883	306	1091
BOILER SS	-	149	621
TECHNICAL SOLUTION 3 (2020)			
ME	32911	-	-
GS	4883	306	1091
BOILER SS	-	149	621
TECHNICAL SOLUTION 4 (2020)			
ME	32911	-	-
GS	4883	309	1102
BOILER SS	-	149	621
TECHNICAL SOLUTION 5 (ECA)			
ME	33485	-	-
GS	5017	315	1121
BOILER SS	-	149	621
TECHNICAL SOLUTION 6 (ECA)			
ME	33815	-	-
GS	5068	318	1132
BOILER SS	-	149	621

Table 4.19 reports the amount of CO_2 emitted in one year for the considered ferry and the variation compared to the current layout for each technical solutions studied. The calculation of CO_2 emitted is calculated considering the consumption of fuel as reported in Table 4.18 and the conversion factor C_F as reported in the guidelines issued by the IMO (MEPC.245 (66), 2014).

Table 4.19. CO_2 emission

LAYOUT	**Total CO_2 [tons/year]**	**Δ CO_2 [%]**
Original	125224	0
Technical solution 1	88435	-29.4
Technical solution 1 + WHRS	85437	-31.8
Technical solution 2	128707	2.8
Technical solution 3	126223	0.8
Technical solution 4	126270	0.8
Technical solution 5	131885	5.3
Technical solution 6	129841	3.7

The LNG-fuelled ship option equipped with WHRS is the best-performed layout solution. Table 4.20 reports the CO_2 emissions when ship is at berth in term of tons and percentages of the total annual emission, and the variation compared to the current layout for each technical solutions examined.

Table 4.20. CO_2 emission at berth

LAYOUT	CO_2 at berth [tons/year]	Share of CO_2 at berth [%]	Δ CO_2 [%]
Original	3779	3.02	0
Technical solution 1	2694	3.05	-28,71
Technical solution 1 + WHRS	2694	3.15	-28,71
Technical solution 2	3779	2.94	0
Technical solution 3	3779	2.99	0
Technical solution 4	3815	3.02	0.96
Technical solution 5	3593	2.72	-4.92
Technical solution 6	3921	3.02	3.76

Table 4.22 reports the annual cost of fuel (for propulsion, electric generation and oil-fired boilers), and the part of fuel cost relating to the time spent at berth. The cost of LNG, HFO and MDO was found in literature, (Livanos G. A. et al., 2012) as the cost of MGO (Sames P., 2001). Because of uncertainty about the evolution of fuel prices over the next few years, it is not possible to know the LSHF price; so in this study it is considered that is equal to the price of MDO. Table 4.21 reports the fuel price adopted in this study.

Table 4.21. Fuel price

FUEL	PRICE [euro/ton]
LNG	477
HFO	483
MDO	676
MGO	744

Table 4.22. Ship fuel cost

LAYOUT	Annual fuel cost [ml euro/year]	Annual fuel cost at berth [ml euro/year]	Share of fuel cost at berth [%]
Original	19.839	0.796	4.01
Technical solution 1	15.314	0.796	3.04
Technical solution 1 + WHRS	14.795	0.876	3.15
Technical solution 2	27.292	0.876	3.21
Technical solution 3	21.157	0.804	4.14
Technical solution 4	21.065	0.804	3.82
Technical solution 5	30.589	0.833	2.72
Technical solution 6	21.093	0.826	3.9

A shore side power when ship is at berth could be an advantage because some points of percentage of CO_2 emitted could be saved. Regarding some information about a preliminary cost assessment, concerning the cost of main engines and generating sets, the equation (4.5) has been adopted.

$$C_E = \alpha_E P_E^{0.9} \tag{4.5}$$

Where:

- P_E is the main engine power;
- α_E is a coefficient calibrated by technical information found in literature according to the case considered (Masaki A. et al., 2014; Livanos G. A. et al., 2012).

Tank and gas supply costs have been considered as the sum of several terms, as reported in equation (4.6).

$$C_{T\&E} = C_{GVU} + C_{DWP} + C_{VR\&M} + C_{BS\&P} + C_V + C_{TANK} \quad (4.6)$$

Where:

- C_{GVU} is the cost of the Gas Valve Unit (HEC & CCDTT, 2013);
- C_{DWP} is the cost of the double walled pipe, evaluated as in equation (4.7);
- $C_{VR\&M}$ is the cost of the vent riser, evaluated as in equation (4.8);
- $C_{BS\&P}$ is the cost of bunkering station and pipe, evaluated as in equation (4.9);
- C_V is the cost if the ventilation system, evaluated as in equation (4.10);
- C_{TANK} is the cost of LNG tank, evaluated as in equation (4.11).

$$C_{DWP} = \alpha_{DWP}\sqrt{P}\, l_{DWP} \quad (4.7)$$

Where:

- α_{DWP} is a coefficient calibrated through technical information found in literature (HEC & CCDTT, 2013);
- P is the total power of users;
- l_{DWP} is the distance between the engine considered and the tanks.

$$C_{VR\&M} = \alpha_{VR\&M}\sqrt{P}\, l_{VR\&M} \quad (4.8)$$

Where:

- $\alpha_{VR\&M}$ is a coefficient calibrated through technical information found in literature (HEC & CCDTT, 2013);
- P is the total power of users;
- $l_{VR\&M}$ is the distance between the tanks and the vent mast.

$$C_{BS\&P} = \alpha_{BS\&P}\, l_{BS\&P} \quad (4.9)$$

Where:

- $\alpha_{BS\&P}$ is a coefficient calibrated through technical information found in literature (HEC & CCDTT, 2013);
- $l_{BS\&P}$ is the distance between the tanks and the bunkering station.

$$C_V = \alpha_V\, P \quad (4.10)$$

Where:

- α_{TANK} is a coefficient calibrated through technical information found in literature (HEC & CCDTT, 2013);
- V is the capacity of tanks.

$$C_{TANK} = \alpha_{TANK} V \tag{4.11}$$

Where:

- α_V is a coefficient calibrated through technical information found in literature (HEC & CCDTT, 2013);
- P is the total power of users.

The cost of the scrubber has been evaluated through the equation (4.12).

$$C_{SCRUBBER} = \alpha_{SCRUBBER} P \tag{4.12}$$

Where:

- $\alpha_{SCRUBBER}$ is a coefficient calibrated through technical information found in literature (ECDGE, 2005a);
- P is the power of the engine.

The cost of the SCR has been evaluated through the equation (4.13).

$$C_{SCR} = \alpha_{SCR} P \tag{4.13}$$

Where:

- α_{SCR} is a coefficient calibrated through technical information found in literature (Livanos G. A. et al., 2012);
- P is the power of the engine.

Table 4.23 shows the estimated plant costs for the various scenarios considered.

Table 4.23. CapEx and OpEx vs Technical solution investigated

Economical Investigations				
Technical Solutions	**CapEx [ml euro]**	**Fuel Cost [ml euro/year]**	**Maintenance [ml euro/year]**	**Total Cost [ml euro/year]**
1	37.651	15.314	2.449	19.269
2	20.094	27.292	2.449	30.545
3	24.059	21.157	2.534	24.654
4	25.206	21.065	2.538	24.611
5	23.171	30.589	3.817	35.333
6	27.524	21.093	3.919	26.112

The fuel cost was found in (Livanos G. et al., 2012). The cost of engine maintenance was found in (V.T.P. Engineering), the cost of scrubber maintenance was found in (ECDGE, 2005a), and the cost of the SCR maintenance was found in (ECDGE, 2005b). Total cost appearing in Table 4.23 is the sum of CapEx divided by 25 years (ship lifetime considered), fuel cost and maintenance cost. Figure 4.10 shows the payback time of the full LNG system solution with respect to solution 4. The ratio between the costs of fuel is the same as the ones calculated from Table 4.21.

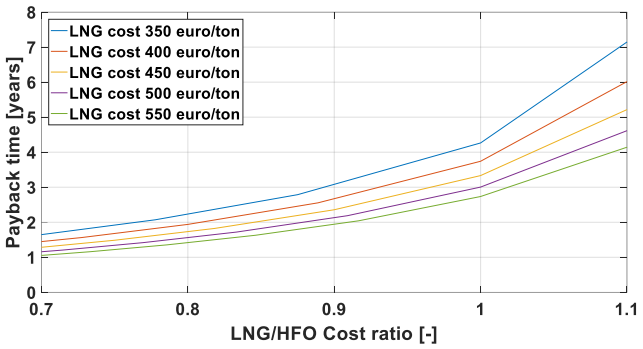

Figure 4.10. Payback time, gas-fuelled propulsion

Figure 4.11 reports the payback time of the gas solution with respect to TECHNICAL SOLUTION 4, taking into account the net payload reduction due to the presence of the LNG tanks but also the benefits represented by a lower weight of the LNG fuel. In case of HFO fuelled ship, the penalty is represented by the weight of the scrubber. As a payload unit, it was considered a car carried on board and whose dimensions and weights were found in (Di Natale N., 2013). The revenue of each car was considered equal to 60 euros per trip, value obtained by consulting the online page of the shipping company. The weight of the scrubber was found in literature (ABS, 2013). The lower fuel consumption, due to the lower weight of the fully loaded gas-fuelled ship, has been evaluated through the admiralty equation, considering a direct correlation between the propulsive power and fuel consumption.

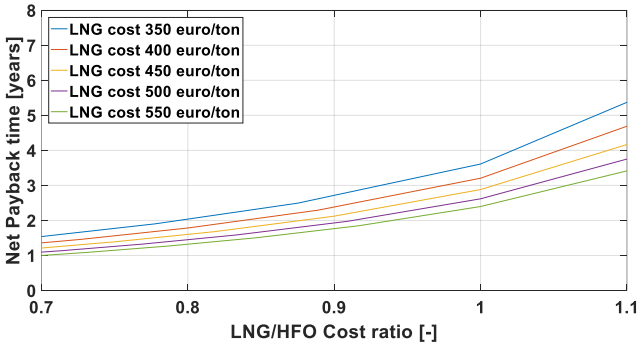

Figure 4.11. Net Payback time, gas-fuelled propulsion

4.7 CONSIDERATIONS ON ENERGY EFFICIENCY DESIGN INDEX

The Energy Efficiency Design Index (EEDI) allows to evaluate the ship's efficiency in terms of energy, by expressing the amount of CO_2 emitted per unit of transport work. The evaluation of this index was carried out through the guidelines issued by the IMO (MEPC.245 (66), 2014). In such guidelines is reported the general formulation to calculate the index, as reported in equation (4.14) and that for the case study in question, due to the absence of PTO system on board the ship, the suitable formulation to calculate the index is reported in equation (4.15).

$$\frac{\left(\prod_{j=1}^{n} f_j\right)\left(\sum_{i=1}^{nME} P_{ME(i)} \cdot C_{FME(i)} \cdot SFC_{ME(i)}\right) + \left(P_{AE} \cdot C_{FAE} \cdot SFC_{AE}*\right) + \left(\left(\prod_{j=1}^{n} f_j \cdot \sum_{i=1}^{nPTI} P_{PTI(i)} - \sum_{i=1}^{neff} f_{eff(i)} \cdot P_{AEeff(i)}\right) C_{FAE} \cdot SFC_{AE}\right) - \left(\sum_{i=1}^{neff} f_{eff(i)} \cdot P_{eff(i)} \cdot C_{FME} \cdot SFC_{ME}**\right)}{f_i \cdot f_c \cdot f_l \cdot Capacity \cdot f_w \cdot V_{ref}} \tag{4.14}$$

The "correction factors" $\mathbf{f_i}$, $\mathbf{f_w}$, $\mathbf{f_{eff}}$ have a value of 1 for this kind of ship.

$$\frac{\left(\prod_{j=1}^{n} f_j\right)\left(\sum_{i=1}^{nME} P_{ME(i)} \cdot C_{FME(i)} \cdot SFC_{ME(i)}\right) + \left(P_{AE} \cdot C_{FAE} \cdot SFC_{AE}*\right) - \left(\sum_{i=1}^{neff} f_{eff(i)} \cdot P_{AEeff(i)} \cdot C_{FAE} \cdot SFC_{AE}\right)}{f_c \cdot Capacity \cdot V_{ref}} \tag{4.15}$$

The EEDI threshold value, referred to the year 2020 is calculated by using formula (4.16).

$$\text{Required EEDI} = (1\text{-X}/100) \cdot (\text{Reference EEDI}) \tag{4.16}$$

The values of terms required for the calculation of EEDI are reported in Table 4.24.

Table 4.24. Main features for EEDI evaluation

SHIP CHARACTERISTICS		
Length b.p.	[m]	186.2
Breadth (maximum)	[m]	30.4
Draught	[m]	7.83
Gross tonnage	[gt]	49257
Speed	[kt]	28
Capacity (DWT)	[ton]	9720
Displacement	[ton]	28358
Propulsion power	[kW]	4*17500
P_{ST} WHRS	[kW]	1198

Figure 4.12 shows the values of the EEDI indices obtained for the different investigated solutions. As it can be noted, only the gas-fuelled ship solution equipped with WHRS can comply with this rule.

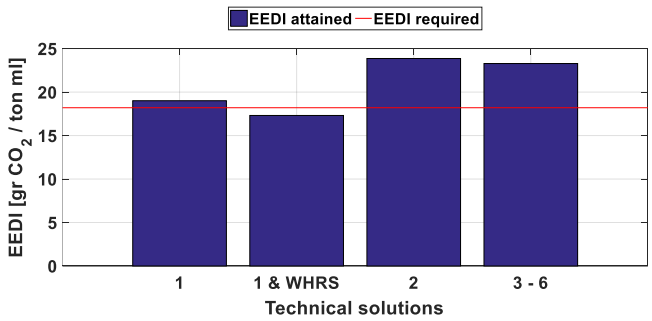

Figure 4.12. EEDI for different investigated solutions

4.8 COLD IRONING SYSTEM

Supplying of electricity to the ships at berth, through a shore-side power solution, can further reduce polluting emissions in port area. Table 4.25 shows the costs of electricity generation on board the ship during the time spent at berth (considering the sum of fuel and maintenance costs) calculated by equation (4.17), and the maximum cost that it may be convenient for ship owner accepting a return on investment of 5 years, calculated by equation (4.18). The initial cost of shore-to-ship power equipment was considered to be 440000 euros (Yorke ENGINEERING, LLC., 2007).

Table 4.25. Cold ironing energy cost evaluation

Cold Ironing system		
Technical Solutions	**Energy cost by ship [euro/kWh]**	**Max energy price [euro/kWh]**
1	0.090	0.076
2	0.159	0.144
3	0.159	0.144
4	0.147	0.132
5	0.152	0.137
6	0.151	0.136

$$C_{ENERGY\_SHIP} = \frac{F_{CONSUMPTION}\, F_{PRICE}}{E_{PORT}} + C_{MAINTENANCE} \tag{4.17}$$

Where:

- $F_{CONSUMPTION}$ is the fuel consumption in port, as reported in Table 4.18;
- F_{PRICE} is the fuel price [euro/tons] (Livanos G. A. et al., 2012);
- E_{PORT} is the electricity required by ship in one year during the time spent in port;
- $C_{MAINTENANCE}$ is the maintenance cost [euro/kWh] (V.T.P. Engineering).

$$E_{PORT\_PRICE} = C_{ENERGY\_SHIP} - \frac{C_{COLD\ IRONING}}{PT\ \ E_{PORT}} \tag{4.18}$$

Where:

- $C_{COLD\ IRONING}$ is the initial cost of shore-to-ship power equipment ship side;
- PT is the payback time of the initial investment.

As reported in Table 4.25, the use of LNG as fuel to run electric generators when the ship is at berth (Technical solution 1 in the table) allows to reach the lowest cost of the energy produced, consequently the energy price due to the cold ironing operation needs to be lower. Therefore, if the ship burns LNG also when is at the berth, the amount of LNG necessary for the ship is superior and consequently the frequency of bunkering increases. As reported in a study carried out by the Korea Register of Shipping (KR, 2016), the frequency of bunkering is a key factor related to the probability of failures during the bunkering operation. In addition, a further reason to prefer the cold ironing solution could be due to possible LNG rising prices. Then, the ship should use the LNG in navigation and shore-connection when it is at berth.

5 MARINE SYSTEMS FOR SHIP POWER SUPPLY AT BERTH

5.1 SUPPLY INFRASTRUCTURE SCENARIOS

The LNG supply infrastructure in the Italian ports is under discussion due to the EU Directive 2014/94/EU. So, two different possible scenarios are considered (Altosole et al., 2017d):

- A possible LNG storage tank located in the port of La Spezia where a regasification plant is in service since long time (Figure 5.1). Therefore, it would be possible to install in this area an LNG storage tank and to use a shuttle tanker to carry the LNG from La Spezia to Genoa
- The installation of LNG storage tanks in the port of Genoa. In Figure 5.2 some possible locations of such LNG storage tanks are reported

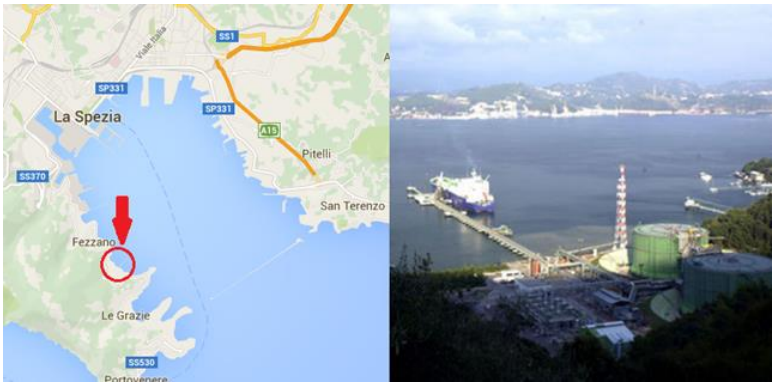

Figure 5.1. Regasification plant in Panigaglia – La Spezia

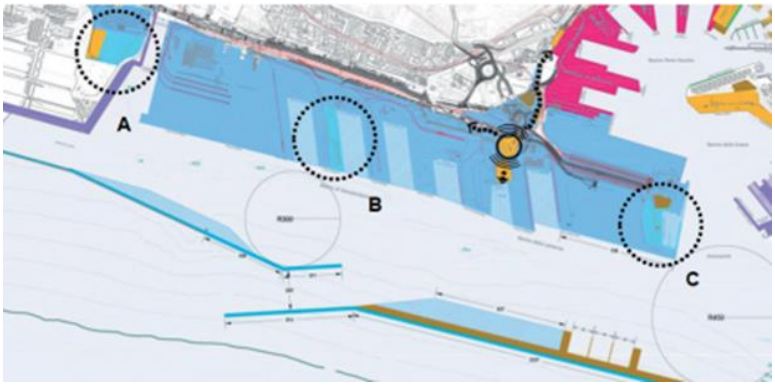

Figure 5.2. Possible locations of LNG storage tanks in the port of Genoa (Capocaccia F., 2015)

5.2 ELECTRIC ENERGY DEMAND IN PORT

A cleaner source of electric energy to feed ships in port should be designed analysing the energy demand in the considered area. The first step of this study dealt with the assessment of the electric energy demand of the ships at berth. Starting from collecting data regarding the time spent at berth by each ship, an analysis of the port calls in the port of Genoa referred to the year 2012 has been carried out. The ship energy demand at berth has been estimated considering different algorithms according to the several vessel typologies, namely ferries, cruise ships and containerships. For the ferries, a linear correlation between energy demand and gross tonnage is considered, the reference value adopted has been found in (Randazzo D., 2014). For the cruise ships, the correlation is based on the on-board maximum installed power; the electrical power demand has been obtained considering the 13% of the total installed power on board (Parenti G., 2014). Regarding the case of containerships, the electric power demand in port is evaluated taking into account the number of TEUs carried. This correlation has been assessed considering a single data found in scientific literature (Nielsen B., 2009). The total amount of electric energy required per year by all the ships considered is about 54 GWh. As it can be noticed from Figure 5.3, the ferries electric energy demand is the most significant, being about 68% of the total amount.

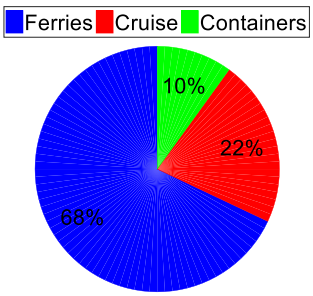

Figure 5.3. Gross electric energy demand in port for several ship typologies – comparison

Considering the net amount of electric energy required by the ships, so not including the time needed for connection and disconnection operations (Tetra Tech, 2007), the total amount of electric energy is near 47.9 GWh. Figure 5.4 shows the total energy demand during the year 2012, distributed in a step of one hour.

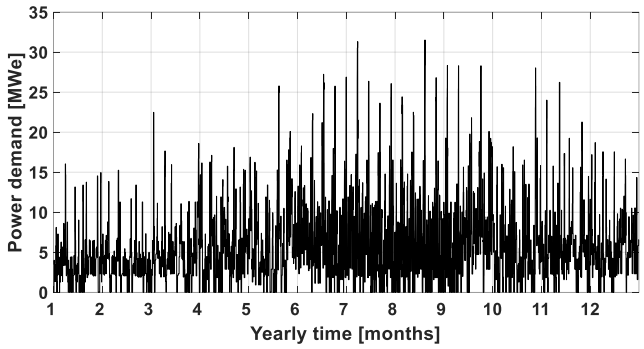

Figure 5.4. Electric energy demand in port

Figure 5.5 shows the total energy demand during the year 2012, subdivided by calendar months, while in Figure 5.6 the average daily energy required by ships is presented.

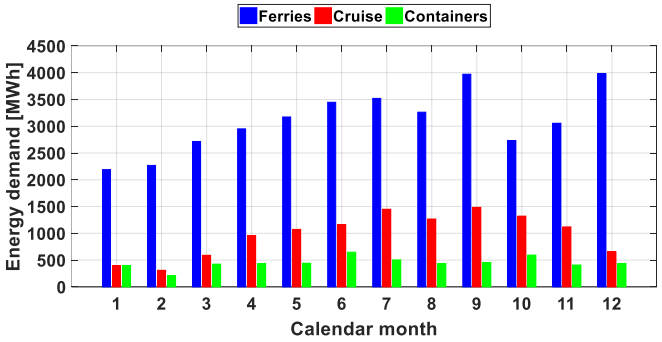

Figure 5.5. Monthly electrical energy demand

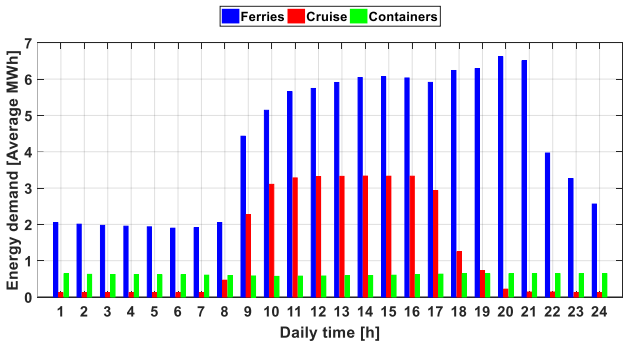

Figure 5.6. Hourly electric energy average demand

Figure 5.7 shows the distribution of time at berth versus the electric power demand.

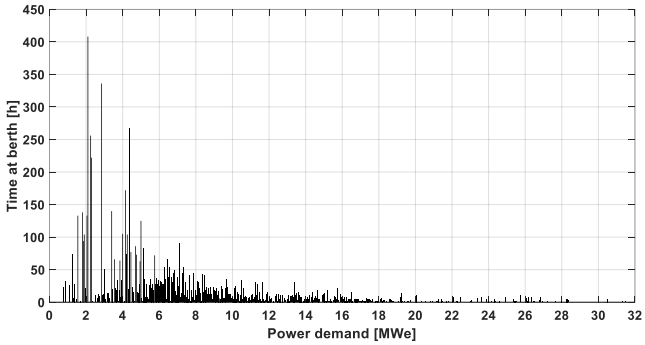

Figure 5.7. Distribution of time at berth vs electric power demand

As shown in Figure 5.8, most of the port calls regarding the ferries traffic is concentrated in the range of required power of 2 – 2.5 MWe while concerning the cruise distribution, there is a similar amount of port calls in the power range between 5 – 6 MWe and 9 – 10 MWe. The containerships power required is concentrated almost all in the range 2 – 2.5 MWe.

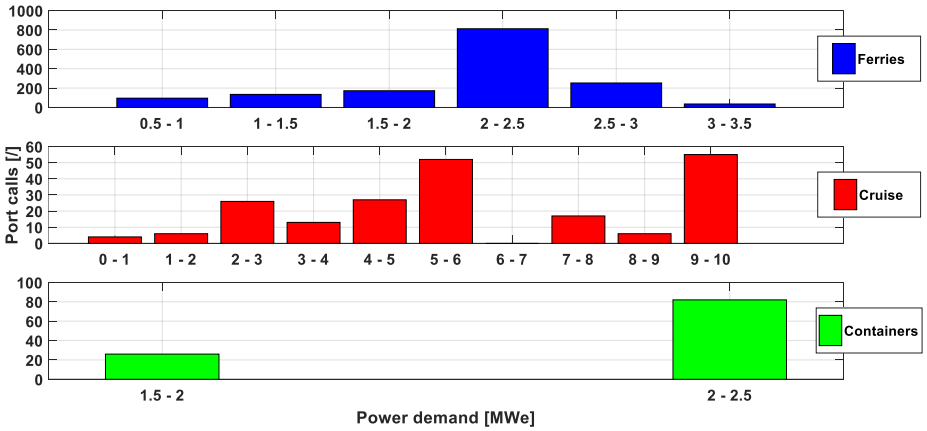

Figure 5.8. Port calls vs power demand

Figure 5.9 represents the distribution of the time spent at berth relating to the power required by each typology of ships investigated.

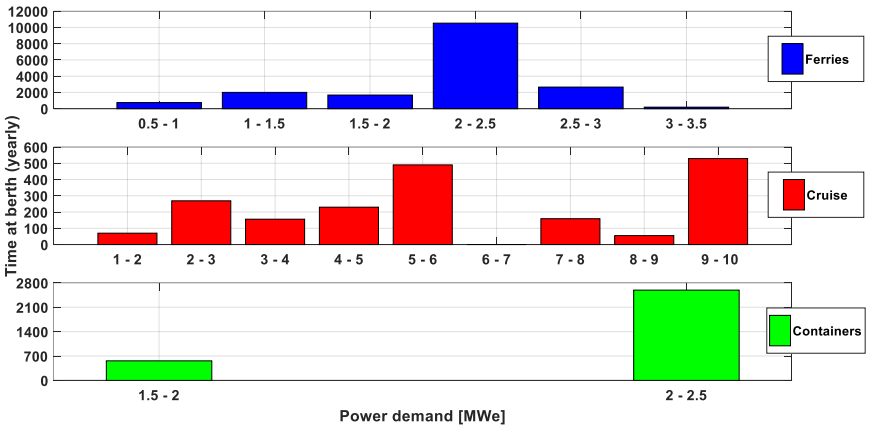

Figure 5.9. Time at berth vs power demand

Figure 5.10 and Figure 5.11 depict the amount of port calls related to the time of arrival and departure respectively.

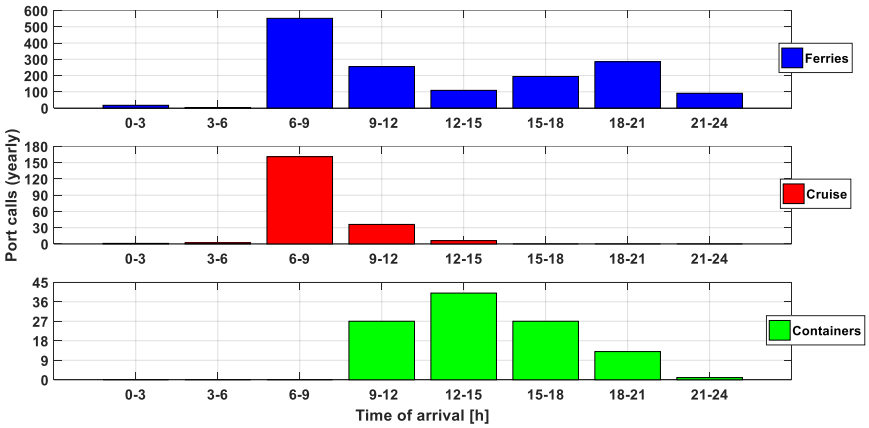

Figure 5.10. Port calls vs time of arrival

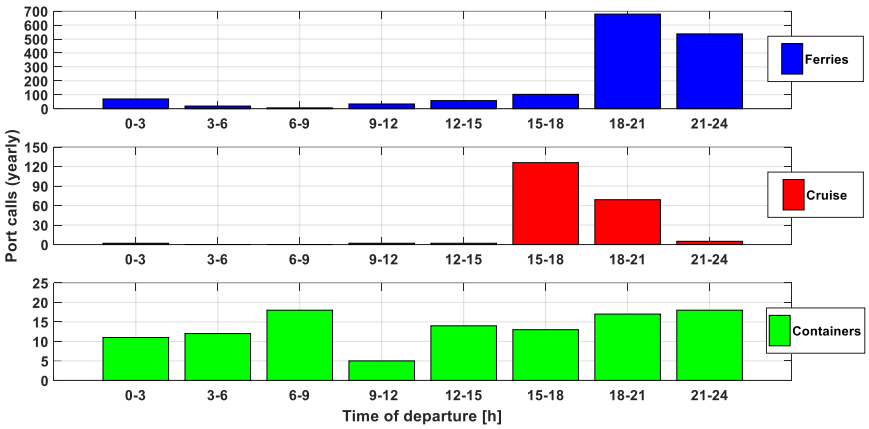

Figure 5.11. Port calls vs time of departure

As concerns the technical features of the electrical system on board the ships engaged in the port of Genoa (in terms of voltage and frequency), there are not specific information but in most European ports, the ships operate at 60 Hz (IEC/ISO/IEEE 80005-1, 2012). Regarding the voltage, the "high voltage shore connections" rules (Erikson P. & Fazlagic I., 2008) recommended a specific value according to the ship type.

5.3 POSSIBLE TECHNICAL SOLUTIONS

Due to the novelty of the problem, a design procedure has been developed, taking into account the target energy market and the possible supply chain options. The design procedure aims at exploring different feasible solutions and ranking them through a cost-benefit approach. If the target energy market is focused on feeding all the ships calling the old port of Genoa, a suitable solution could be a fixed power barge moored in port, connected to a dedicated electric network for energy distribution at each berth. If the target energy market is to feed just a limited number of ships calling the old port of Genoa, two technical solutions have been identified:

- towed power supply barge
- self-propelled power supply vessel

In particular, the self-propelled vessel could be a valid solution in case the LNG storage tanks are located in the port of La Spezia. The best candidate ships for the energy market should have the following characteristics:

- high electric power demand
- long layover time in port
- frequent port calls

5.4 POWER SUPPLY BASIC DESIGN

The number of generator units installed on board the barge includes one considered in stand-by mode (ready to run in case of shutdown of a running engine or in no working condition for maintenance reason). For each considered engine layout, once known the power required by the ship, it is possible to set the number of working generators and the related engine load to get the minimum fuel consumption. The number of running engines (N_{RE}), for each electric power required by ships ($P_{EL\ SHIP}$), is obtained through the equation (5.1).

$$N_{RE\ j} = \min \left| \frac{P_{EL\ SHIP\ j}}{\eta_{EL}} - \sum P_{MCR\ i}\ EL_R \right| \tag{5.1}$$

Where:

- η_{EL} is the global electric efficiency (Attah E. E. & Bucknall R., 2015);
- P_{MCR} is the power of each engine considered at MCR condition;
- EL_R is the engine load at normal operating condition (set at 0.8).

In case of the $P_{EL\ SHIP}$ exceeds the MCR condition of the total installed power on board the barge, the possible power supplied is referred at the engine load at normal operating condition. The barge energy is calculated as the product of the power provided by the barge and the relating time period which the power is rated. The engine load is obtained through the equation (5.2).

$$EL_j = \frac{P_{EL\ SHIP\ j}}{\eta_{EL}\ (N_{RE\ j}\ P_{MCR})} \tag{5.2}$$

Knowing the load factor for each supplied power request, the time period T which the engine operates and the specific fuel consumption SFC of the considered engine (that can be presented as function of the engine load) is possible to calculate the total fuel consumption LNG_{cons} in the considered time period through the equation (5.3).

$$LNG_{cons} = \sum (SFC_j\ N_{RE\ j}\ P_{MCR}\ EL_j\ T_j) \tag{5.3}$$

The average thermal efficiency of the power station $\overline{\eta_E}$ is calculated through the equation (5.4).

$$\overline{\eta_E} = \frac{E}{LNG_{cons}\ LHV}\ 100 \tag{5.4}$$

Where E is the energy supplied to ships in one year of time and LHV is the lower heat value of the natural gas.

The evaluation of the main dimensions of the barge has been carried out considering the footprint of the generators and an additional clearance. The layout of the engines is in the transverse direction of the barge. The beam, the height and length are calculated respectively as in equation (5.5), (5.6) and (5.7).

$$B = l_E \ c_l + DS \tag{5.5}$$

Where:

- l_E is the greater length of the engines installed on board (found in the product guide of the engines);
- c_l is a coefficient taking in consideration an appropriate clearance round the engine, the value used has been found in (Potapov V., 2012);
- DS is the double side (it has been assumed 800 mm).

$$H = h_E \ c_h + h_E \ c_{hb} \tag{5.6}$$

Where:

- h_E is the greater height of the engines installed on board (found in the product guide of the engines);
- c_h is a coefficient taking in consideration an appropriate vertical clearance; the value used has been found in (Potapov V., 2012);
- c_{hb} is a coefficient taking in consideration the height of the engine foundation; the value used has been found in (Potapov V., 2012).

$$L = L_B + L_{ECR} + L_{ER} + L_S \tag{5.7}$$

Where:

- L_B is the length of the bow, the assumed value has been taken from a similar project, as found in (becker marine systems, 2015);
- L_{ECR} is the length of the engine control room; the value has been taken from a similar project as found in (becker marine systems, 2015);
- L_{ER} is the length of the engine room, calculated as in equation (5.8).
- L_S is the length of the stern; the considered value has been found in (Potapov V., 2012).

$$L_{ER} = b_E \ N_E \ c_b \tag{5.8}$$

Where:

- b_E is the greater beam of the engines installed on board (found in the product guide of the engines);
- N_E is number of the engines installed on board;
- c_b is a coefficient taking in consideration an appropriate transversal clearance; the value used has been found in (Potapov V., 2012);

The capacity of the LNG tank is evaluated through the equation (5.9).

$$LNG_{Tank} = \frac{LNG_{cons} \ BT}{UF \ \rho_{LNG} \ Days \ N_{Tanks}} \tag{5.9}$$

Where:

- UF is the utilization factor of the tanks, considered equal to 0.85, considering that the filling limit is 0.95 (WARTSILA Gas Systems, 2014) and 0.1 (Sungtae Yun et al., 2014) is recommended to be left in the tank for keeping cool down;
- BT are the days between two bunkering operations, equal to 7 days;
- $Days$ are the 365 days in one year;
- ρ_{LNG} is the density of the liquefied natural gas considered equal to 0.43 kg/m^3 (WARTSILA Gas Systems, 2014);
- N_{Tanks} is the number of LNG tanks installed on board: 2 tanks have been considered.

Knowing the calculated capacity of the tank, it is possible to select an LNG tank from the product guide (WARTSILA Gas Systems, 2014). The placement of the LNG tanks is planned on the deck. It can be carried out considering the LNG tanks aligned in transversal disposition (considering a clearance between them as recommended by the product guide) as first choice if the distance from the side of the barge and the tank is on compliance with minimum distance recommended by the IGF code. Otherwise, the disposition of the LNG tanks is planned to be carried out considering the LNG tanks aligned in longitudinal disposition (considering a clearance between them as recommended by the product guide) and so the L_{ER} to be considered is the greater between this one calculated and the one estimated in equation (5.8). The estimation of the barge displacement W has been carried out considering the sum of four items, as reported in equation (5.10):

$$W = W_H + W_O + W_{GG} + W_T \tag{5.10}$$

Where:

- the weight of hull W_H and the weight of outfitting W_O have been derived from available data of similar units;
- the weight of gas-fuelled generators W_{GG} and LNG tank W_T have been found in the product catalogue.

The investment cost has been assessed considering the sum of four items, as reported in equation (5.11):

$$CapEx = C_H + C_O + C_{GG} + C_{T\&E} \tag{5.11}$$

Where:

- C_H is the cost of hull, estimated through the correlation found in literature (Vernengo G. & Rizzuto E., 2014);
- C_O is the cost of the outfitting, estimated through the technical information collected in (Peckham J., 2013);
- C_{GG} is the cost of the gas-fueled electric generator, estimated using the information found in (Masaki A. et al., 2014) as shown in equation (4.5);
- $C_{T\&E}$ is the cost of LNG tank and gas processing equipment, estimated consulting technical information in (HEC & CCDTT, 2013) as detailed in equation (4.6).

The cost of energy EC has been estimated through equation (5.12):

$$EC = \frac{\frac{CapEx}{LT} + OpEx}{E} \tag{5.12}$$

Where:

- LT represents the lifetime of the power barge considered for economic investigations: 30 years is an appropriate value (Engblom K., 2014);
- E is the energy consumed per year by ships in port;
- $OpEx$ represents the yearly operational costs, estimated by equation (5.13).

$$OpEx = O_{fuel} + O_{maint} + O_{lo} + O_{crew} + O_{ins} \tag{5.13}$$

The cost of fuel (O_{fuel}) has been obtained considering a unit value of 477 €/ton (Livanos G. A. et al., 2012), while the cost related to the maintenance of generators (O_{maint}), lubricating oil (O_{lo}), crew (O_{crew}) and insurance (O_{ins}) have been found in (V.T.P. Engineering). Equation (5.14) has been used to calculate the annual operating rate index ($\text{Index}_{\text{AOR}}$) of the power station.

$$\text{Index}_{\text{AOR}} = \frac{\sum P_{EL\ SHIP}\ \text{h}}{P_{\text{BARGE}}\ h_{Yearly}} \tag{5.14}$$

Where:

- P_{BARGE} represents the total power installed on board the barge;
- h_{Yearly} represents the 8760 hours including in one solar year.

5.5 INVESTIGATIONS ON POSSIBLE FIXED POWER SUPPLY BARGE LAYOUTS

In order to carry out the study on the possible layout of the fixed power supply barge, a MATLAB code has been written in house. The code has been populated with the main features of power generation units by different manufacturers (marked with the letter C, R and W in the next figures). The main characteristics of the generating set considered in this study are reported in Table 5.1. As far as vessels are concerned, the input data deal with the electric power request and the time spent in port from each considered ship. The layout definition, in terms of size and number of electrical generators, has been achieved taking into account both technical and economic aspects. At last, just active power demand has been considered for the electrical generators, and the energy required by the ships berthed has been computed over a time period that does not include the time needed for connection and disconnection operations (Tetra Tech, 2007). Considering these technical times, the total amount of electric energy supplied by the cold ironing operation per year by all the ships considered is about 47.93 GWh.

Table 5.1. Main characteristics of the generating sets

Generators type	Mark	Power [kW]	Efficiency [%]	Length [mm]	Width [mm]	Height [mm]	Dry weight [kg]
CG260 - 12	C	3471	45.94	8000	2660	3390	42500
CG260 - 16	C	4479	45.94	9420	2690	3390	51450
B35:40L9AG	R	3780	47.68	10848	2630	4445	79545
B35:40L12AG	R	5472	48.16	10112	3110	4667	97070
9L34SG	W	4342	47.81	10400	2780	3840	77000
16V34SG	W	7743	47.92	11300	3300	4240	12000

Figure 5.12 shows the achievable percent energy coverage as a function of the rated electrical power available for the different layouts investigated. The available power has been considered as the total power of the engines minus one (considering a single engine in maintenance condition as suggested in (Solem S. et al., 2015) running at MCR. Each dot represents one of the generation configurations, which range from 6 to 10 units of different manufacturers (C,R,W) and different power ratings.

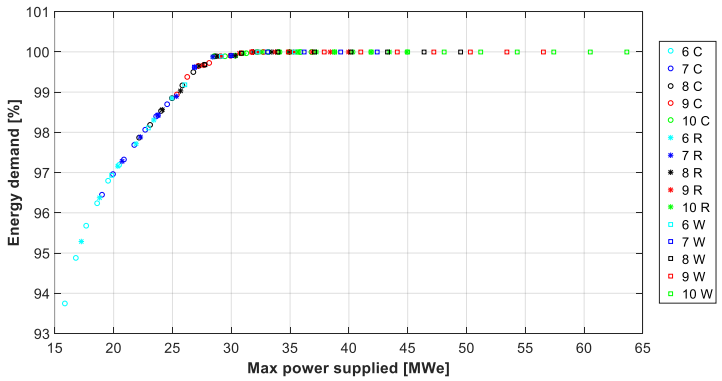

Figure 5.12. Energy demand vs Maximum power supplied by barge

Considering a power of about 31.5 MW, all the right configurations (dots) allow to cover 100% energy demand at port. The average engine efficiency of the generation units is reported in Figure 5.13, while Figure 5.14 reports the cost of the produced energy considering only the fuel cost, once again as a function of the available installed electrical power.

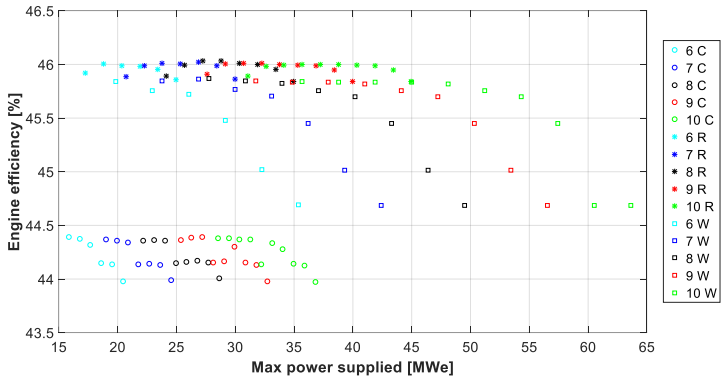

Figure 5.13. Average energy efficiency vs Maximum power supplied by barge

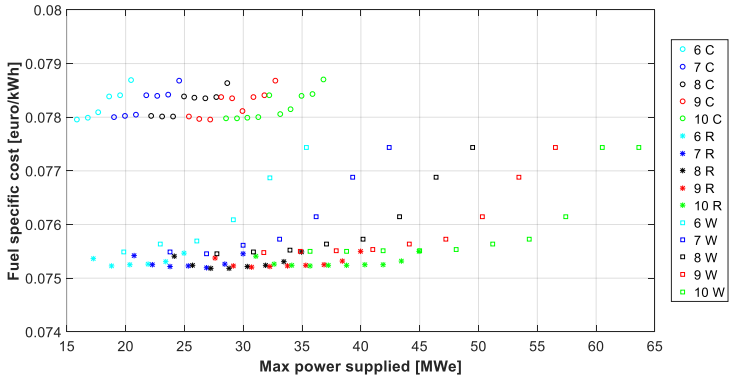

Figure 5.14. Average fuel specific cost vs Maximum power supplied by barge

Figure 5.15 reports the fuel consumption considering one year as time horizon.

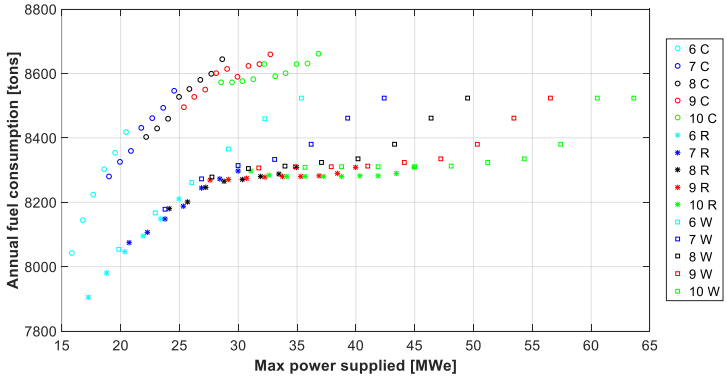

Figure 5.15. Annual fuel consumption vs Maximum power supplied by barge

Figure 5.16 depicts the average load factor of the running engines. Depending on the selection, a load factor from 0.55 to about 0.72 can be achieved.

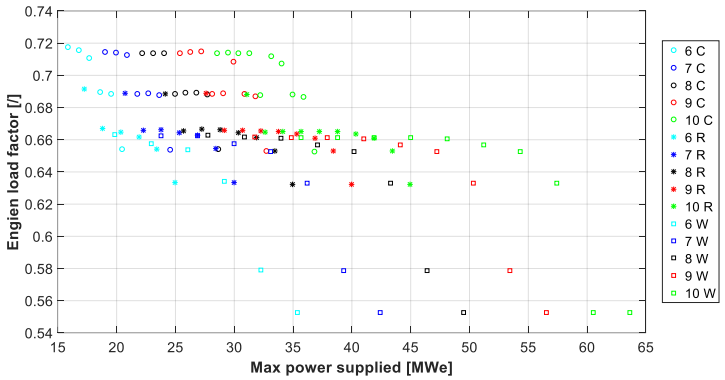

Figure 5.16. Average engine load factor vs Maximum power supplied by barge

In Figure 5.17, the rate of time, at which the engine runs below the minimum load factor threshold, is reported (0.2 has been considered as threshold as found in literature (Solem S. et al., 2015)). The Figure 5.18 shows the corresponding time spent above the maximum load factor (0.9 has been considered as threshold as found in literature (Solem S. et al., 2015)).

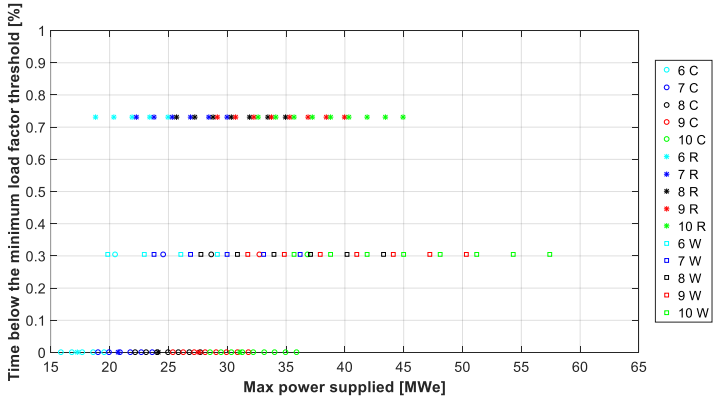

Figure 5.17. Time spent below the minimum load factor threshold vs Maximum power supplied by barge

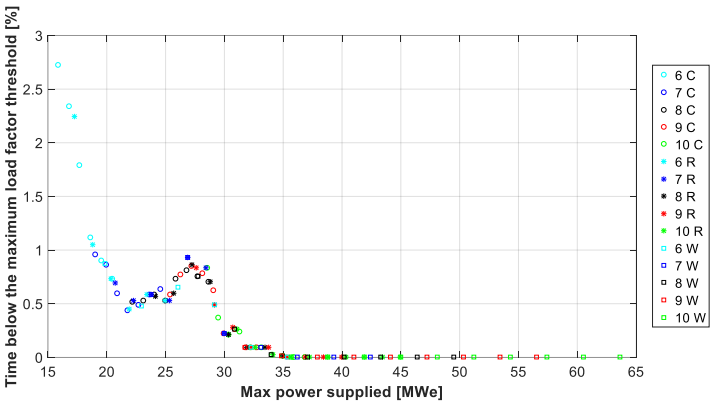

Figure 5.18. Time spent over the maximum load factor threshold vs Maximum power supplied by barge

Figure 5.19 reports the total power installed on board as a function of the available power usable for cold ironing operation.

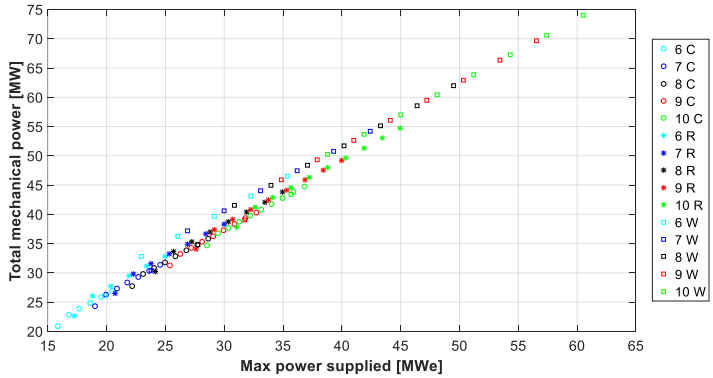

Figure 5.19. Total power installed on board vs Maximum power supplied by barge

Figure 5.20 shows the annual operating rate of the power generation station, while Figure 5.21 represents the engine running hours in one year of cold ironing operation.

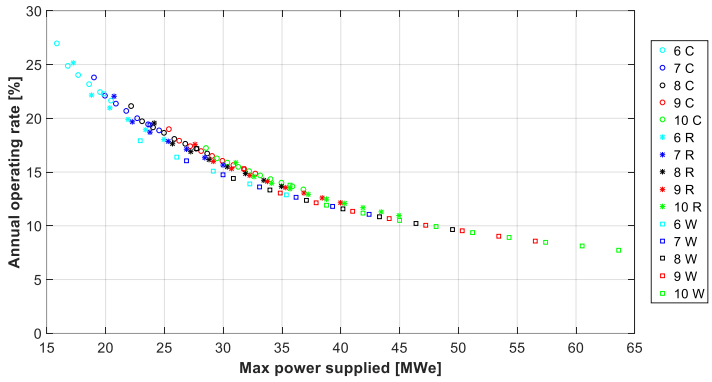

Figure 5.20. Annual operating rate vs Maximum power supplied by barge

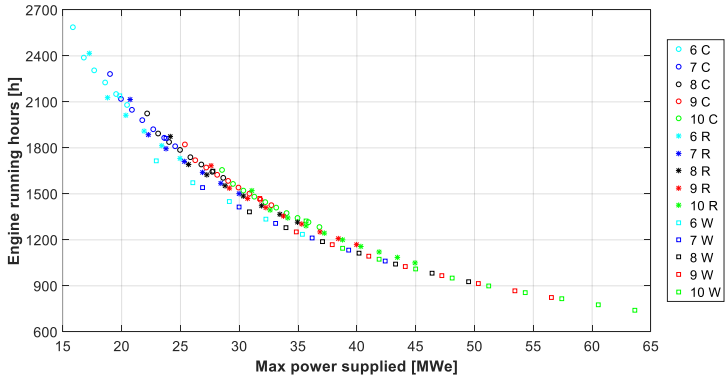

Figure 5.21. Engine running hours vs Maximum power supplied by barge

Regarding the barge weight and size, as it can be noticed from Figure 5.22 and Figure 5.23 respectively, the displacement ranges are from 4000 to about 7000 tons, while the length ranges are from about 40 to about 80 m, depending on the layout selection.

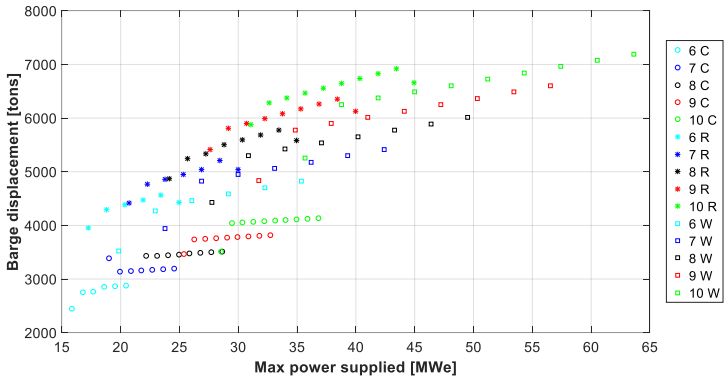

Figure 5.22. Barge displacement vs Maximum power supplied by barge

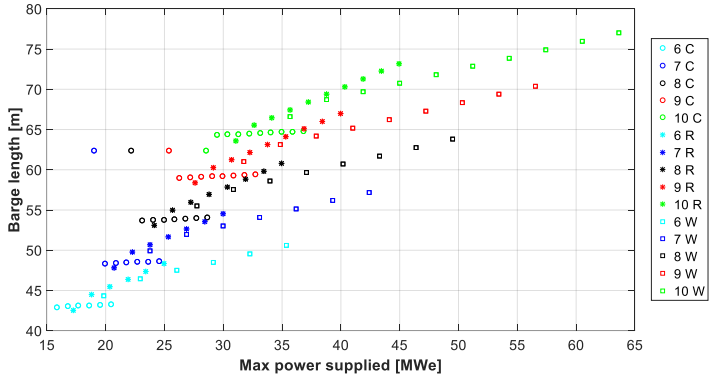

Figure 5.23. Barge length vs Maximum power supplied by barge

Figure 5.24, Figure 5.25 and Figure 5.26 depict the beam, the height and the draft of the barge respectively.

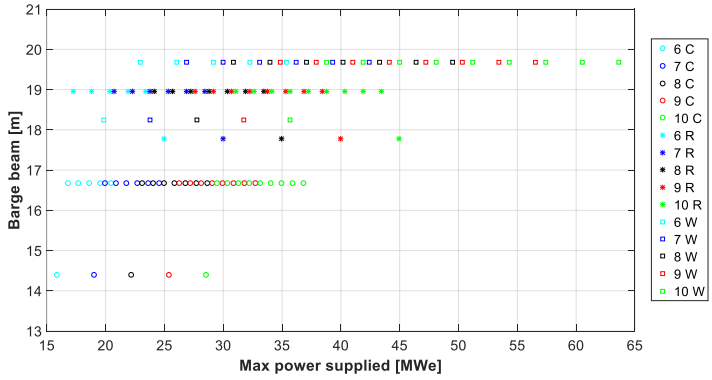

Figure 5.24. Barge beam vs Maximum power supplied by barge

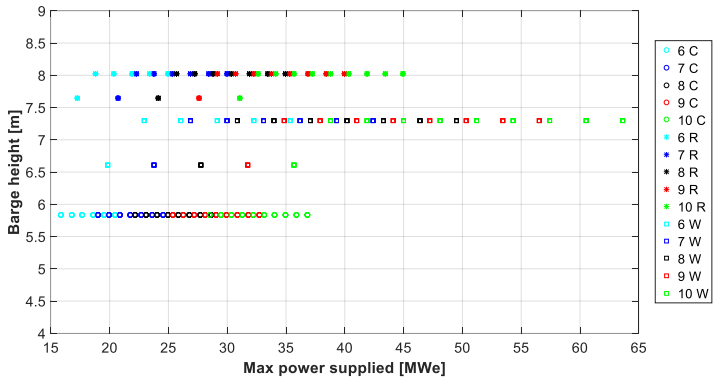

Figure 5.25. Barge height vs Maximum power supplied by barge

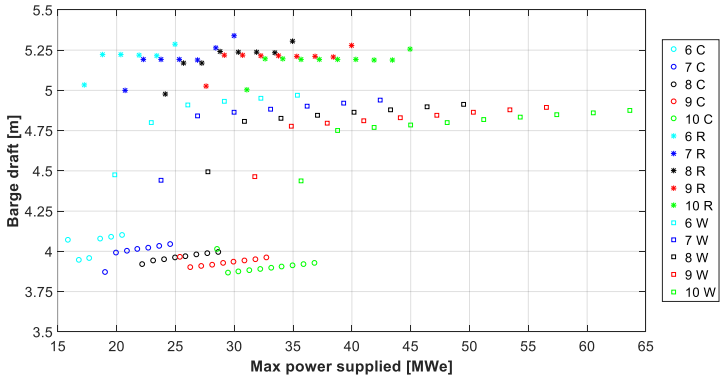

Figure 5.26. Barge draft vs Maximum power supplied by barge

Regarding the preliminary cost assessment, a first estimation of the investment cost has been performed; the results are reported in Figure 5.27, while the cost of energy is reported in Figure 5.28.

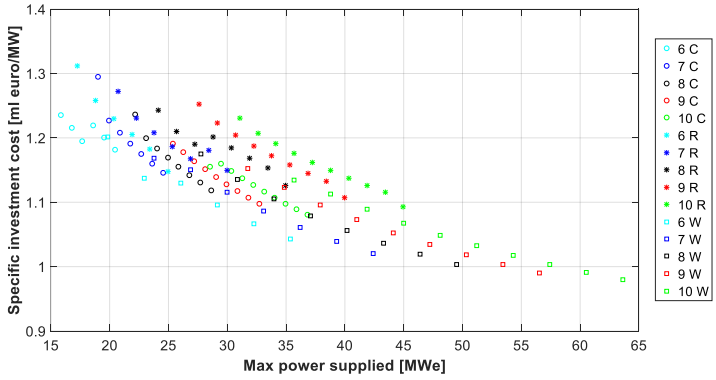

Figure 5.27. Specific investment cost vs Maximum power supplied by barge

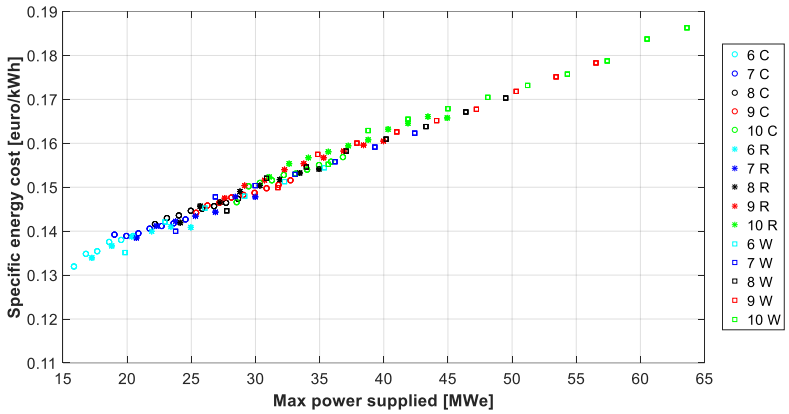

Figure 5.28. Specific energy cost vs Maximum power supplied by barge

As target for the choice of the generators layout, the minimum energy cost and the 100% of the energy required have been taken into account. The main characteristics of the proposed floating unit solution are reported in Table 5.2. In Appendix I, a simplified drawing, representing the general arrangement of the proposed solution, is reported.

Table 5.2. Main characteristics of the barge selected

FIXED POWER SUPPLY BARGE		
POWER GENERATION		
Generators Layout		9 * 9L34SG
Total mechanical power	[MW]	39.084
Max power supplied	[MWe]	31.719
Energy supplied at berth	[%]	100
Average engine efficiency	[%]	45.848
Fuel specific cost	[€/kWh]	0.0755
Annual fuel consumption	[tons]	8307.4
Average engine load	[/]	0.6618
Annual operating index	[%]	15.33
Engine running hours	[h]	1471
Time at lower threshold load	[%]	0.3
Time at upper threshold load	[%]	0.09
BARGE CHARACTERISTICS		
Displacement	[tons]	4839
Length	[m]	61.04
Beam	[m]	18.24
Height	[m]	6.60
Draft	[m]	4.46
LNG tank capacity	[m^3]	2 * 239
Bunkering	[days]	7
PRELIMINARY COST ASSESSMENT		
Specific investment cost	[ml €/MW]	1.152
Energy cost	[€/kWh]	0.15

It is not easy to predict how many ships will be equipped with an on-board system able to receive energy from the shore connection, so the variation of the cost of energy provided by the barge, as a

function of the electric energy demand from ships, has been analysed. The results are shown in Figure 5.29.

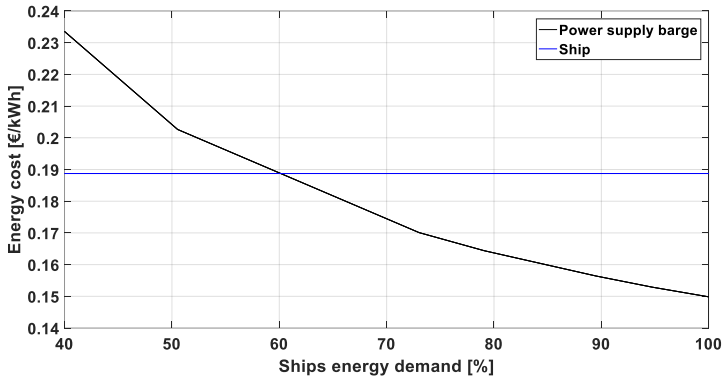

Figure 5.29. Barge specific energy cost vs percent ships energy demand

As result of Figure 5.29, the cost-effectiveness of the power supply barge is possible if around the 60% of the ships demand occurs, considering an average fuel consumption of 217 g/kWh (Ballini F., 2013) and a maintenance cost for diesel generators of 0.012 euro/kWh (V.T.P. Engineering). To further cut the cost of the energy produced by the barge, it would be necessary to increase the amount of energy delivered by such a system. Table 5.3 reports the specific cost of energy for different scenarios of production by the barge, to feed both the ships and other at land industrial activities in port. To this aim, the land factor αLF of Table 5.3 allows to identify the latter amount of energy delivered by the barge generators (αLF times the amount of energy still remaining, once the ships demand has been satisfied, taking into account the available gross total based on the installed electrical power). The cost reported in Table 5.3 does not consider any cost due to distribution on electric energy and the cost of frequency converter regarding the possibility to supply power to land activities.

Table 5.3. Specific cost of energy [€/kWh] vs ships and at land activities energy request

α_{LF}	**Energy yearly delivered to ships [GWh]**						
	17.10	24.22	35	37.90	42.90	45.41	47.93
0	0.2411	0.1976	0.1658	0.1604	0.1528	0.1495	0.1465
	(0)	(0)	(0)	(0)	(0)	(0)	(0)
0.2	0.1423	0.1373	0.1319	0.1307	0.1287	0.1278	0.1269
	(35.48)	(34.06)	(31.91)	(31.33)	(30.35)	(29.87)	(29.38)
0.4	0.1227	0.1214	0.1197	0.1193	0.1186	0.1183	0.1180
	(70.97)	(68.11)	(63.82)	(62.66)	(60.71)	(59.74)	(58.77)
0.6	0.1146	0.1141	0.1136	0.1135	0.1133	0.1130	0.1129
	(106.45)	(102.17)	(95.73)	(93.98)	(91.06)	(89,61)	(88.16)
0.8	0.1111	0.1108	0.1105	0.1105	0.1103	0.1103	0.1102
	(141.94)	(136.22)	(127.65)	(125.31)	(121.42)	(119.48)	(117.55)
1	0.1079	0.1079	0.1079	0.1079	0.1079	0.1079	0.1079
	(177.42)	(170.28)	(159.56)	(156.64)	(151.77)	(149.36)	(146.93)

Another important aspect is the possibility to receive the boil off gas from the coastal storage tanks (assuming in this study the possible installation of this infrastructure). The amount of the boil off has

been calculated considering a boil off ratio of 0.1% (Myang Wook Shin et al., 2008) of the LNG in tanks, assuming the total capacity of the storage tanks equal to 10000 m^3 (SANECO, 2014) and considering the mass density of LNG equal to 0.43 ton/m^3. The amount of boil-off gas results to be equal to 0.1792 tons/h. The cost of boil off has been considered 25% less than the cost of LNG (Engblom K. & Reinlund J., 2016). In such a context, Table 5.3 also reports, for the different scenarios, the value of the energy yearly delivered to the industrial activities at land (GWh within brackets). The results of the analysed case studies show that, if full power is continuously delivered all the year, the minimum cost is achieved, up to a value of about 11 cents € per kWh. As mentioned by the Masterplan issued by the Italian Government for promoting the use of natural gas as fuel, the potential LNG bunkering demand in 2025 could be about 323951 m^3. Figure 5.30 represents the percentage of this amount of LNG that could be used to feed the power supply barge.

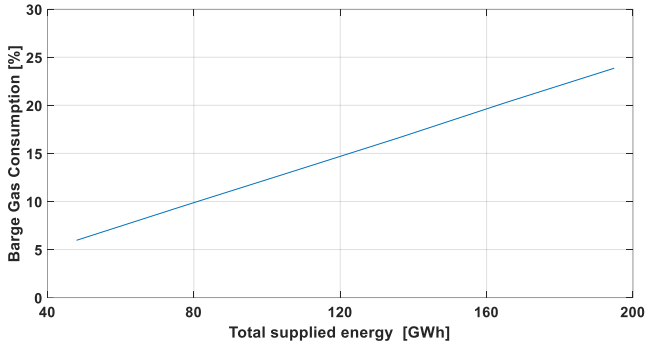

Figure 5.30. Barge gas consumption related to Potential LNG bunkering demand

As represented in Figure 5.30 maximum use of the power supply barge (including power supplied to land activities) could ensure the 25% of the potential LNG bunkering demand.

5.6 PORT INFRASTRUCTURE: ELECTRICAL GRID

Shore-to-ship electricity supply system is intended as the set of equipment to distribute electrical energy from the main energy source (power supply barge) to the final users, through an electrical infrastructure. The proposed layout of the grid is represented in Figure 5.31. The location of the power supply barge (PSB in the figure) has been assumed near the future LNG storage tank. The electrical power produced by the barge is convoyed to 4 main sub stations (green label in the figure) so distributed to the pier terminal supply energy (red labels in the figure). Table 5.4 reports the max electrical power absorbed by ship at berth and the layout of electrical grid. Table 5.5 reports the lengths of electric cables needed for energy distribution. The cost of harbour canalization (to bury cables in the ground) are 150 euro per meter (MariTermAB, 2004) and high voltage cable cost is 15 euro per meter (MariTermAB, 2004). The pier installation cost (including cables, transformer and other equipment) has been evaluated considering a cost of 587740 euros per MWe regarding containerships and ferries piers (Yorke engineering, 2007), and 212722 euros per MWe for cruise pier (Yorke engineering, 2007).

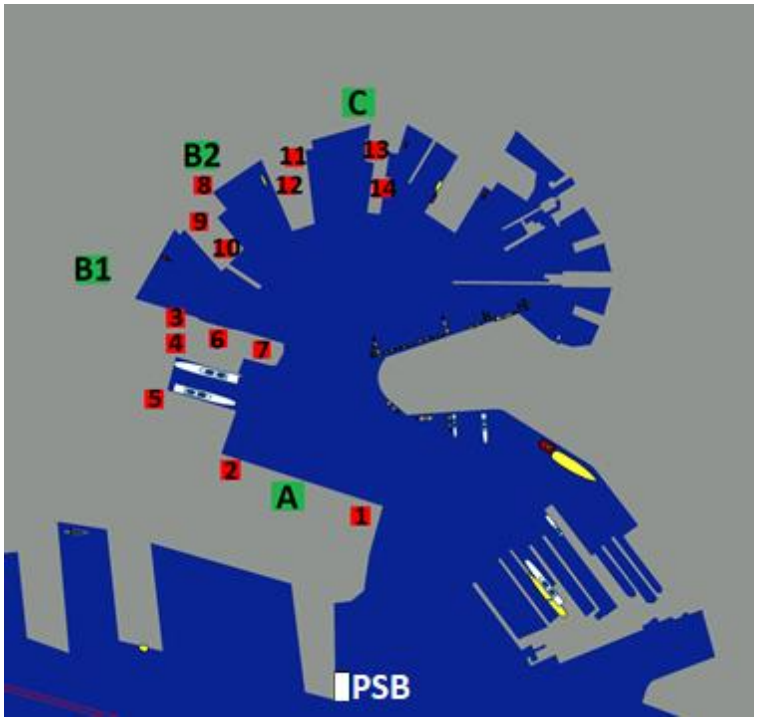

Figure 5.31. Port electrical infrastructure. Proposed layout

Table 5.4. Electrical power distribution layout

POWER SUPPLY DISTRIBUTION			
Substation	**Pier**	**Ship typology**	**Max power supplied [MWe]**
A	1	Containerships	2,00
	2	Containerships	2,00
B1	3	Ferries	3,13
	4	Ferries	3,13
	5	Ferries	3,13
	6	Ferries	3,13
	7	Ferries	3,13
B2	8	Ferries	3,13
	9	Ferries	3,13
	10	Ferries	3,13
	11	Ferries	3,13
	12	Ferries	3,13
C	13	Cruise	10,00
	14	Cruise	10,00

Table 5.5. Port electrical grid, electric cable length

POWER SUPPLY DISTRIBUTION			
Substation	**PSB - Substation distance [m]**	**Pier**	**Substation – Pier distance [m]**
A	1008	1	250
		2	250
B1	1958	3	300
		4	300
		5	440
		6	440
		7	480
B2	2308	8	200
		9	200
		10	320
		11	320
		12	440
C	3000	13	200
		14	200

The total initial cost calculated is around 28 million euro. The operating cost of the electrical grid has been calculated considering the labour cost (for cable connection and disconnection) as 441 euro per ship visit and assuming a maintenance cost as 30 % of the initial cost split in 25 years (typical lifetime for return of investment of harbour infrastructure). The cost of electrical energy distribution (summing investment cost and operating cost) reached 0.047 euro/kWh in case of 100% of ship energy demand required.

5.7 ELECTRICAL CONNECTION FOR SUPPLYING ENERGY TO LAND ACTICIVITIES

As regards the possibility to supply electrical power to land, a converter frequency is required and significant improvements to the electrical grid facilities of the city too. Any information about the cost of converter frequency has been found but considering a frequency converter consisting of an electric motor (60 Hz) coupled to alternator (50 Hz). The unit cost could be assumed as the cost unit of a diesel generator (Masaki A. et al., 2014; Livanos G. A. et al., 2012). The max power to supply to land could be evaluated as the max power at 80% MCR of total power installed, excepted two engines (assuming one in standby mode and one turned off for maintenance reason). The cost regarding electrical equipment for to supply energy to land is considered as 1.15 ml euros per MW (Yorke engineering, 2007). Considering a maintenance cost near to 20% of the initial cost, it is possible to calculate the total cost of the facilities required for supplying power to land. The cost of this initial investment, adding maintenance cost split in 30 years and referred to a maximum energy delivered of 146.93+47.93 GWh (as reported in Table 5.3), it is about 0.007 euro per kWh. Considering that no energy is supplied to land, the drawbacks of the unused facility is about 0.028 euro per kWh.

5.8 AIR EMISSION AND EXTERNALITIES COST

The evaluation of externalities cost starts from the calculation of air emission by ships at berth. In fact, pollution, for example is a well-known negative externality. The air emission factor (using MGO as fuel) is reported in Table 5.6 (Yorke engineering, 2007) while the specific externalities cost, based on (MariTermAB, 2004), is reported in Table 5.7.

Table 5.6. Emission factor (Yorke engineering, 2007)

AIR EMISSION FACTOR WITH MGO [g/kWh]			
NOx	**PM 10**	**PM 2.5**	**SOx**
13.9	0.42	0.23	2.05

Table 5.7. Externalities cost (MariTermAB, 2004)

EXTERNALITIES WITH [euro/kg]			
NOx	**PM 10**	**PM 2.5**	**SOx**
2.6	165	165	30

The air emission and externalities cost referred to the Old port of Genoa is reported in Table 5.8.

Table 5.8. Old port of Genoa. Air emission and Externalities cost with MGO

	AIR EMISSION by SHIPS at berth [tons/year]	**EXTERNALITIES COST [ml euro/year]**
NOx	829	2.155
PM 10	25	4.133
PM 2.5	13.7	2.263
SOx	122.3	3.667
Total	990	12.219

The Figure 5.32 reports the reducing air emissions thanks to the cold ironing operation through the power supply barge. The NOx emission is considered equal to 3 g/kWh (WARTSILA Engines, Wartsila 50 DF Product guide) in case of gas-fuelled engine while the other pollutant emissions are considered negligible.

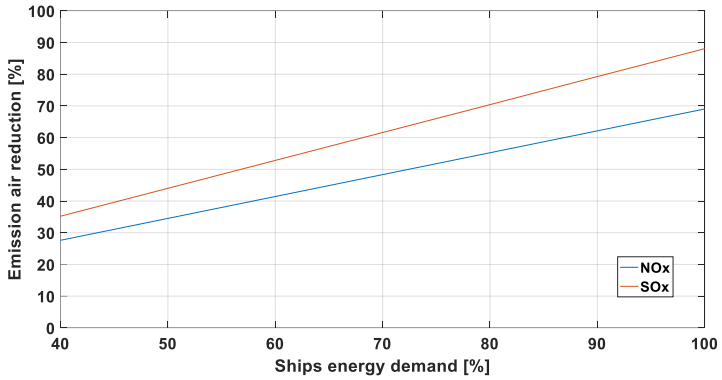

Figure 5.32. Air emission reduction with power supply barge

Figure 5.33 reports the reduction of CO2 emission due to the use of the power supply barge. The calculation of ship CO2 emission is carried out considering the conversion factor referred to the use of MGO as found in the guidelines issued by the IMO (MEPC.245 (66), 2014). Total emission of CO_2 in port by ship is about 41491 tons, value calculated considering a specific consumption of 217 g/kWh (Ballini F., 2013). To calculate the production of CO2 by barge is sufficient to know the fuel consumption (calculated through the MATLAB code) and the conversion coefficient.

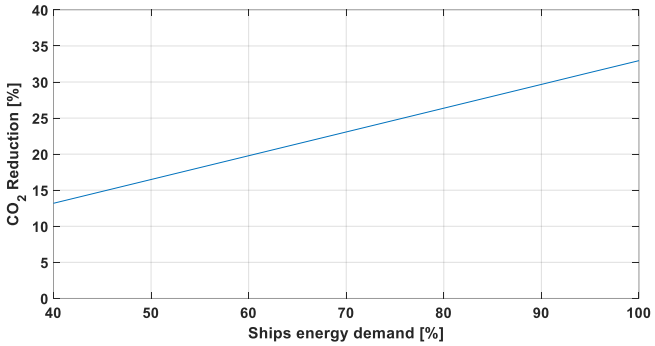

Figure 5.33. CO_2 reduction

The saving cost for the Italian government is reported in the Figure 5.34.

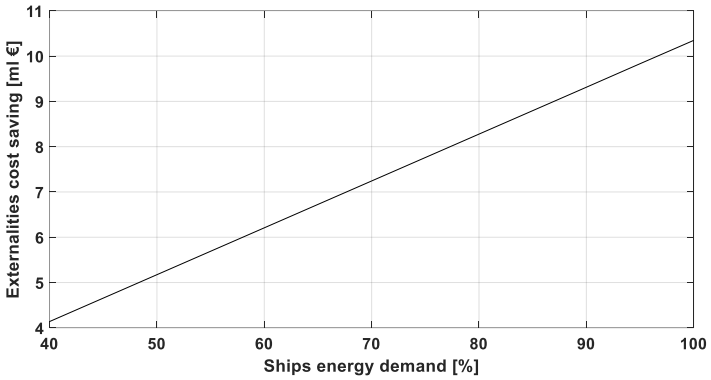

Figure 5.34. Externalities cost saving for government

The specific externalities cost is 0.22 euro/kWh (this value is calculated considering the ratio between the annual externalities cost as reported in Table 5.8 and the total electric energy required by ships at berth during one year). The energy cost shown in Figure 5.35 has been calculated as in equation (5.15). The cost of electrical energy produced on board and reported in Figure 5.35 (Ship in the legend) has been calculated considering a very efficient engine, whose specific consumption is 180.6 g/kWh and summing a maintenance cost, as found in (V.T.P. Engineering).

$$\mathrm{EC} = EC_1 + EC_2 - \%EXC \tag{5.15}$$

Where:

- EC_1 is the energy cost produced by the power supply barge;
- EC_2 is the cost due to the distribution of energy;
- $\%EXC$ is a percentage (Benefit in the legend of Figure 5.35) of the specific externalities cost.

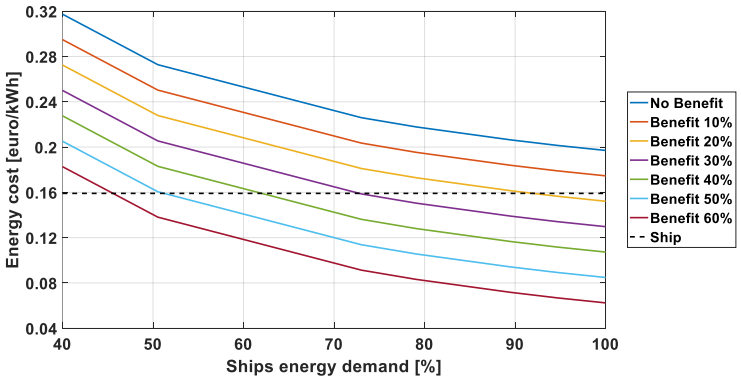

Figure 5.35. Energy cost by cold ironing system for different benefit scenarios

Taking in account the possibility to supply energy to all ships in port, the energy cost of the power supply barge needs almost a governmental benefit equal to the 20% of externalities cost saved thanks to the cold ironing system adopted.

5.9 INVESTIGATIONS ON POSSIBLE TOWED POWER SUPPLY BARGE LAYOUTS

As for a towed barge, serving one ship at each time, the selection of the most interesting ships has been carried out introducing an index of merit, calculated as in equation (5.16).

$$SHIP_{INDEX} = \frac{h}{h_{MAX}} * \frac{PC}{PC_{MAX}} * \frac{P_{EL}}{P_{EL\,MAX}} \tag{5.16}$$

Where at the numerator the following quantities appear:

- h indicates the hours spent at berth by ship at every port call;
- PC are the number of port calls of each vessel;
- P_{EL} is the electric power required by ship at berth.

At the denominator, the maximum of these quantities are considered at the maximum value verified in the reference year of this study. In the case in which there are two or more vessels in port at the same time, the ship with the higher index of merit has been selected. The containerships, whose electricity demand is lower than the other type of vessels, stand for long times at the berth, and this is a very restrictive design constraint, and for this reason the containerships will be not taken into account hereinafter. The total amount of net electric energy is near 11.1 GWh. Figure 5.36 shows the distribution of time at berth relating to the electric power demand for the considered case study.

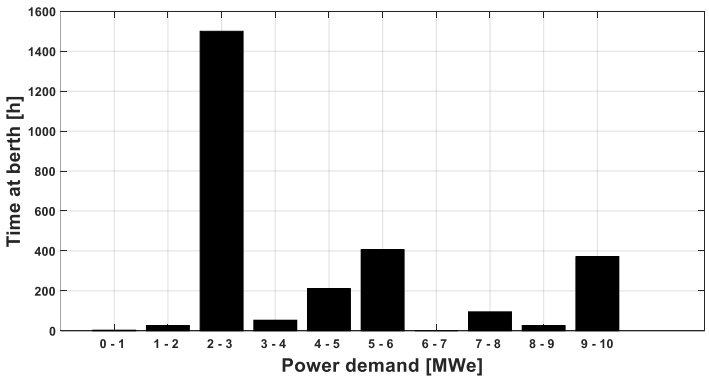

Figure 5.36. Distribution of time at berth vs electric power demand

The design of the towed power supply barge has been carried out considering the same equations of the fixed barge. Regarding the operative costs, the towing by tug has been considered too (information about cost has been found online). The main characteristics of the generating set considered in this study are reported in Table 5.9. The investigated power layouts are a combination of different engines having the same bore and of the same manufacturer.

Table 5.9. Main characteristics of the generating sets

Generators type	Mark	Power [kW]	Efficiency [%]	Length [mm]	Width [mm]	Height [mm]	Dry weight [kg]
CG170-16	C	1625	45.1	5360	1810	2210	12600
G3516H	C	2111	46.56	7395	2139	2402	18315
CG260 - 12	C	3471	45.94	8000	2660	3390	42500
CG260 - 16	C	4479	45.94	9420	2690	3390	51450
C26:33L6AG	R	1460	48.33	7011	2304	3161	33905
C26:33L8AG	R	1940	48.33	7771	2304	3161	42820
C26:33L9AG	R	2190	48.33	8151	2304	3161	46020
B35:40L9AG	R	3780	47.68	10848	2630	4445	79545
B35:40L12AG	R	5472	48.16	10112	3110	4667	97070
9L34SG	W	4342	47.81	10400	2780	3840	77000
16V34SG	W	7743	47.92	11300	3300	4240	12000

Figure 5.37 shows the energy demand covered by different power plant layouts. The full demand is satisfied by a minimum of 10 MWe supplied by the plant

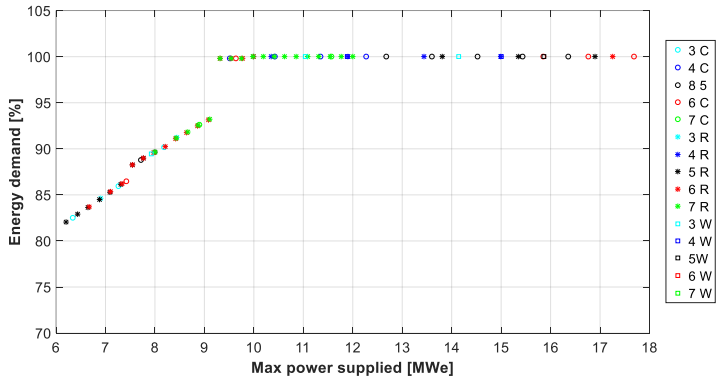

Figure 5.37. Energy demand vs max power supplied

Figure 5.38 shows the average engine efficiency of the power plant while Figure 5.39 represents the average engine load.

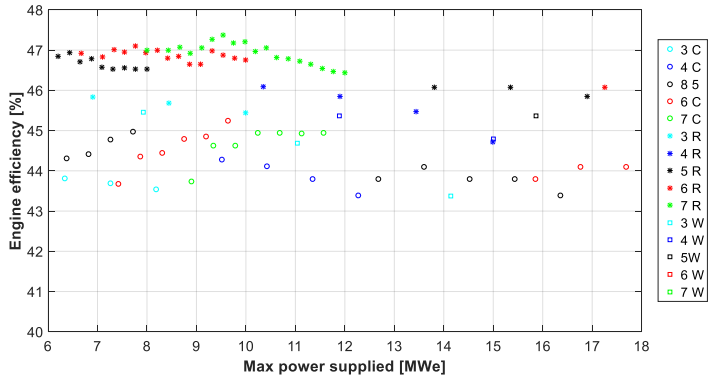

Figure 5.38. Engine efficiency vs max power supplied

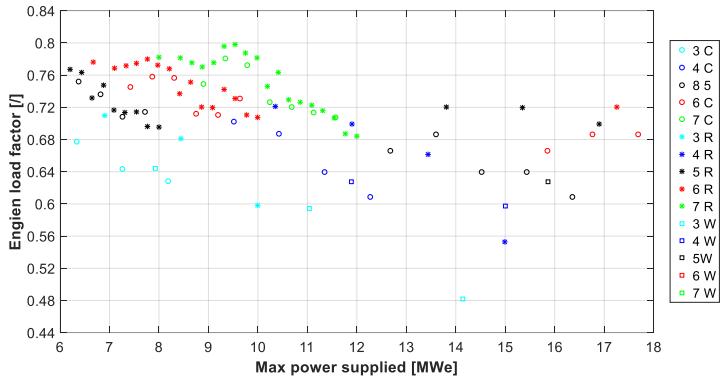

Figure 5.39. Engine load factor vs max power supplied

Figure 5.40 depicts the annual fuel consumption while Figure 5.41 shows the time required between two bunkering operations. The bunkering time is calculated considering the smallest tanks available on product catalogue (WARTSILA Gas Systems, 2014). This size allows a good bunkering time.

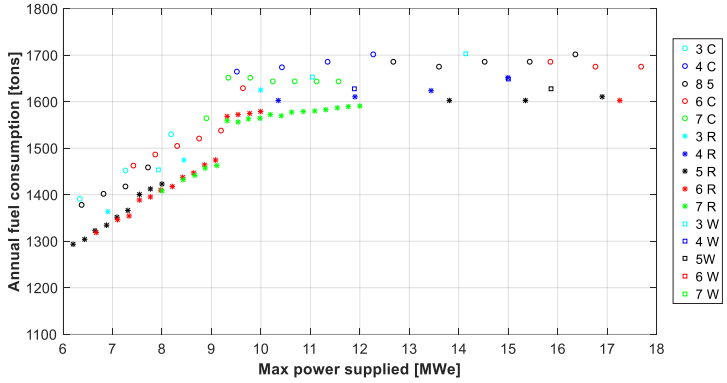

Figure 5.40. Annual fuel consumption vs max power supplied

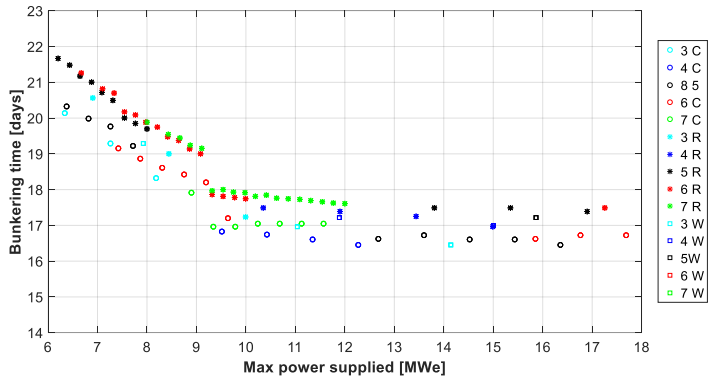

Figure 5.41. Bunkering time vs max power supplied

Figure 5.42 shows the displacement of the barge while the length is reported in Figure 5.43. The layout of the engine is intended as maximum two engines side by side placed in longitudinal way.

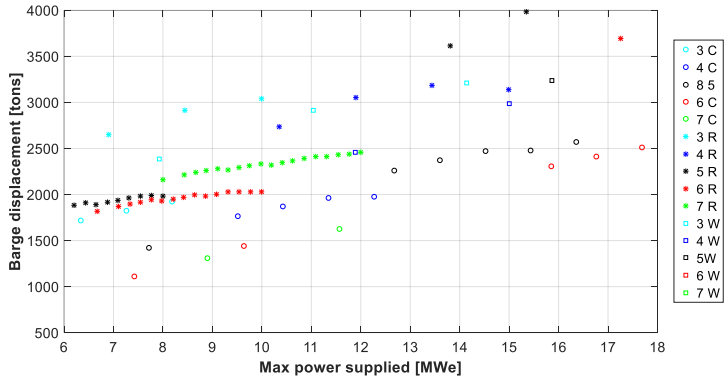

Figure 5.42. Barge displacement vs max power supplied

The beam and height of each power plant layout are reported in Figure 5.44 and Figure 5.45 respectively, while the draft is shown in Figure 5.46.

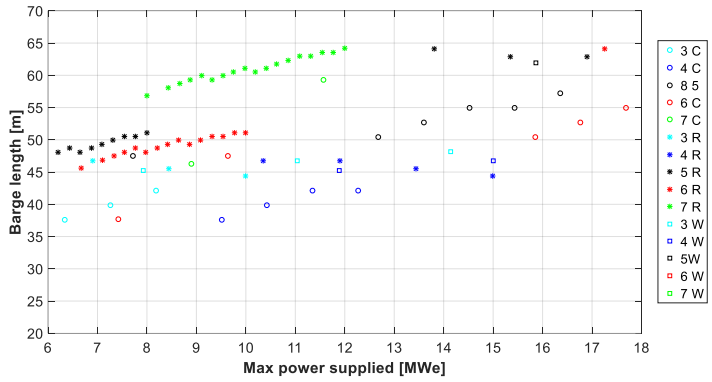

Figure 5.43. Barge length vs max power supplied

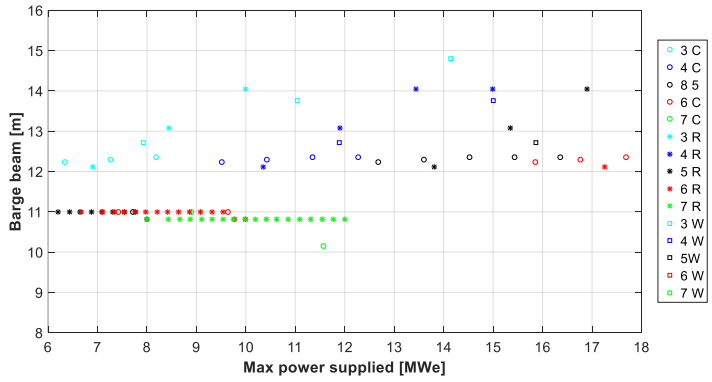

Figure 5.44. Barge beam vs max power supplied

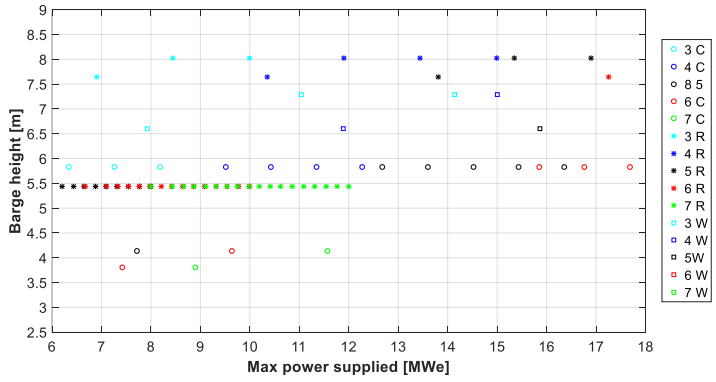

Figure 5.45. Barge height vs max power supplied

Regarding a preliminary cost assessment, the initial cost is reported in Figure 5.47, while the Figure 5.48 shows the energy cost.

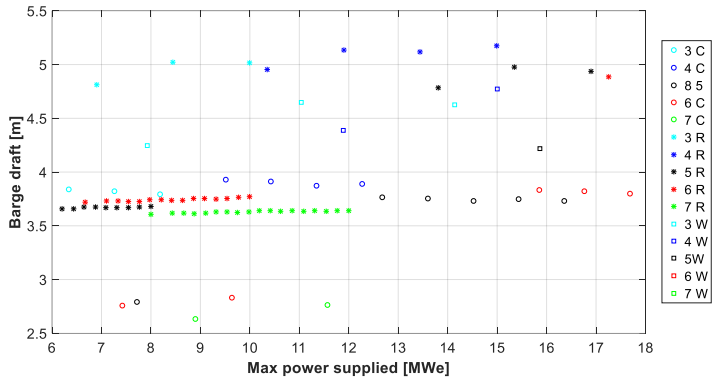

Figure 5.46. Barge draft vs max power supplied

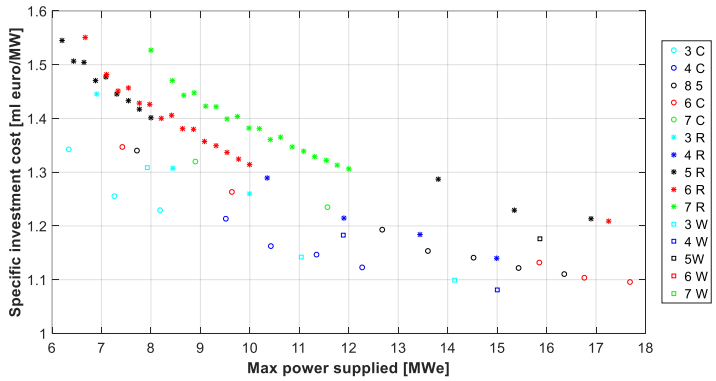

Figure 5.47. Barge specific investment cost vs max power supplied

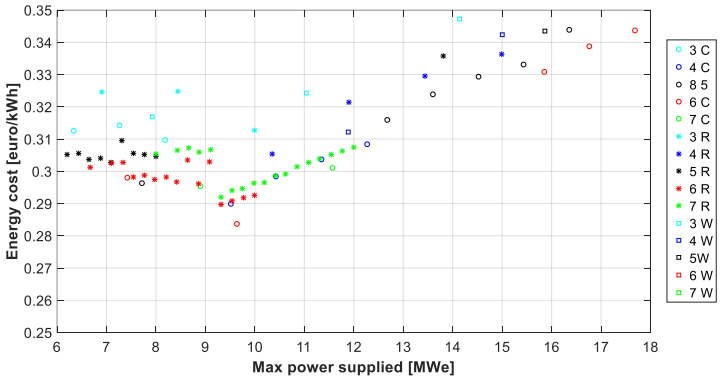

Figure 5.48. Energy cost vs max power supplied

Figure 5.49 reports the time spent above the load factor limit.

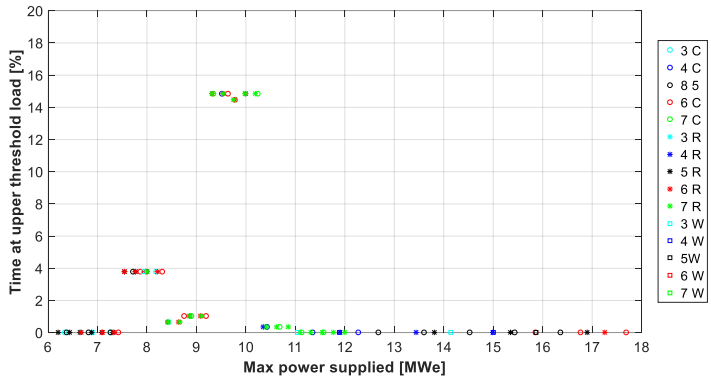

Figure 5.49. Time spent over the maximum load factor threshold vs max power supplied

The choice of the layout of the different power supply barges could be addressed by the minimum energy cost and the 100% of energy supplied. Another important aspect is the time spent over the maximum (90% MCR). The main characteristics of the layout that satisfies these technical requests are reported in Table 5.10. In Appendix II, a simplified drawing representing the general arrangement of the proposed solution is reported.

Table 5.10. Main characteristics of the towed power supply barge selected

TOWED POWER SUPPLY BARGE		
POWER GENERATION		
Generators Layout		1 * C26:33L6AG; 4 * C26:33L8AG; 2 * C26:33L9AG.
Total mechanical power	[MW]	13.60
Max power supplied	[MWe]	10.42
Energy supplied at berth	[GWeh]	9.3
Average engine efficiency	[%]	47.05
Fuel specific cost	[€/kWh]	0.074
Annual fuel consumption	[tons]	1569
Average engine load	[/]	0.7635
Annual operating index	[%]	8.54
Engine running hours	[h]	820
Time at lower threshold load	[%]	0
Time at upper threshold load	[%]	0.36
BARGE CHARACTERISTICS		
Displacement	[tons]	2397
Length	[m]	61.13
Beam	[m]	10.81
Height	[m]	5.44
Draft	[m]	3.72
LNG tank capacity	[m^3]	2 * 105
Bunkering	[days]	17.8
PRELIMINARY COST ASSESSMENT		
Specific investment cost	[ml €/MW]	1.432
Energy cost	[€/kWh]	0.289

Table 5.11 reports the pollutant air emission and the externalities cost due to the abatement pollution system.

Table 5.11. Old port of Genoa. Air emission and Externalities cost with power supply barge

	AIR EMISSION by SHIPS at berth [tons/year]	AIR EMISSION reduction [%]	EXTERNALITIES COST [ml euro/year]
NOx	718	13.40	1.86
PM 10	20.8	17.08	3.42
PM 2.5	11.4	17.08	1.87
SOx	10.4	17.08	3.04
Total	851	14.00	10.21

Figure 5.50 report the cost of energy in case of the power supply barge could supply electric energy to land. The Power to Land Factor (appearing on x axis) means the load of the power station considering 0 in case of not suppling energy to land and 1 considering the engines (in this case is considered that all engines installed on board excepted 2 running to supply energy to land) at 80% of the load. The max power produced by the barge is 6.73 MWe. The time considered for suppling energy is 8 hours per day (in the night time) so a possible energy supplied of about 19.65 GWh. The cost achieved does not take into account the cost of the frequency converter required by supplying electrical energy to land activities. The cost of a converter frequency could be compared to the cost unit of a diesel generator (Masaki A. et al., 2014; Livanos G. A. et al., 2012). The cost regarding electrical equipment to supply energy to land is considered as 1.15 ml euros per MW (Yorke engineering, 2007). Considering a maintenance cost near to 20% of the initial cost is possible to calculate the total cost of the facilities required for supplying power to land. The cost of this initial investment, adding maintenance cost split in 30 years and referred to a maximum energy delivered equal to 19.65+9.3 GWh (as reported in Table 5.10) is about 0.013 euro per kWh. Considering that no energy is supplied to land, the drawbacks of the unused facility is about 0.02 euro per kWh.

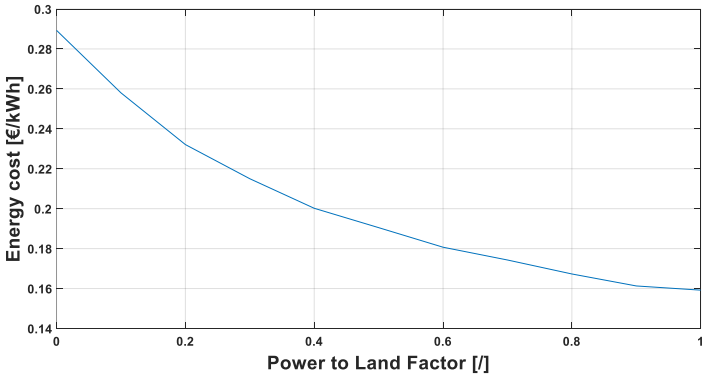

Figure 5.50. Energy cost vs Power to Land Factor

5.10 INVESTIGATIONS ON POSSIBLE POWER SUPPLY VESSEL LAYOUTS

As regard the power supply vessel, the same energy demand scenario is considered. The same approach has been used to investigate different layouts, so the set of equations previously cited has been used apart from the equation used to assess the length of the vessel and the cost, weight and fuel consumption related to the propulsion system (consisting of two azimuth thruster driven by one electrical motor per shaft).

The length of the vessel has been evaluated considering that the space L_S (the term appearing in equation (5.7)) has been calculated as in equation (5.17).

$$L_S = L_{AT} + L_{EM} \tag{5.17}$$

Where:

- L_{AT} is the part of length to place the azimuth thruster, calculated through the equation (5.18);
- L_{EM} is the part of length to place the electrical motor, calculated through the equation (5.19).

$$L_{AT} = c_{AT} \; P_{EM} \tag{5.18}$$

Where:

- c_{AT} is a coefficient calibrated through technical information related to a vessel equipped with azimuth thruster;
- P_{EM} is the maximum power produced by the electrical motor calculated through the admiralty equation (the admiralty coefficient has been evaluated from technical information of a ship that are known) for a max speed of 16 knots and split in two parts.

$$L_{EM} = c_{EM} \; P_{EM} \tag{5.19}$$

Where c_{EM} is a coefficient calibrated through technical information related to a vessel equipped with electrical motors.

The weight of the electrical propulsion system has been evaluated through the equation found in literature (Vernengo G. & Rizzuto E., 2014). The cost of the propulsion system has been evaluated as in equation (5.20).

$$C_{PS} = c_{PS} \; P_{EM} \; n_{EM} \tag{5.20}$$

Where:

- c_{PS} is a coefficient which value is found in (Masaki A. et al., 2014);
- n_{EM} is the number of electrical motors installed on board.

The fuel consumption for sailing from the port of Genova to La Spezia (54 nml) has been calculated considering a cruise speed reached at the 80% of the maximum installed power (cruise speed

evaluated through the equation of admiralty). The specific fuel consumption adopted for this calculation has been taken equal to 163 g/kWh (the average value of specific consumption at 80% load of the gas-engine considered in this study). Figure 5.51 shows the displacement of the power supply barge while Figure 5.52 and Figure 5.53 report the length and draft respectively and for different layouts.

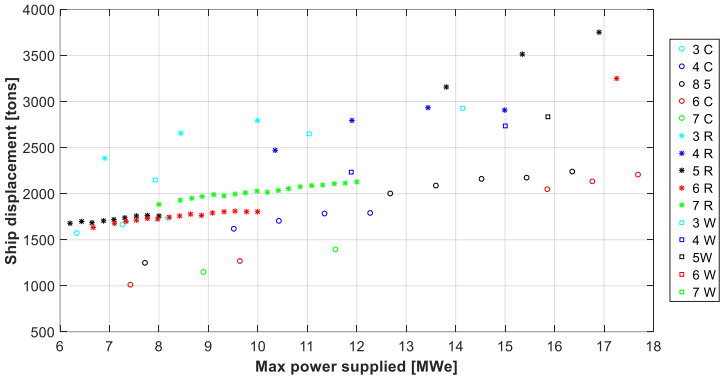

Figure 5.51. Displacement vs max power supplied

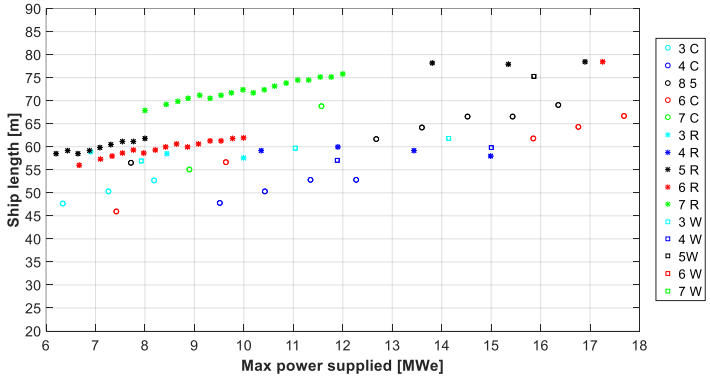

Figure 5.52. Length vs max power supplied

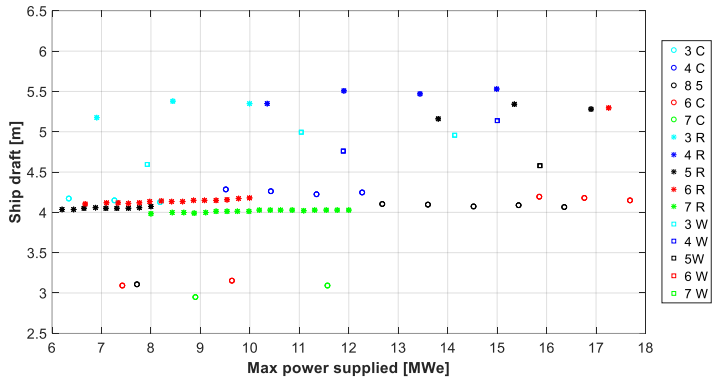

Figure 5.53. Draft vs max power supplied

Regarding a preliminary cost assessment, Figure 5.54 and Figure 5.55 report the specific cost investment and the energy cost respectively. The cost of energy is less than the one of the power barge due to self-propulsion, that allows cutting an important part of operative cost (tug service).

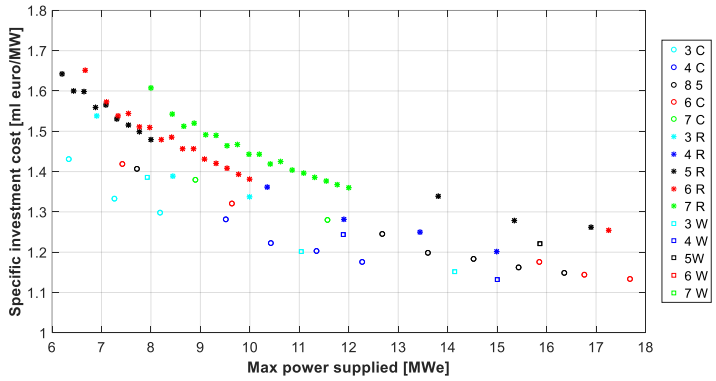

Figure 5.54. Specific investment cost vs max power supplied

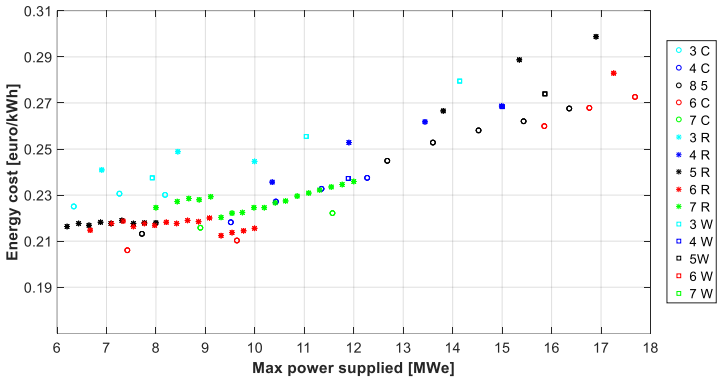

Figure 5.55. Energy cost vs max power supplied

The Figure 5.56 reports the percentage of fuel consumption related to the annual consumption of fuel for the cold ironing system.

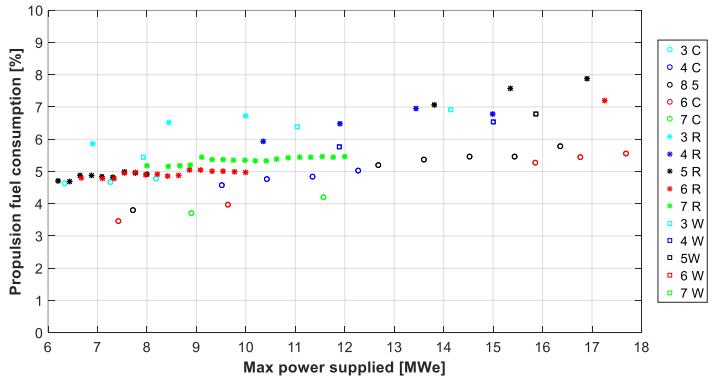

Figure 5.56. Fuel consumption for sailing vs max power supplied

As regards the choice of layout, the energy cost results to be less in case of the adoption of 7 C engines (11.5 MWe) but the same choice as for the barge could be more interesting due to high efficiency of the engines. In Table 5.12, the main characteristics that differ from those reported in Table 5.10 are shown. In Appendix III, a simplified drawing representing the general arrangement of the solution proposed is reported.

Table 5.12. Main characteristics of selected solution

POWER SHIP CHARACTERISTICS		
Displacement	[tons]	1690
Length	[m]	72.37
Beam	[m]	10.81
Height	[m]	5.44
Draft	[m]	4.03
Fuel consumption for sailing	[%]	5.33
PRELIMINARY COST ASSESSMENT		
Specific investment cost	[ml €/MW]	1.420
Energy cost	[€/kWh]	0.226

As regards the air emission, the same value reported in Table 5.11 could be representative also in case of power supply vessel. Figure 5.57 reports the cost of energy in case the power supply vessel could supply electric energy to land. The cost achieved does not take into account the cost of the frequency converter required by supplying electrical energy to land activities. The cost of energy due to the installation of a frequency converter is 0.0026 euro per kWh, as calculated for the power supply barge.

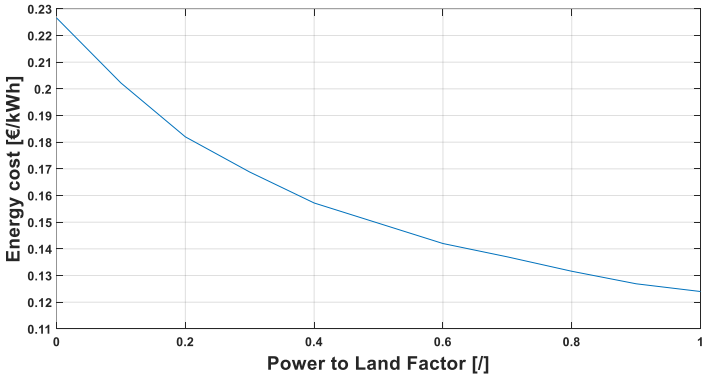

Figure 5.57. Energy cost vs power to land factor

5.11 WHRS UPGRADE ON POWER SUPPLY BARGE

In this session, a study on a possible WHR system installation on board the fixed power supply barge is carried out. The scientific approach used is the same as described in the chapter "WASTE HEAT RECOVERY SYSTEM FOR MARITIME SECTOR". The input data for the design condition of the power turbine, fed by the steam generated by the waste recovery system, are listed in Table 5.13. The design condition selected to size the waste heat recovery system is the average power supplied by the power plant that is 5.5 MWe (power produced by 2 running engines at 0.693 of load).

Table 5.13. Input data design point

INPUT DATA		
Engine Type		9L34SG
Running engines	[-]	2
Nominal power MCR	[kW]	4342
Load factor	[-]	0.693
Exhaust gas temperature after turbine	[°C]	383
Exhaust air flow	[kg/s]	5.428
Exhaust fuel flow	[kg/s]	0.132
Fuel	[-]	NG

The geometrical characteristics of the finned tubes of the heat exchangers are the same as reported in Table 4.6. The max extension of the heat exchangers is set as the length of the gas-generators (placed in transversal way). The cross area of the heat exchangers is set to be 1.3 m * 1.3 m (value calculated in affinity knowing the technical data of a heat exchanger fitting an engine whose power is given). To accommodate the heat exchangers, the horizontal arrangement is preferable to not increase the vertical centre of gravity and to have an easy access for maintenance operation. Because this arrangement, the placement of the LNG tanks is made possible considering an extension of the length. One-pressure waste heat recovery system is considered in this study, due to the cost-effective considerations (the average power of heat source is low related to the suggestions of MAN (MAN Diesel & Turbo, 2012) for WHRS). The set of parameters that maximize the power of the steam turbine are reported in Table 5.14.

Table 5.14. Set of parameters values for optimized design

SELECTED VALUES		
p_{HP}	[bar]	7.4
p_{COND}	[bar]	0.14
$\Delta T_{pp\,HP}$	[°C]	11

The main performances of the WHRS selected are reported in Table 5.15.

Table 5.15. Results of optimized solution

MAIN RESULTS OF STUDY		
P_{ST}	[kW]	427
$Fuel\ saving$	[%]	7
$\Delta \dot{m}_{fuel}$	[%]	0.5
Δp_{HRSG}	[mmWC]	52
T_{EG}	[°C]	168
x_S	[-]	0.9
L_{HRSG}	[m]	8.89
W_{HRSG}	[ton]	10.79
Payback time	[years]	36

By using the off design condition code written by the author, it is possible to deeply calculate the performance of the WHRS, having as input data the electrical power of the energy port scenario of this study and the related time of energy supplied. The related load factor of gas-generator and the number of running machines are associated at each electrical power value. Figure 5.58 reports the fuel saving due to WHRS. The average fuel saving is 4.6 % that differs from the value reported in Table 5.15 because the load factor less than 0.5 has not been taken in consideration, due to the fact that a low speed of exhaust gas can negatively affects the heat exchangers (MAN Diesel & Turbo, 2004). Furthermore, the characteristics of exhaust gas associated at the running of gas-engines at different loads are different in comparison with the design condition. With increasing of power demand, the fuel saving percentage decreases because even of the steam production increases, the steam turbine can receive only until a max of steam (the surplus is bypassed at the condenser). The max steam flowing to turbine is 1.17 kg/s (the design point condition is set as the 90% of the max power of steam turbine).

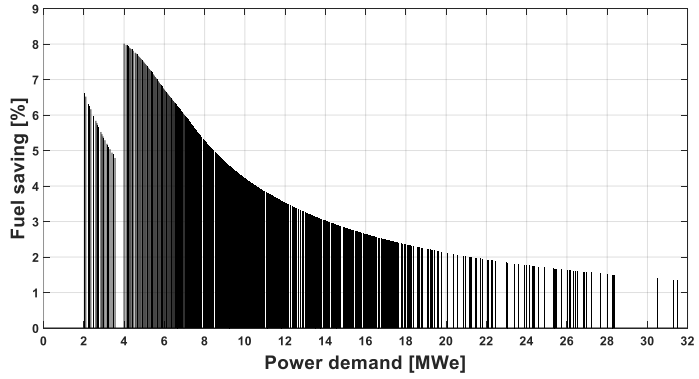

Figure 5.58. Fuel saving vs power demand by ships

The extension of the length of the power supply barge is 26 m to accommodate the LNG tanks. Considering the 100% of energy supplied to ships (47.9 GWh per year), the cost of energy (excluding the cost related to the distribution grid or the need of a frequency converter in case of supplying energy to land activities) is calculated as in equation (5.12). To the original CapEx is added the cost of WHRS (steam turbine generator + condenser + 9 heat exchangers) calculated described in the chapter “WASTE HEAT RECOVERY SYSTEM FOR MARITIME SECTOR” and the cost of the

extension of the hull barge (Vernengo G. & Rizzuto E., 2014). The OpEx is calculated at net of fuel saving. The new cost of energy is 0.15 euro/kWh that is slightly more than the cost reached without waste recovery. This because the renewed CapEx affects the fuel saving that remains low. One possible solution to cut the cost of energy is to supply it for more users. Figure 5.59 shows the electric energy cost as function of the barge energy divided by the value of 47.9 GWh (the total energy required by ships at berth).

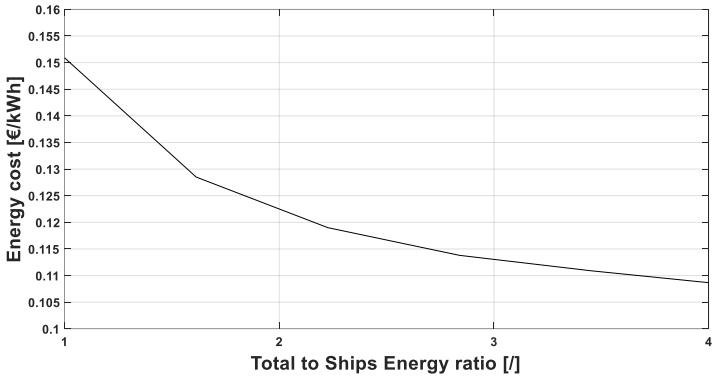

Figure 5.59. Energy cost vs Total to Ships Energy ratio

The minimum value reached is around 0.11 euro/kWh. The benefit of WHRS decreases considering more power produced by power plant because the steam turbine is sized for a design point of an average power of 6 MWe. Considering a waste recovery system designed for an operating profile of the power supply barge including to fully running 7 generators for all the year (design point condition is reported in Table 5.16), the parameters selected by the calculation code are reported in Table 5.17. The features of the waste heat recovery system are presented in Table 5.18.

Table 5.16. Input data design point for 100% power supply barge operating

INPUT DATA		
Engine Type		9L34SG
Running engines	[-]	7
Nominal power MCR	[kW]	4342
Load factor	[-]	0.8
Exhaust gas temperature after turbine	[°C]	379
Exhaust air flow	[kg/s]	5.846
Exhaust fuel flow	[kg/s]	0.15
Fuel	[-]	NG

Table 5.17.Selected parameters for maximizing energy efficiency

SELECTED VALUES		
p_{HP}	[bar]	7
p_{COND}	[bar]	0.13
$\Delta T_{pp\,HP}$	[°C]	8

Table 5.18. Steam turbine features for 100% power supply barge operating

MAIN RESULTS OF STUDY		
P_{ST}	[kW]	1606
$Fuel\ saving$	[%]	6.6
$\Delta \dot{m}_{fuel}$	[%]	0.65
Δp_{HRSG}	[mmWC]	66.4
T_{EG}	[°C]	164
x_S	[-]	0.9
L_{HRSG}	[m]	9.81
W_{HRSG}	[ton]	12.06
Payback time	[years]	6.28

To the original CapEx of the power supply barge, the cost of WHRS (steam turbine generator + condenser + 9 heat exchangers) is added calculated as described in the chapter "WASTE HEAT RECOVERY SYSTEM FOR MARITIME SECTOR" and the cost of the extension of the hull barge (Vernengo G. & Rizzuto E., 2014). The OpEx is calculated at net of fuel saving. The cost of energy could achieve a value of 0.105 euros per kWh.

CONCLUSIONS

In this research study, several technical solutions, using LNG as marine fuel, have been investigated to make ships more eco-friendly and complying with latest rules. The use of LNG as ship fuel has been investigated in terms of plant installation (analysing the main working and safety requirements) and performance of the engine. In particular, a simulation code for a marine gas engine behaviour has been developed to evaluate efficiency and pollutants emissions. Gas-fuelled ships, equipped with a waste heat recovery system to increase energy efficiency, can fully comply with the new stringent environmental rules. The benefits are in economics terms too. A power supply barge could satisfy the electric energy demand of a ship at berth. The cost of energy achieved by the barge could be supported in part from a governmental incentive (that is, as demonstrated in this study, lower respect to the saving of externalities cost, thanks to the installation of a power supply barge fuelled by LNG). To cut furtherly the cost of energy, the power supply barge could deliver energy to land-based activities and the further amount of LNG represents the 25% of the potential demand of LNG in 2025. The installation of a power barge could be a pull factor for investors who want to invest in the installation of LNG storage tanks. The initial cost of a power supply barge is similar to the cost of a direct connection facility from land electrical grid but the power supply barge has the advantage that it can be moved and so usable in another harbour. Due to sudden variation of the electrical power required by ships at berth, a direct connection to the land electrical grid could overload and disturb the electrical transmission. Furthermore, in order to use energy from the electrical land grid, a converter frequency is required with a further initial cost, energy loss during the conversion of frequency and an available area of the port to place this equipment. The floating energy generation plant could be a valid option for supplying energy to ships at berth. The towed power barge and the self-propelled vessel need less capital investments and are characterized by small dimensions and weight but can supply energy just to a small number of ships. On the other hand, due to their size, both solutions can offer flexibility of movement in port and allow to feed ships by approaching each of them. Another important benefit of a fixed power supply barge is the possibility to receive the boil off from the LNG storage tanks. The introduction of LNG in the maritime sector could represent a pull factor for all the ship-owners interested to switch on a greener fuel for moving cargo and passengers in a new era.

REFERENCES

ABS, 2013. Exhaust Gas Scrubber System Status and guidance.

ABS, 2015. Guide for propulsion and auxiliary systems for gas fueled ships.

Alberto Quarati, 2015. Gas, nove porti italiani in corsa per il rifornimento. *LA STAMPA.*

Altosole M., Campora U., Martelli M., 2014. Performance decay analysis of a marine gas turbine propulsion system. *J Ship Res* 2014; 58(3): 117-129.

Altosole, M., Laviola, M., Trucco, A., Sabattini, A., 2015. Waste heat recovery systems from marine diesel engines: Comparison between new design and retrofitting solutions. *(2015) Maritime Technology and Engineering - Proceedings of MARTECH 2014: 2nd International Conference on Maritime Technology and Engineering, pp. 735-742.*

Altosole M., Campora U., Laviola M., Zaccone R., 2017a. Waste Heat Recovery from Dual-Fuel Marine Engines. *Proceedings of IMAM 2017.*

Altosole, M., Benvenuto, G., Campora, U., Laviola, M., Trucco, A., 2017b. Waste heat recovery from marine gas turbines and diesel engines *Energies, 10 (5), art. no. 718.*

Altosole, M., Benvenuto, G., Campora, U., Laviola, M., Zaccone, R., 2017c. Simulation and performance comparison between diesel and natural gas engines for marine applications. *Proceedings of the Institution of Mechanical Engineers Part M: Journal of Engineering for the Maritime Environment, 231 (2), pp. 690-704.*

Altosole M., Figari M., Laviola M., Savio S., 2017d. LNG Fueled Barge for Cold Ironing: Feasibility Study for the Emission Abatement in the Port of Genoa. *WMU Stud.Maritime Affairs, Vol. 6, Aykut I. Ã–lÃ§er et al. (Eds): Trends and Challenges in Maritime Energy Management, 978-3-319-74575-6.*

Andreola M. 2011. Rolls-Royce Bergen Single Fuel Gas Engines. Cross Industry Seminar on LNG as fuel – Lloyd's Register, London, UK, 20 April 2011.

Attah E. E., Bucknall R., 2015. An analysis of the energy efficiency of LNG ships powering options using the EEDI. *Ocean Engineering*, Volume 110, Part B, 1 December 2015, Pages 62–74.

Ballini F., 2013. Air pollution from Ships in Danish Harbours: Feasibility Study of Cold Ironing Technology In Copenhagen. *Thesis for degree of doctor of philosophy*. DITEN, University of Genoa.

Becker marine systems, 2015. Il Sistema Hamburg, energie sostenibili per le città portuali.

Benvenuto G., Campora U., Carrera G., 1998. A Two-Zone Diesel Engine Model for the Simulation of Marine Propulsion Plant Transients. *In: Proceedings of the 2nd International Conference on Marine Industry*, MARIND 98, Varna, Bulgaria, 28 September– 2 October 1998.

Benvenuto G., Laviola M. and Campora U., 2013. Simulation model of a methane-fuelled four stroke marine engine for studies on low emission propulsion systems. *In: Guedes Soares C & López Peña F (eds.) Developments in Maritime Transportation and Exploitation of Sea Resources*, 2013, CRC Press, pp. 591-597.

Benvenuto, G., Laviola, M., Campora, U., 2015a. Assessment of steam cycle layouts for COGAS ship propulsion systems. *(2015) Maritime Technology and Engineering - Proceedings of MARTECH 2014: 2nd International Conference on Maritime Technology and Engineering, pp. 743-754.*

Benvenuto, G., Campora, U., Laviola, M., Zaccone, R., 2015b. Comparison of waste heat recovery systems for the refitting of a cruise ferry. *(2015) 18th International Conference on Ships and Shipping Research, NAV 2015, pp. 404-415.*

Benvenuto, G., Laviola, M., Zaccone, R., Campora, U., 2016. Comparison of a natural gas engine with a diesel engine for marine propulsion. *(2016) Proceedings of 3rd International Conference on Maritime Technology and Engineering, MARTECH 2016, 2, pp. 725-734.*

Bond S., 2011. Practical applications of class requirements to LNG fueled vessels. LNG Fuel Forum, 2011, Stockholm, Sweden.

Campora, U., Laviola, M., Zaccone, R., 2016. An overall comparison between natural gas spark ignition and compression ignition engines for a ro-pax propulsion plant. *(2016) Proceedings of 3rd International Conference on Maritime Technology and Engineering, MARTECH 2016, 2, pp. 735-744.*

Capocaccia F., 2015. Dal Green Shipping Summit il punto su LNG. *TTM.* Genova

Cohen H, Rogers GFC and Saravanamuttoo HIH. Gas Turbine Theory. 3rd ed. Harlow, Essex, England: Longman Scientific & Technical, 1987

Di Natale N., 2013. Full gas Ro-Ro PAX ferry: feasibility study and preliminary design. *Master Thesis in naval architecture and marine engineering*. University of Genoa.

Dimopoulos G. G., Georgopoulou C. A., Kakalis N. M. P., 2011. Modelling and optimization of an integrated marine combined cycle system. *Proceedings of ECOS 2011*, Novi Sad, Serbia.

ECDGE (European Commission Directorate General Environment), 2005a. Service Contract on Ship Emission: Assignment, Abatement and Market-based Instruments Sox Abatement

ECDGE (European Commission Directorate General Environment), 2005b. Service Contract on Ship Emission: Assignment, Abatement and Market-based Instruments NOx Abatement

Engblom K., 2014. Features and parameters of various power plant technologies. *Wärtsilä Technical Journal*.

Engblom K., Reinlund J., 2016. LNG value chain optimisation – Case Aruba. *Wärtsilä Technical Journal*.

Erikson P. & Fazlagic I., 2008. Shore-side power supply. A feasibility study and a technical solution for an on-shore electrical infrastructure to supply vessels with electric power while in port. Chalmers University of Technology.

Esoy, V., Einang, P., Stenersen, D., Hennie, E., Valberg, I., 2011. LNG-fuelled engines and fuel system for medium-speed engines in maritime applications, *Society of Automative Engineers of Japan*, Inc., JSAE 20119212, SAE 2011-01-1998.

Farzaneh-Gord M. The first and second law analysis of a spark ignited engine fuelled with alternative fuels. *Archives of thermodynamics* 2009, 30: 73-92.

Fast Ferry Management, INC., 2007. SCR Project – M/V SOLANO.

Ferrari G., 2008. Motori a combustione interna. 4th ed. Torino, Italy: Il Capitello.

HEC, CCDTT, 2013. LNG as Ship Fuel, Effects on ship design, operations and supporting infrastructure. New Technologies for the Marine Highway.

Henriksson D., Nymanvierto R., 2016. Exhaust gas economizer on auxiliary engines. *Diploma thesis in the Marine Engineering Programme*. Chalmers University of Technology.

IEC/ISO/IEEE 80005-1, 2012. Utility connections in port – part 1: high voltage shore connection (HVSC) systems – general requirements. Geneva: IEC/ISO/IEEE, 2012.

IMO, International Code of Safety for Ships using Gases or other Low-flashpoint Fuels (IGF Code).

Karlsson S., Hognabba T., Kuusisaari M., 2013. The Wärtsilä Gas Valve Unit Enclosed Design (GVU-ED™) for marine applications. *Wartsila, marine in detail*.

Kokarakis J., 2015. Standards and Guidelines for Natural Gas Fuelled Ship Projects. *Bureau Veritas.*

KR, 2013. Evaluation of safety zone for LNG bunkering station for LNG-fuelled ships. Amendments to the IGF code and development of guidelines for low-flashpoint fuel.

Laviola M and Martelli M., 2014. A Thermodynamic Four Stroke Diesel Engine Model for Pleasure Craft Application. In: Proceedings of SEA – MED V Congress, Messina, Italy, 4 July 2014.

Livanos G. A., Theotokatos G., Pagonis D., 2012. Techno-economical investigation of alternative propulsion concepts of ferries operating in Mediterranean sea – introduction of LNG as alternative fuel. *3rd International Conference on Contemporary Problems of Thermal Engineering CPOTE*, Gliwice, Poland.

Livanos G. A., Theotokatos G., Pagonis D., 2014. Techno-economic investigation of alternative propulsion plants for Ferries and RoRo ships. *Energy Conversion and Management*. 79 (2014) 640-651.

MAN 51/60DF Project Guide – Marine.

MAN B&W Diesel A/S.: TCS-PTG Savings with Extra Power. Copenhagen Denmark.

MAN Diesel & Turbo, 2004. Soot Deposits and fires in Exhaust Gas Boilers.

MAN Diesel & Turbo, 2007. Thermo Efficiency System for Reduction of Fuel Consumption and CO2 Emission.

MAN Diesel & Turbo, 2012. Waste Heat Recovery System (WHRS) for Reduction of Fuel Consumption, Emissions and EEDI.

MariTermAB, 2004. Shore-side electricity for ships in ports, case studies with estimates of internal and external costs, prepared for the North Sea Commision. Report.

Masaki A., Hiroyuki K., Tetsugo F., Shota O., Kazuyoshi H., 2014. Economic analysis of trans-ocean LNG fueled. *J Mar Sci Technol* 19:470–478. doi:10.1007/s00773-014-0262-5.

MEPC.245(66), 2014. GUIDELINES ON THE METHOD OF CALUCLATION OF THE ATTAINED ENERGY EFFICIENCY DESIGN INDEX (EEDI) FOR NEW SHIPS.

MEPC, 2012. Marine Environment Protection Committee, Guidelines to the Method of Calculation of the Attained Energy Efficiency Design Index (EEDI) for New Ships. Resolution MECP 212 (63/23), Annex 8, March 2012.

MHI, Steam turbine generator. Website: https://www.mhi-mme.com/products/boilerturbine/steam_turbine.html

MITSUBISHI HEAVY INDUSTRIES, LTD. Steam Turbine Generator

Myang Wook Shin, Dongil Shin, Soo Hyoung Choi and En Sup Yoon, 2008. Optimal operation of the boil-off gas compression process using a boil-off rate model for LNG storage tanks. *Korean journal chemical engineering*.

Mylaudy Dr. S. Rajadurai, Naveen. S., 2015. Muffler Optimization for Increased Fuel Efficiency Iterations Using Taguchi Orthogonal Array for Controlling CO2, IJISET

Nichita C., Nabergoj T., Sonechko D., 2014. The ultimate Jones Act dry cargo carrier: An innovative LNG fueled container RO-RO vessel, Design & Operation of Container Ships, 21-22 May 2014, *Wartsila Ship Design.* London, UK.

Nielsen B., 2009. 8500 TEU Container Ship Green Ship of the Future Concept study. *Odense Steel Shipyard Ltd Book*. Published: 4th December 2009 Project: 4-4383

Parenti G., 2014. La produzione di potenza elettrica per le utenze di bordo di navi da crociera e la sua relazione con il potere inquinante durante le soste in porto. *Master Thesis in naval architecture and marine engineering*, Università degli Studi di Napoli Federico II.

Peckham J., 2013. Becker Touts ‘World’s First Hybrid LNG Barge’ for Cold-Ironing Cruise Ships. *Diesel fuel News*.

Perdichizzi A., 2011. Cicli Combinati, *Dispense del corso di Sistemi Energetici*. Università degli Studi di Bergamo.

Potapov V., 2012. DF Integrated propulsion system and LNG pack – Technical developments, benefits and operational experience. Wartsila http://www.korabel.ru/filemanager/OTHER/0/0/7.pdf

Qiang Guo, Zheshu Ma, Dong Yang, 2012. Conceptual Design and Performance Analysis of an Exhaust Gas Waste Heat Recovery System for a 10000 TEU Container Ship, POLISH MARITIME RESEARCH

Randazzo D., 2014. Proposte di soluzioni impiantistiche per il recupero del calore di scarto dei motori diesel di una nave traghetto. *Master Thesis in naval architecture and marine engineering*. Università degli Studi di Genova.

Rolls-Royce, 2012. Diesel and Gas Engines Generator Set and Propulsion Systems. Report.

SAACKE MARINE SYSTEMS, Technical data sheet, Exhaust gas marine economizer EME-

Sames P., 2011. Costs and benefits of LNG as ship fuel for container vessels. Key results from a GL and MAN joint study.

SANECO, 2014. Studio su analisi preliminare di rischio e prefattibilità tecnico-economica riguardante la dislocazione di determinate attività di movimentazione e stoccaggio di prodotti chimici, petrolchimici, petroliferi e LNG nel porto di Genova.

SCHMI H., 2005. Marine engine Technologies for Reduced Emissions Waste Heat recovery. *Application Technology*, Wartsila.

Singh D. V., Pedersen E., 2016. A review of waste heat recovery technologies for maritime applications, *Energy Conversion and Management*. 111 (2016) 315-328.

Solem S., Fagerholt K., Erikstad S. O., Patricksson O., 2015. Optimization of diesel electric machinery system configuration in conceptual ship design. *Journal of Marine Science and Technology*. September 2015, Volume 20, Issue 3, pp 406–416.

Sungtae Yun, Jinheon Ryu, Suwon Seo, Sangick Lee, Hyun Chung, Yutaek Seo, Daejun, 2014. Conceptual design of an offshore LNG bunkering terminal: a case study of Busan Port. *Journal of Marine Science and Technology*. June 2015, Volume 20, Issue 2, pp 226–237.

Tadros M., Ventura M. and Guedes Soares C., 2015. Numerical simulation of a two-stroke marine diesel engine. In: *Guedes Soares C, Dejhalla R & Pavletic D (eds.) Towards Green Marine Technology and Transport*, 2015, Taylor & Francis Group, pp. 609-618

Tellkamp J., Mohn H., 2015. Small-scale LNG infrastructure development. *IN FOCUS-LNG AS SHIP FUEL*, DNV GL.

Tetra Tech, Inc., 2007. Draft use of shore-side power for ocean-going vessels white paper.

The Engineering ToolBox, website www.engineeringtoolbox.com

Theotokatos G., Livanos, G. A., Dimitrellou, S., Strantzali, E., Pagonis, D.N., Politis, K., Theodoulides, A., Peirounakis, D. Mizithras, P., 2015. Design of LNG storage and feeding system for an open type ferry. Towards Green Marine Technology and Transport: *Proceedings of the 16th International Congress of the International Maritime Association of the Mediterranean (IMAM 2015)*, Pula, Croatia, 21-24 September 2015. ed. / C. Guedes Soares; R. Dejhalla; D. Pavletić. Leiden, The Netherlands, 2015. p. 473-481.

Theotokatos G., Stoumpos S., Lazakis I., Livanos G., 2016. Numerical study of a marine dual-fuel four stroke engine. *MARTECH 2016 - 3rd International Conference on Maritime Technology and Engineering*, Lisbon, 4-6 July.

Tigges K., 2011. SISHIP SGM References 101103 Shaft Generators and Booster Plants. *SIEMENS References*

Unipv, Università degli Studi di Pavia Dipartimento di Ingegneria Civile e Architettura Sezione Idraulica, Ambiente ed Energetica. Impianti motori a vapore. Turbine a vapore. website: http://www-3.unipv.it/webidra/materialeDidattico/sala/014.pdf

V.T.P. Engineering. COLD IRONING, Una nuova soluzione eco-compatibile per l'alimentazione delle navi in porto. Website: http://www.vtpengineering.it/allegati/coldironing/brochure_cold_ironing_ita.pdf

Van Kreij J., 2015. LNG ship fuel systems update, *2015 GREEN4SEA Forum*. Chart Industries.

Vernengo G., Rizzuto E., 2014. Ship synthesis model for the preliminary design of a fleet of compressed natural gas carriers. *Ocean Engineering* 89 (2014) 189-199.

WARTSILA GAS SYSTEM, 2014. LNG PAC PRODUCT GUIDE.

Wärtsilä. LNG Shipping, 2013. Wärtsilä dual-fuel. Internal report.

Woschni G., 1967. A universally applicable equation for the instantaneous heat transfer coefficient in the internal combustion engine. *Society of Automotive Engineers Trans* 1967; 76, SAE paper 670931: 3065.

WPCI-LNG FUELLED VESSELS, website: http://www.lngbunkering.org/lng/technical-solutions/tank-types.

Wursig G., 2013. LNG fuel tank – benefits and challenges. *DNV*.

Yorke engineering, 2007. Port of San Diego: Cold ironing study.

Zel'dovich YB., 1946. The Oxidation of Nitrogen in Combustion Explosions. Acta Physicochimica U.S.S.R. 1946, 21: 577–628.

APPENDIX

APPENDIX I

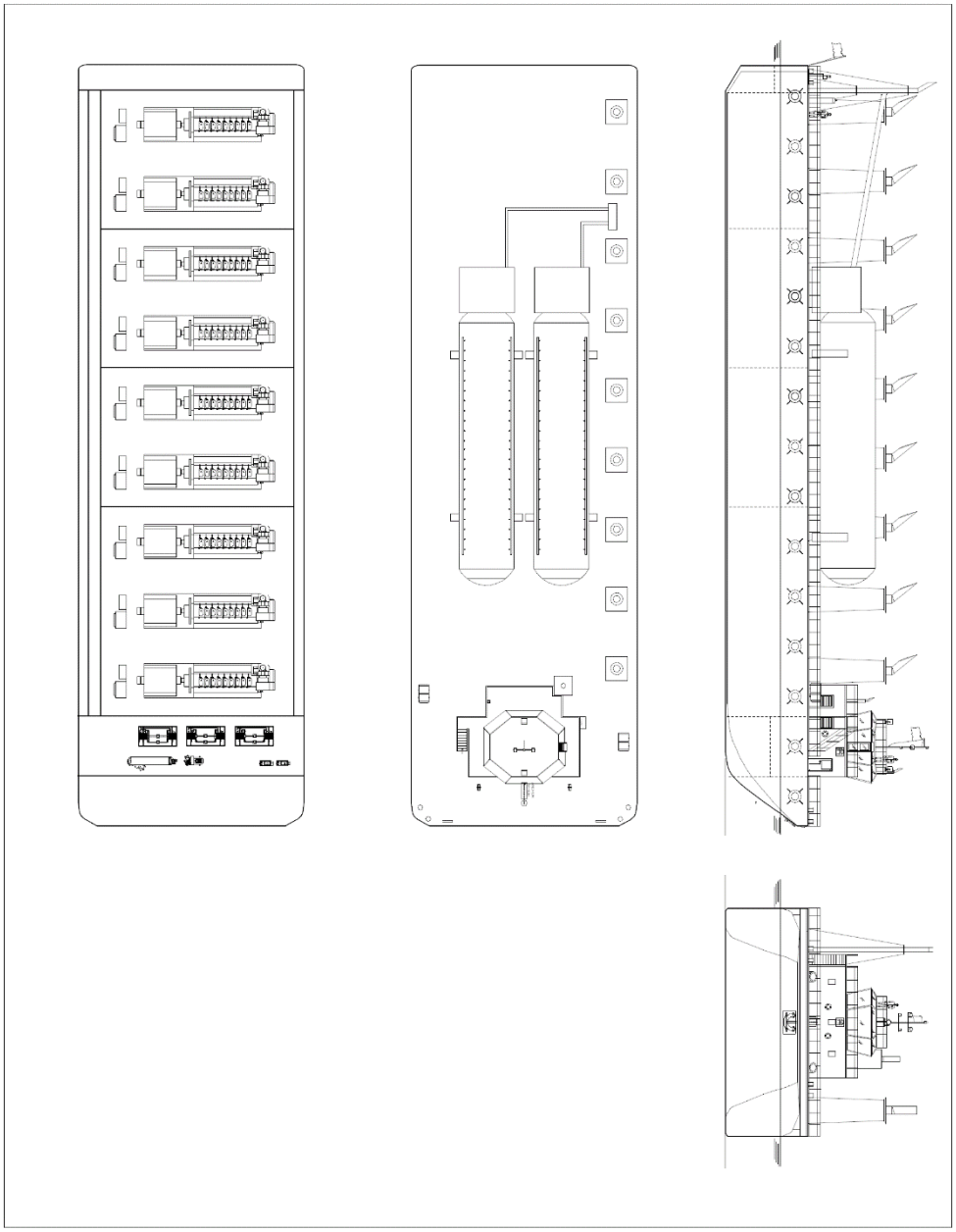

General arrangements of the fixed power supply barge

APPENDIX II

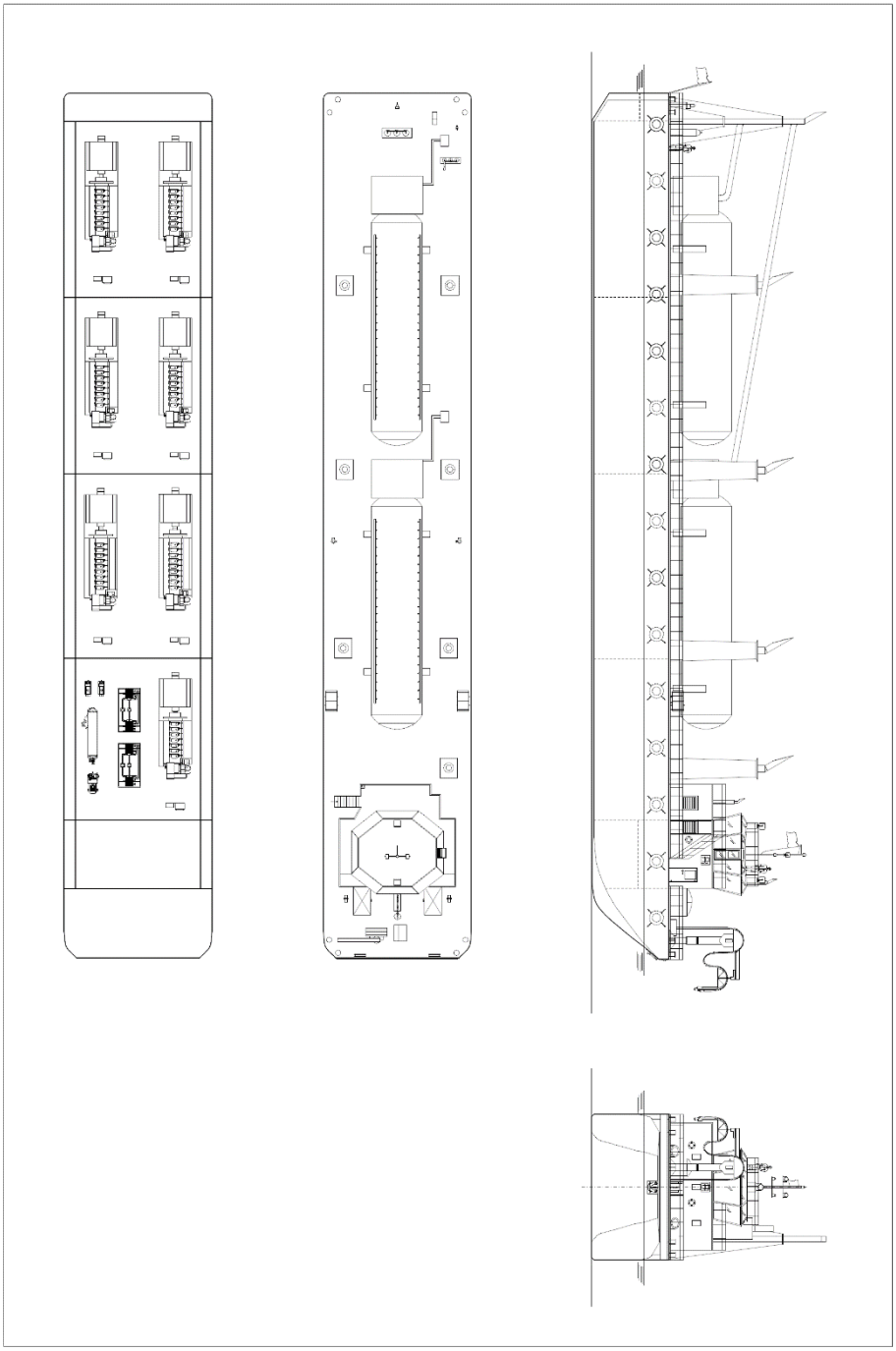

General arrangements of the towed power supply barge

APPENDIX III

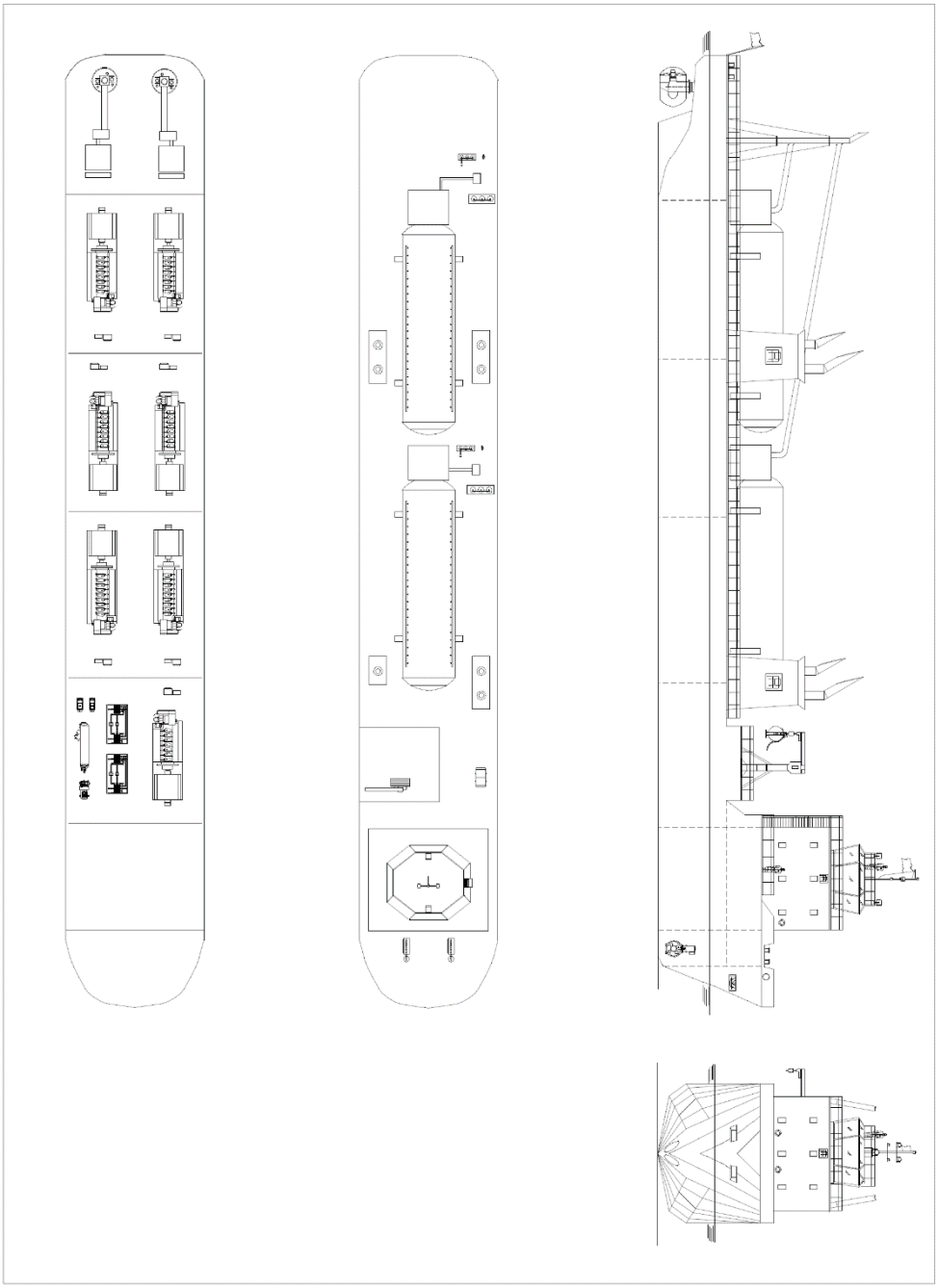

General arrangements of the power supply vessel